Development and characterization of radiochromic and radiofluorogenic solid state polymer dosimeter material

Bernal Zamorano, Maria del Rocio

Publication date:
2018

Document Version
Publisher's PDF, also known as Version of record

Development and characterization of radiochromic and radiofluorogenic solid state polymer dosimeter material

PhD dissertation

María del Rocío Bernal-Zamorano

Center for Nuclear Technologies
Technical University of Denmark
January, 2018

Preface

The work described in this thesis was carried out at the Center for Nuclear Technologies of the Technical University of Denmark (DTU Nutech) placed at Risø Campus (Røskilde), under the supervision of Lars R. Lindvold as main supervisor, and Claus E. Andersen as co-supervisor.

Acknowledgements

I would like to thank all the people who made this project possible. Lars René Lindvold, thanks for sharing your extensive knowledge in chemistry and optics with me, for sharing also your wonderful library, for being always available and for your support at every moment. Claus E. Andersen, thanks for helping me with dosimetry concepts, statistics and R-programming, for your good advices, and your support. Thanks to both of you for your good guidance in these three years.

Thanks to Mark Bailey for reviewing the thesis, for doing the Monte Carlo simulation of the gammacell, for helping me with interesting discussions, and for personal support. Thanks to Mark Bailey, Arne Miller and Torben Esmann Mølholt for helping me with irradiations and EPR measurements. Thanks to Fedor Zhuravlev, who introduced me to the design of experiments method and helped me with its analysis.

Thanks to my fellow PhD student Nicolai H. Sanders, who developed the fluorescence setup that was used in this project. Thanks to Grichar Valdés Santurio, who helped me with Monte Carlo simulations. Thanks to the rest of the PhD office: Nikola Markovic, Patrik Sibolt, Martin Autzen, Susanne Nørring Bekke, and also Jeppe Brage Christensen and Christina Ankjærgaard who visit us often, for being a very good company.

Thanks to Bent Lauritzen, Jens-Peter Lynov, Pia Elhauge, Merete Holmegaard Larsen, Nina Jensen, Finn Jørgensen and Claus Bang for their support; and to everyone in the department for making my stay more pleasant.

Finally, I want to thank my friends for their support and for the good moments.

This thesis is dedicated to my parents and my sister Miriam, for their encouragement and support.

Thank you. Tak. Gracias.

Rocío Bernal Zamorano, January 2018, Røskilde

Abstract

Due to the complexity of external radiotherapy based on, e.g., LINAC, gamma knife and particle therapy, it is important that the treatment plans and the actual absorbed dose distribution received by the patient is in agreement. Radiochromic films, radiochromic and polymerizing gels, and radiochromic solid state dosimeters have been developed over the years for that purpose. However, 3D dosimetry is still not in use in the clinic.

This PhD-project proposes a novel method that potentially could lead to a polymer-based solid-state dosimeter suitable for use as 3D dose verification using optical fluorescence tomography.

In this PhD project a radiochromic and radiofluorogenic solid state dosimeter was developed. The radiation-sensitive component of the dosimeter is pararosaniline leuco dye, originally used for its radiation-induced color change in the Risø B3 radiochromic film. This material is well-known from high-dose (> 1kGy) dosimetry in radiation sterilization of, e.g., disposable medical devices. In this PhD project, a solid-state polymer material doped with this dye has been developed. The material has maintained its radiochromic properties even at thickness 500 times thicker than the conventional film dosimeter. This property has been achieved by the use of two biocompatible monomers. The first one, poly(ethylene glycol) diacrylate (PEGDA), possesses two important properties in this context, namely, tissue equivalence and ion-mobility. Ion-mobility is very important as it facilitates mobility of the free radicals formed during irradiation and their subsequent reaction with the radiochromic dye. The second polymer, 2-hydroxyethyl methacrylate (HEMA), facilitates mechanical stability of the dosimeter after it has been polymerized.

The fabrication process of the dosimeter is fast and easy. The radiochromic leuco-dye is dissolved in PEGDA and HEMA together with a photoinitiator. Subsequently, the mixture is photopolymerized using a 385 nm UV LED light source. The use of photopolymerization makes it possible to control the process temporally and spatially.

The absorbance and fluorescence responses of this dosimeter were characterized using a Co-60 gamma-source. Within clinical dose range (0-30 Gy) the material had linear response of absorbance and fluorescence. The main contributing factors to the dosimeter response were identified, mainly related to the effect of the photoinitiator, the secondary polymer, and the photocuring process. The contribution from the dye and from the matrix to the radiation response was determined by absorbance, fluorescence, and EPR measurements.

This new solid state dosimeter does not need a container, it presents good optical and mechanical properties, it is tissue equivalent, and it can be made in any shape. The studies carried out along this PhD project have shown that this dosimeter is a potential candidate for use in 3D dosimetry, but further investigation is required to increase the fluorescence sensitivity to low doses (< 10 Gy).

Resumé (Danish abstract)

På grund af kompleksitets graden ved medicinsk strålebehandling baseret på eksterne strålekilder som f.eks. LINAC, gammakniv og partikel terapi, er det vigtigt, at kunne verificere, at den planlagte stråledosis er i overensstemmelse med den absorberede stråledosis som patienten faktisk har modtaget under behandlingen. Der er i årenes løb blevet udviklet en række metoder baseret på radiokrome film, radiokrome gel og radiokrome polymere med henblik på at dække dette behov. Disse metoder har, indtil videre, dog ikke vist sig at kunne anvendes i daglig klinisk 3D dosisverifikation.

I dette ph.d. projekt er der blevet gjort forsøg på at udvikle og karakterisere et nyt radiokromt og radiofluorogent polymer materiale, der potentielt kan anvendes til 3D dosisverifikation baseret på optisk fluorescens tomografi.

Det dosimeter materiale, der er udviklet i dette ph.d. projekt er baseret på et pararosanilin leuco farvestof, der skifter farve ved bestråling med ioniserende stråling. Farvestoffet er også kendt som Risø B3 i forbindelse med tyndfilm dosimetre til måling af høje strålingsdoser (> 1 kGy) ved f.eks. sterilisering af medicinske eengangsartikler. I dette ph.d. projekt er det lykkedes at fremstille et faststof polymer materiale doteret med dette farvestof, hvor de radiokrome egenskaber kendt fra tyndfilms materialet er bevaret ved en tykkelse som er 500 gange tykkere end film dosimetret. Dette er sket ved at anvende to biokompatible polymer materialer. Det ene materiale, polyethylenglykol diakrylat (PEGDA), der har to vigtige egenskaber i denne sammenhæng, nemlig vævsækvivalens og ionmobilitet. Ionmobiliteten gør det muligt for de frie radikaler, der dannes ved bestråling at reagere med den radiokrome farvestof, som giver dosimeter responset. Det andet materiale, 2-hydroxyethyl methakrylat (HEMA), gør dosimetret mekanisk stabilt efter polymerisering.

Fremstillingsmetoden for dette dosimeter materiale er hurtig og enkel. Det radiokrome farvestof opløses i PEGDA og HEMA, der desuden er tilsat en fotoinitiator. Derefter fotopolymeriseres blandingen med en 385 nm UV LED lyskilde. Brugen af fotopolymerisering gør det muligt at styre polymeriseringsprocessen både i tid og sted.

Absorbans- og fluorescens respons fra polymer dosimeter ved bestråling med en Co-60 gammakilde er blevet karakteriseret. Inden for kliniske relevante doser 0-30 Gy har materialet et lineært respons både i absorbans- og fluorescens signal. De primære faktorer, der bidrager til dosimeter respons er blevet identificeret som fotoinitiator, sekundær polymer og fotopolymeriserings processen. Bidraget til dosimeter respons fra det radiokrome farvestof og primær polymer er blevet undersøgt ved måling af absorbans, fluorescens og elektron paramagnetisk resonans (EPR) fra dosimeter.

Den nye faststof dosimeter kræver ikke en beholder og kan derfor støbes i vilkårlige geometrier. Det er desuden vævsækvivalent og har gode optiske og mekaniske egenskaber. Resultaterne fra dette ph.d. projektet indikerer, at materialet kunne være en god kandidat som 3D dosimeter til medicinsk dosimetri såfremt dets fluorescens egenskaber kan forbedres, især ved lave absorberede stråledoser (< 10 Gy).

List of Publications

Publications included in this thesis:

I. Bernal-Zamorano, M.R., Sanders, N.H., Lindvold, L., Andersen, C.E. (2017). Radiochromic and radiofluorogenic 3D solid polymer dosimeter; initial results for high doses. *Journal of Physics: Conference Series*, 847, 012016. Published. DOI: 10.1088/1742-6596/847/1/012016.

II. Bernal-Zamorano, M.R., Sanders, N.H., Lindvold, L., Andersen, C.E. (2017). Radiochromic and radiofluorogenic 3D solid polymer dosimeter; effect of the photoinitiator. *Radiation Measurements*, 106, 192-195. Published. DOI: 10.1016/j.radmeas.2017.03.012.

III. Bernal-Zamorano, M.R., Sanders, N.H., Lindvold, L., Andersen, C.E. Radiochromic and radiofluorogenic 3D solid polymer dosimeter; a third signal: Electron Paramagnetic Resonance (EPR). Submitted to Radiation Measurements on December 2017.

Conference contributions

Results from this PhD project presented at international conferences.

First-authored contributions:

I. Bernal-Zamorano, M.R., Sanders, N.H., Lindvold, L., Andersen, C.E. (2016). 3D dosimetry material with absorbance and fluorescence responses to ionizing radiation. Poster presentation. 18th SSD conference, Munich (Germany).

II. Bernal-Zamorano, M.R., Sanders, N.H., Lindvold, L., Andersen, C.E. (2016). Radiochromic and radiofluorogenic 3D solid polymer dosimeter; initial results for high doses. Oral presentation. 9th IC3DDose conference, Houston (Texas).

III. Bernal-Zamorano, M.R., Sanders, N.H., Lindvold, L., Andersen, C.E. (2017). Increasing the sensitivity of a radiofluorogenic 3D solid polymer dosimeter. Oral presentation. 5th Øresund Workshop on Radiotherapy, Helsingborg (Sweden).

IV. Bernal-Zamorano, M.R., Sanders, N.H., Lindvold, L., Andersen, C.E. (2017). Presentation of 3D RayTrack. Exhibitor at Medico Bazar, Lyngby (Denmark).

V. Bernal-Zamorano, M.R., Sanders, N.H., Lindvold, L., Andersen, C.E. (2017). Electron paramagnetic resonance (EPR) signal from a new solid polymer material

aimed for 3D dosimetry. Poster presentation. 36th ESTRO conference, Vienna (Austria).

VI. Bernal-Zamorano, M.R., Sanders, N.H., Lindvold, L., Andersen, C.E. (2017). Radiochromic and radiofluorogenic solid state dosimeter based on triphenyl methane dyes. Oral presentation. Dosimetry Workshop, Aarhus (Denmark).

Second-authored contributions:

I. Sanders, N.H., Bernal-Zamorano, M.R., Lindvold, L., Andersen C.E. (2016). Novel material for high resolution dosimetry, utilizing radiation induced changes in fluorescence response. Poster presentation. 35th ESTRO conference, Turin (Italy).

II. Sanders, N.H., Bernal-Zamorano, M.R., Lindvold, L., Andersen C.E. (2016). Measuring radiation dose in 3D in a radiofluorogenic sample; a proof of concept setup. Oral presentation. 18th SSD conference, Munich (Germany).

III. Sanders, N.H., Bernal-Zamorano, M.R., Lindvold, L., Andersen C.E. (2017). Recovering dose distribution from fluorescence data. Oral presentation. 5th Øresund Workshop on Radiotherapy, Helsingborg (Sweden).

IV. Sanders, N.H., Bernal-Zamorano, M.R., Lindvold, L., Andersen C.E. (2017). Challenges in optical 3D dosimeter readout of a fluorogenic solid state dosimeter. Oral presentation. Dosimetry Workshop, Aarhus (Denmark).

Third-authored contributions:

I. Høye, E.M., Sadel, M., Bernal-Zamorano, M.R., Muren, L.P., Petersen, J.B.B., Skyt, P.S., Swakon, J., Bassler, N., Balling, P. (2017). Saturation dose and quenching in proton beams in a radiochromic 3D dosimeter. Poster presentation. BiGART conference, Aarhus (Denmark).

Abbreviations and symbols

3D	Three dimensional
^{60}Co	Cobolt-60
CPTX	1-chloro-4-propoxy-9H-thioxanthen-9-one
CQ	Camphorquinone
CT	Computed tomography
DMAEM	2-(Dimethylamino)ethyl methacrylate
DoE	Design of experiments
EDB	Ethyl 4-dimethylaminobenzoate
EPR	Electron Paramagnetic Resonance
FTIR	Fourier transform infrared
Gy	Gray. Unit of dose (J/kg)
HEMA	2-hydroxyethyl methacrylate
ITX	Isopropyl-9H-thioxanthen-9-one
LED	Light emitting diode
LINAC	Linear accelerator
MEHQ	Monomethyl ether hydroquinone
M_w	Molecular weight
Nd:YAG	Neodymium-doped yttrium aluminium garnet
PEGDA	Poly(ethylene glycol) diacrylate
QA	Quality assurance
TCPO	Bis(2,4,6-trichlorophenyl) oxalate
T_g	Glass transition temperature
TPO	Diphenyl(2,4,6-trimethylbenzoyl)phosphine oxide
UV	Ultraviolet

V	Volt. Unit to electric potential (J/C). Used to quantify the energy of e.g. diagnostic x-rays devices (kV), radiotherapy photon beams (MV) or radiotherapy electron beams (MeV, megaelectron volt)
W	Watt. Unit of power (J/s)
Z_{eff}	Effective atomic number
ρ	Mass density
ρ_{el}	Electronic density
μ/ρ	Mass attenuation coefficient (photons)
L_{Δ}/ρ	Restricted mass stopping power (electrons)

Contents

Chapter 1

Introduction

Cancer is still the leading cause of death globally. About 14.1 million of new cases per year are estimated worldwide, from which 8.2 million people die (*Ferlay et al., 2013*). Cancers are usually treated with a combination of techniques, such as surgery, chemotherapy, and radiotherapy.

About 60% of people with cancer get radiotherapy, usually external beam radiotherapy, which is predominantly based on the use of high-energy X-rays produced by a linear accelerator (LINAC) to target the tumor from outside the body, rotating around the patient. The purpose of delivering dose to the tumor may be curative by eliminating the tumor or palliative by shrinking it for pain relief.

Accuracy and precision are crucial factors in radiotherapy: radiation must hit the tumor while avoiding the healthy tissue that is next to it (accuracy) and this must occur over and over again (precision). The treatment is usually divided into small doses (fractions) to allow the healthy tissue to recover. To ensure that radiation targets just the tumor and not the healthy tissue, and thereby minimize the incidence of severe side effects arising from the irradiation of healthy tissue, individualized treatment plans and high-precision delivery techniques have been developed during the last decades.

Treatment planning is carried out by using a computed tomography (CT) scan of the patient; radiation oncologists define empirically the planning target volume (PTV), and commercial treatment planning systems are used to calculate the dose distribution in the target tumor and in organs at risk. Regarding the LINAC, the beam is shaped to conform to the specific three dimensional (3D) shape of the tumor by intensity-modulated radiation therapy (IMRT), delivering multiple beams of different intensities. Imaging of the tumor during treatment is possible by image-guided radiotherapy (IGRT), allowing making necessary adjustments in the beam guiding (*Baskar et al., 2012*).

The 3D dose distribution in the patient is determined by advanced computerized dose calculation algorithms. However, due to the complexity of these dose distributions,

experimental verification of the treatment plan is necessary (*Low, 2015*). A measurement of the 3D distribution would ensure that the treatment is delivered as intended. This demand is present both, for everyday patient safety, and for quality assurance of clinical trials aiming to establish the benefits of new treatment modalities. Here it is when the need for 3D dosimetry arises.

1.1. 3D Dosimetry

Radiation measurements are carried out by dosimeters. Point dosimeters, like ionization chambers, thermoluminescent dosimeters (TLD), diodes, alanine and scintillators, measure the absorbed dose in a single point, usually inside a water tank or a solid water phantom while irradiated by the LINAC (figure 1.1a). They are mainly used for beam calibration and quality assurance (QA).

In 2 dimensions (2D), GafChromic™ radiochromic film is widely used in the clinic for QA. It is a polydiacetylene-based film in which radiation induces polymerization of the diacetylene monomers, leading to a series of polyconjugated carbon double bonds and therefore it is accompanied by a color change (*ICRU, 2008*). The green film darkens its color with radiation and the absorbed dose is obtained by measuring the color change of the film with an optical scanner. There are several GafChromic™ films with different dose ranges and applications (*Ashland, 2017)*). GafChromic™EBT3 film (0.1 cGy – 10 Gy) is used for IMRT treatment plan verification by placing it in different sections of a phantom (figure 1.1b). Then, the 3D dose distribution in the phantom obtained by the treatment planning system is compared to the film measurements (*Borca et al., 2013*). However, this is not a real 3D measurement. Since absorbed dose distributions from IMRT are complex, a full 3D measurement with high spatial resolution is required.

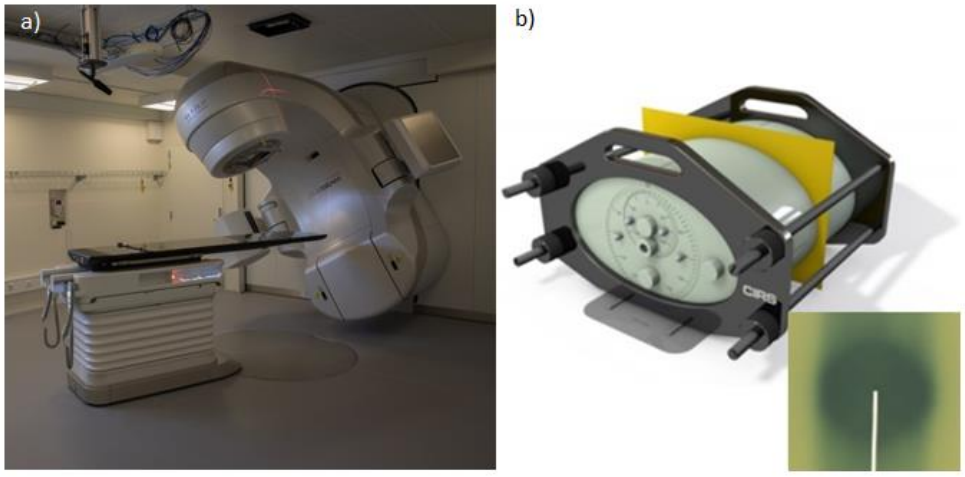

Figure 1.1: a) Varian TrueBream™ LINAC at DTU Nutech. b) GafChromic™ film inserted in a thorax-like phantom (*Supertech*, 2017). Detail of an irradiated film (*Wang et al., 2012*).

3D dosimetry systems are radiation sensitive volumes that change their chemical properties with ionizing radiation. This response, quantifiable by a measurement system, should be stable and reproducible. The dosimeter would be capable of rendering a 3D dose profile from an external radiation treatment session by placing it in lieu of the area targeted for treatment. Some 3D dosimetry systems that will be following discussed are presented in table 1.1.

Table 1.1: 3D dosimetry systems.

Dosimeter	State	Response	Measurement	Readout
Fricke	Gel	Radiochromic	Concentration of Fe^{3+}	OCT, MRI
RGD	Gel	Radiochromic	Color change of MG dye	OCT, MRI
PAG, MAG, VIPAR, PABIG	Gel	Polymerizing	Scattering	OCT, MRI
Presage™	Solid	Radiochromic	Color change of MG dye	OCT
RFG	Gel	Radiofluorogenic	Fluorescence of MPy dye	OFT

The first 3D dosimeters that were developed were radiochromic gels, polymer gels that change color with radiation. In 1950, methylene blue and indo-phenol dyes contained in gelatin or agar matrices were investigated (*Day and Stein, 1950*). A well-known radiochromic gel is the Fricke gel, a ferrous sulfate dosimeter that oxidizes by effect of radiation, changing the ionization state of ferrous ions (Fe^{2+}) to ferric (Fe^{3+}) in proportion to the absorbed dose (*Schreiner, 2004*). Figure 1.2a shows Fricke gels based on polyvinyl alcohol (PVA) irradiated with high-energy X-rays (*d'Errico et al., 2017*). The increase in color intensity corresponds to the increase in absorbed dose. The figure also includes the magnetic resonance imaging (MRI) maps used to determine the ferric ion distribution. A major problem of Fricke gels is the diffusion of the ions, resulting in a blurring image and therefore in a poor spatially-resolved dose distribution. Another radiochromic gel dosimeter (RGD) is the one based on malachite green (MG) leuco dye, contained in an aqueous gelatin matrix. The leuco dye is oxidized by free radicals produced upon irradiation, leading to a color change (*Vandecasteele and De Deene, 2013*).

Alongside, another type of gel dosimeters was developed: polymerizing gels (*Baldock et al., 2010*), in which radiation induces a chain polymerization converting them into solids. They are usually formed by an aqueous gelatin base, a monomer, a crosslinker, and an antioxidant compound since oxygen inhibits polymerization by scavenging the radicals form after irradiation. They can be grouped according to their monomer into polyacrylamide gelatin (PAG) gels and methacrylic acid gelatin (MAG) gels (*Watanabe et al., 2017*). Other versions have been developed, such as the VIPAR gel, with N-vinylpyrrolidone (NVP) as monomer; and the PABIG gel, with poly(ethylene glycol)

diacrylate (PEGDA, M_w = 700 g/mol). The last one is shown in figure 1.2b after 10 Gy irradiation with a ^{192}Ir brachytherapy source. The opaque region in the middle is due to radiation-induced polymerization (*Sobotka et al., 2012*).

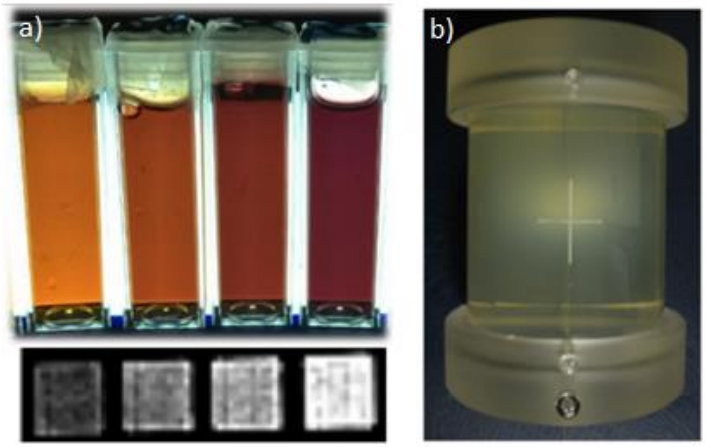

Figure 1.2: a) Radiochromic Fricke gels, based on PVA, with their correspondent MRI maps, irradiated with high-energy X-rays to increasing doses (*d'Errico et al., 2017*). b) Polymerizing PABIG gel, based on PEGDA, showing opaque polymerized region in the middle due to ^{192}Ir brachytherapy source irradiation to 10 Gy (*Sobotka et al., 2012*).

A dosimetry system comprises not only the dosimeter itself, with its correspondent storage conditions and calibration, but also the measurement process (instrument and procedure). The measurement technique for gels was traditionally MRI but due to its high cost it is mostly dedicated to patients, so an alternative read-out based on optical methods started to be used: optical computed tomography (OCT). Therefore, the dose would be obtained by measuring the change in the optical properties of the dosimeters after irradiation. In polymerizing gels, the transparent unirradiated gel becomes opaque when it solidifies due to radiation, and this transparency can be quantified by measuring the scattered light. In radiochromic gels, the color change is quantified by measuring the optical density or absorbance.

Gel dosimeters can present problems such as blurring of images, diffusion of the dose response inside the gel, and the need of a container that adds artifacts into the read-out. These may be solved by using a solid state dosimeter instead. Already in 1961, a solid in-phantom dosimeter with the form of a human head and neck was presented (*Potsaid and Irie, 1961*). This model, shown in figure 1.3, acts as both phantom and dosimeter. The system, containing methyl yellow dye in a paraffin-wax matrix with chloroform and bromoform, is converted from yellow to red when it is irradiated (see dark area in the section of the model in figure 1.3). The color change is proportional to the absorbed dose.

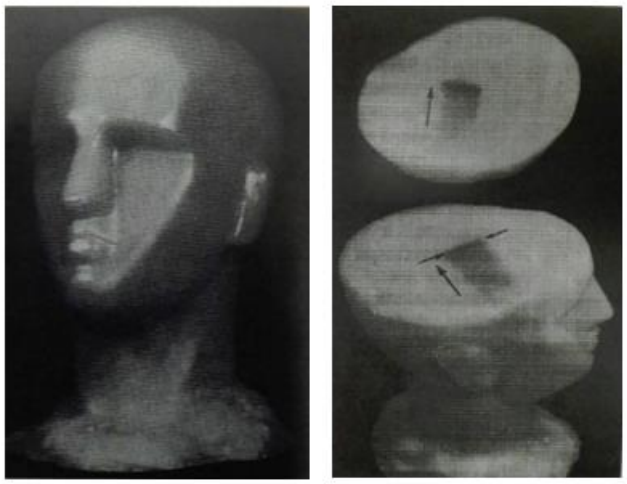

Figure 1.3: In-phantom dosimeter representing head and neck, irradiated with a proton beam (notice the Bragg peak) (*Potsaid and Irie, 1961*).

However, it was not until 2003 that the first commercially available solid state dosimeter, Presage™, was introduced. It can be made in any shape, like the rodent-morphic dosimeter shown in figure 1.4a (*Bache et al., 2015*). Its dose response is due to the color change of the malachite green (MG) leuco dye, contained in a polyurethane matrix. Since then, many studies have been carried out (*Khezerloo et al., 2017*) and new versions have been developed (*Høye et al., 2015*).

Although this dosimeter does not have the limitations of gels, the read-out is very time consuming, which hinders its routine use in the clinic. The solid dosimeter is placed in an aquarium filled with a refractive index matching fluid to avoid refraction at the dosimeter surface. Then, it is scanned in different slices and for different directions in each slice while it rotates. The conventional scanner was the OCTOPUS™, whose scan and image reconstruction required a time of several hours (*Sakhalkar et al., 2009*). New designs have been developed since then, like the in-house DLOS (Duke Large-Field Optical-CT System) (figure 1.4b) (*Thomas et al., 2011*) or the commercially available VISTA™ optical CT scanner (*Modus QA, 2017*), decreasing the overall time to less than 1 hour. However, 3D dosimetry is still not used in the clinic.

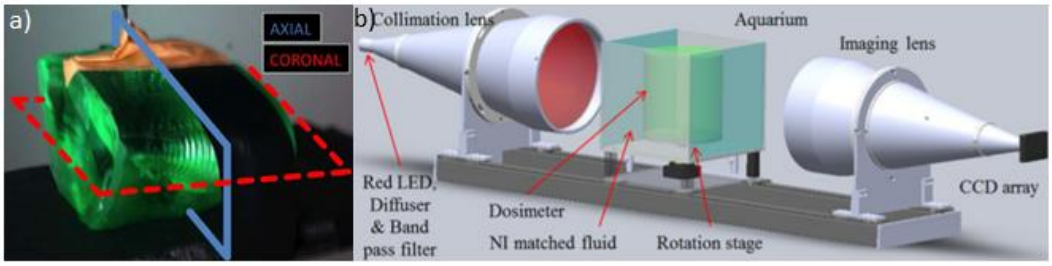

Figure 1.4: a) Rodent-morphic Presage™ made by using 3D printed molds derived from rat CT data (*Bache et al., 2015*). b) DLOS optical CT scanner (*Thomas et al., 2011*).

A simpler, *in-situ*, and faster measurement process with higher spatial resolution is needed to facilitate the use of 3D dosimetry in the clinic. This can be achieved by using optical fluorescence tomography (OFT), which obtains a complete 2D image in one go by using a black and white charged-coupled device (CCD) camera. Besides accelerating the scanning speed, this technique facilitates the detection of small signals and the equipment is simpler. A radiofluorogenic dosimeter gel (RFG) based on maleimido-pyrene (MPy) dye, which becomes fluorescent when co-polymerized with tertiary-butyl acrylate (TBA) by effect of radiation, has been studied so far with this technique for high-energy particle radiotherapy applications (figure 1.5) (*Warman et al., 2013*).

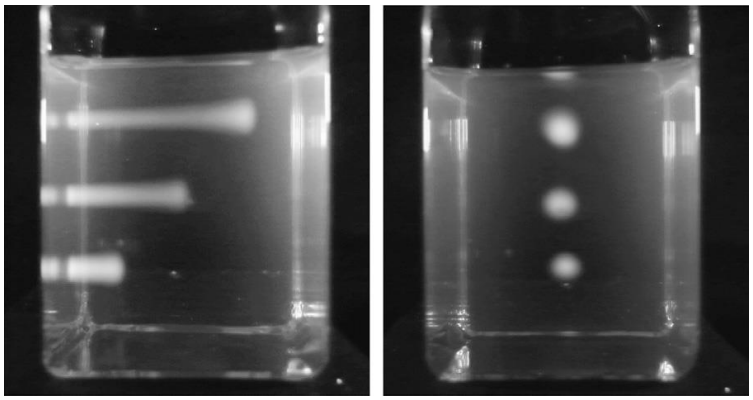

Figure 1.5: Radiofluorogenic gel (40 x 40 mm^2, 50 mm long) exposed to 80 MeV proton beams attenuated by 22, 32 and 42 mm thick polystyrene plates used to slow down and stop the protons at different depths (different Bragg peaks) (*Warman et al., 2013*).

Optical fluorescence tomography is the technique thought for the measurement of the 3D solid state dosimeter presented in this thesis. The equipment is developed in a parallel PhD project (*Sanders, 2017*) and the readout only takes 1.5 min/cm.

1.1.1. Characteristics of a good 3D dosimetry system

In order to design a new and more effective 3D dosimetry system that could be practical for use in the clinic, the following characteristics were regarded as highly desirable:

- Solid state, easy to handle.
- Water equivalent, and therefore tissue equivalent.
- Fast, easy and controllable manufacturing.
- Radiation-induced response linear with dose.
- Stable radiation-induced response.
- Radiation-induced response independent of environmental influence factors, such as temperature, humidity, light, dose rate, and energy.
- Fast, easy and highly spatially-resolved measurement.

1.1.2. The concepts of our 3D dosimeter

The new 3D dosimetry system that we are developing comprises the following characteristics (presented in table 1.1 for other 3D dosimetry systems):

- State: solid.
- Response: radiofluorogenic and radiochromic.
- Measurement: fluorescence of pararosaniline dye.
- Readout: optical fluorescence tomography (OFT).

In this thesis, a dosimeter is developed, which is based on the following concepts:

- A leuco dye capable of forming a stable dye after exposure to ionizing radiation. This dye is fluorescent when embedded in a solid state matrix. It responds to radiation by increasing color intensity (magenta) and fluorescence.
- A light curable hydrophilic polymer capable of facilitating the reaction of the leuco dye. Water equivalent.
- A secondary polymer providing mechanical stability to the first polymer. Preferably also hydrophilic.
- A hydrogen donor compound to abstract the nitrile group leaving from the leuco dye when is transformed to the dye, and thus avoiding reaction reversibility.
- An organic polar solvent with high dielectric constant to promote the reaction.
- A photoinitiator to solidify the matrix by a photocuring process, which allows a better polymerization control and the possibility of 3D printing.

The theory behind these concepts will be explained in the following chapters of the introduction.

1.2. Interaction of radiation with matter

In this chapter, a brief introduction of the processes that occur when radiation interacts with matter is given. First, it is necessary to classify radiation into two categories: ionizing and non-ionizing. Ionizing radiation imparts to materials through which it passes, more than the energy needed to cause a valence electron to escape an atom or molecule, which is of the order of a few eV. It comprises charged particles (usually electrons, protons, alpha particles and heavy ions) and uncharged particles (UV photons, X-rays, and gamma rays; and neutrons). The most frequent range of energies used in radiotherapy is 10 keV – 25 MeV for electrons and photons, up to 100 MeV for neutrons, up to 300 MeV for protons and up to 400 MeV/m_u for heavy ions (m_u is the atomic mass unit). Non-ionizing radiation comprises radiofrequency, microwave, infrared radiation, visible light, and it is insufficiently energetic to ionize matter (*Andreo et al., 2017*).

1.2.1. Ionizing radiation

Ionizing radiation interacts with matter depending on its nature: directly ionizing radiation (charged particles) and indirectly ionizing radiation (uncharged particles). Charged particles interact with nearly every atom along its path, depositing their energy in the medium through direct Coulomb-force interactions with the nearby atoms and losing their energy gradually. These Coulomb-force interactions are characterized in terms of the relative sizes of the impact parameter and the atomic radius into soft and hard collision, and bremsstrahlung radiation (*Andreo et al., 2017*).

Uncharged particles, by contrast, may pass through matter with no interactions at all. They deposit their energy by a two-step process: first they transfer their energy to charged particles, and then these charged particles will deliver their energy to matter as previously mentioned (*Knoll, 2010*). Figure 1.6 shows the interaction of photons (either X-rays or gamma rays) with matter (photoelectric effect, Compton effect and pair production). Figure 1.7 shows the regions in which each photon interaction predominates, depending on the incident photon energy ($h\nu$) and the absorber material atomic number (Z).

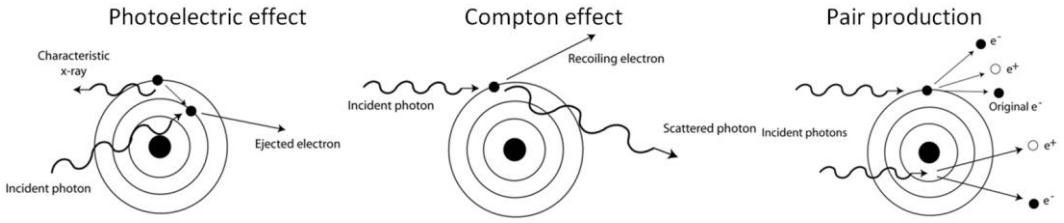

Figure 1.6: Photon interactions (*Beierholm, 2011*).

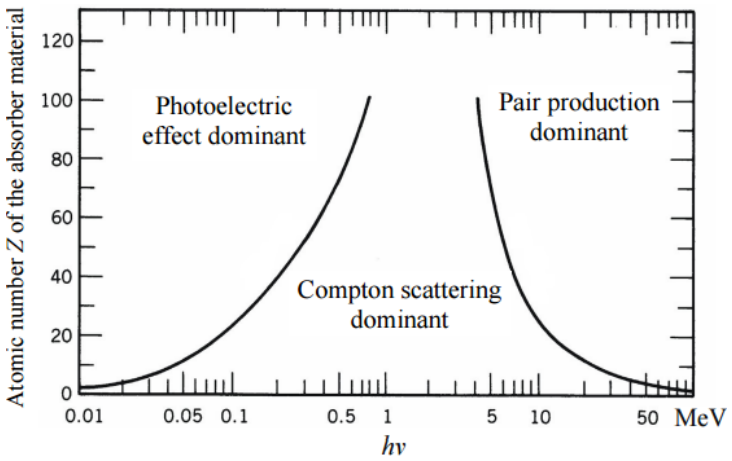

Figure 1.7: Regions of predominance (*Attix, 1986*).

In the case of radiotherapy (X-rays ~0.5 MeV upward, and ^{60}Co 1.17 MeV and 1.33 MeV), the dominant interaction is the Compton effect, which involves the interaction of photons with loosely bound electrons. Photons transfer some of their energy to electrons and the rest is emitted as scattered photons. Then, these electrons transfer

energy to the medium. Therefore, the absorbed dose to a medium is entirely delivered by electrons. These electrons are responsible for most of the biological damage.

Ionization of molecules can lead to radiolysis (breaking chemical bonds) and formation of free radicals (atom, molecule or ion with an unpaired valence electron). These free radicals may then react producing chemical changes in the material. In dosimetry these chemical changes are used to determine the absorbed dose in the material.

1.2.1.1. Absorbed dose in the medium

Some of the most relevant radiation quantities in the interaction of ionizing radiation with matter are the following (*Andreo et al., 2017*):

- Absorbed dose (D) is the mean energy $d\bar{\varepsilon}$ imparted to a mass dm by ionizing radiation. It is expressed by equation 1.1 and its unit is the gray (Gy).

$$D = \frac{d\bar{\varepsilon}}{dm} \quad (1.1)$$

- Fluence (Φ) is the number of particles or photons dN crossing a sphere of cross-sectional area da. The energy fluence (Ψ) is the incident radiant energy on the sphere. They are respectively expressed by equations 1.2 and 1.3. The expressions corresponding to a monoenergetic beam are extended to a beam with a spectrum of energies (expressions with respect to energy, E). For a monoenergetic beam, $\Psi = \Phi E$, where E is the energy of the beam.

$$\Phi = \frac{dN}{da} \rightarrow \Phi_E(E) = \frac{d\Phi}{dE}(E) \quad (1.2)$$

$$\Psi = \frac{dE}{da} \rightarrow \Psi_E(E) = \frac{d\Psi}{dE}(E) = \frac{d\Phi}{dE}(E)E \quad (1.3)$$

- Kinetic energy released per unit mass (Kerma, K) is the mean kinetic energy transferred from uncharged particles to charged particles dE_{tr} in a mass dm. The unit is $J\ kg^{-1}$ and the special name for the unit is the gray (Gy). It is expressed by equation 1.4, where μ_{tr}/ρ is the mass energy transfer coefficient of the material for uncharged particles of energy E. The concept is also extended to a spectrum of energies.

$$K = \frac{dE_{tr}}{dm} = \Psi\frac{\mu_{tr}}{\rho} \rightarrow K = \int \Psi_E(E)\ \frac{\mu_{tr}(E)}{\rho}\ dE \quad (1.4)$$

- Stopping power (S) is the energy lost by charged particles in traversing a distance dx in the medium. It is the rate at which energy is transferred from the charged particles in the medium to the medium itself. Its unit is $MeV\ cm^{-1}$ or $\mathrm{J\ m^{-1}}$. It is expressed by equation 1.5.

$$S = \frac{dE}{dx} \quad (1.5)$$

- Mass attenuation coefficient (μ/ρ) is the fraction of photons interacting in dx in a medium of density ρ. It characterizes how easily a material can be penetrated by a photon beam. Its unit is $\mathrm{cm^2 g^{-1}}$. The mass energy absorption coefficient (μ_{en}/ρ) describes the fraction of photon energy transferred and subsequently resulting in local dose deposition. It is related to μ/ρ by equation 1.6, where $\overline{E}_{ab}$ is the average energy absorbed per interaction and $h\nu$ the photon energy. Equation 1.6 shows the mass energy absorption coefficient averaged over the energy fluence spectrum.

$$\frac{\mu_{en}}{\rho} = \frac{\mu}{\rho}\frac{\overline{E}_{ab}}{h\nu} \rightarrow \frac{\overline{\mu}_{en}}{\rho} = \frac{1}{\Psi}\int_0^{E_{max}} \Psi_E(E)\ \frac{\mu_{en}(E)}{\rho}\ dE \quad (1.6)$$

Since charged particles interact with atomic electrons and nuclei of the medium by soft and hard collisions or by radiative bremsstrahlung, the Kerma and the stopping power can be divided in these two contributions: $K = K_{col} + K_{rad}$ and $S = S_{col} + S_{rad}$ where the subscripts refer to collisional and radiative. Energy from bremsstrahlung is carried away by photons, while energy from the collisional contribution produces ionizations and excitations. This results in locally deposited energy, close to the incident particle track. Two results are derived from that:

Firstly, for a photon spectrum, collisional Kerma is a good approximation for the absorbed dose in the medium if charged particle equilibrium (CPE) exists. That is if each charged particle of a given type and energy leaving the volume is balanced by a particle of the same type and energy entering the volume (secondary electrons are absorbed on the volume). In that way, the dose in the medium (D_{med}) is related to the photon fluence in the medium $(\Phi_E)_{med}$ by equation 1.7.

$$D_{med} = K_{col} = \int_0^{E_{max}} E\ (\Phi_E)_{med} \left(\frac{\mu_{en}(E)}{\rho}\right)_{med} dE \quad (1.7)$$

Secondly, for a charged particles spectrum and if knock-on equilibrium (KOE) exists (always present if CPE exits), the absorbed dose in the medium is related to the electron fluence in the medium by equation 1.8.

$$D_{med} = \int_0^{E_{max}} (\Phi_E)^e_{med} \left(\frac{S_{col}(E)}{\rho}\right)_{med} dE \quad (1.8)$$

1.2.1.2. Cavity theory

To measure the absorbed dose in a medium a dosimeter is needed, which can be seen as a cavity in the medium. According to the size of the dosimeter relative to the range of charged particles (secondary electrons) crossing it, the dosimeter may be considered a small, large or intermediate cavity. Figure 1.8 illustrates the three cavity theories (*Andreo et al., 2017*).

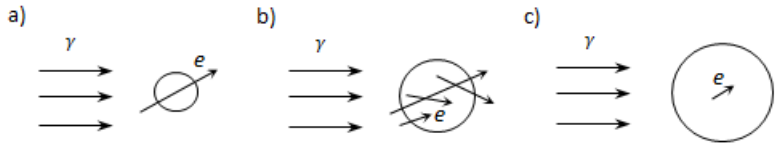

Figure 1.8: Schematic drawings of cavity theory (adapted from *Andreo et al., 2017*): a) small, b) intermediate, c) large.

In the small cavity, the absorbed dose is delivered by secondary electrons that traverse the cavity completely, while in the large cavity it is delivered by secondary electrons starting and stopping within the cavity. In the intermediate cavity, besides the previous two cases, secondary electrons originated in the cavity and stopping in the wall or starting in the wall and terminating in the cavity are also considered.

These theories are expressed by equations that relate the absorbed dose measured in the detector ($\overline{D}_{det}$) with the absorbed dose in the medium (D_{med}).

In the small cavity, the electrons responsible for the absorbed dose are generated outside the detector, so the detector 'senses' electrons whose energy is deposited locally during their path through the cavity. Therefore, the absorbed dose is obtained by using the mass collision stopping power (S_{col}/ρ). In the Bragg-Gray cavity theory (equation 1.9) no secondary electrons generated in the cavity escape it.

$$f(Q) = \frac{D_{med}}{\overline{D}_{det}} = \frac{\int_0^{E_{max}} (\Phi_E)_{med} \left(\frac{S_{col}(E)}{\rho}\right)_{med} dE}{\int_0^{E_{max}} (\Phi_E)_{med} \left(\frac{S_{col}(E)}{\rho}\right)_{det} dE} = s_{med,det}^{BG} \qquad (1.9)$$

The Spencer-Attix cavity theory (equation 1.10) is a more general formulation for the small cavity that uses the restricted mass stopping power (L_Δ/ρ). Electrons with energies below the cutoff energy Δ are locally absorbed, while for larger energies than Δ the electrons have enough kinetic energy to pass through the cavity. Restricted stopping powers are lower than the unrestricted, which include the secondary scattered electrons. This theory was further formulated by Nahum to include track-end terms (TE) that represent local deposition of energy by particles with energies below Δ during their path through the cavity. $s_{med,det}^{BG}$ and $s_{med,det}^{SA}$ are the Bragg-Gray and the Spencer-Attix mass collision stopping power ratios.

$$f(Q) = \frac{D_{med}}{\overline{D}_{det}} = \frac{\int_{\Delta}^{E_{max}} (\Phi_E)_{med}^{tot} \left(\frac{L_\Delta(E)}{\rho}\right)_{med} dE + TE_{med}}{\int_{\Delta}^{E_{max}} (\Phi_E)_{med}^{tot} \left(\frac{L_\Delta(E)}{\rho}\right)_{det} dE + TE_{det}} = s_{med,det}^{SA} \quad (1.10)$$

In the large cavity, the electrons responsible for the absorbed dose are generated inside the detector, so the energy is deposited by the photon-liberated secondary electrons. In that case, the detector reflects internal photon interactions, so the mass energy absorption coefficient (μ_{en}/ρ) is relevant here.

$$f(Q) = \frac{D_{med}}{\overline{D}_{det}} = \frac{\int_0^{E_{max}} E \left(\phi_E^{ph}\right)_{med} \left(\frac{\mu_{en}}{\rho}\right)_{med} dE}{\int_0^{E_{max}} E \left(\phi_E^{ph}\right)_{det} \left(\frac{\mu_{en}}{\rho}\right)_{det} dE} \quad (1.11)$$

In the intermediate cavity, both cases are combined. The parameter d in equation 1.12 approaches 0 for large cavities and 1 for small cavities; $s_{det,med}$ is the stopping power ratio; and $(\mu_{en}/\rho)_{det,med}$ is the mass energy absorption coefficient ratio. The first term of the equation, takes into account the dose due to electrons from the medium, while the second term corresponds to the dose from photon interactions in the cavity. Solid state detectors are considered an intermediate cavity; therefore, this is the theory that is used in chapter 4.7 for the study of the dosimeter presented in this thesis.

$$\frac{1}{f(Q)} = \frac{\overline{D}_{det}}{D_{med}} = d s_{det,med} + (1-d)\left(\frac{\mu_{en}}{\rho}\right)_{det,med} \quad (1.12)$$

1.2.1.3. Water equivalence

One of the characteristics mentioned in chapter 1.1 for a good 3D dosimeter was water equivalence. This is because radiation is absorbed in a different way depending on the density of the medium, as it can be seen in figure 1.9 for different mediums in the body. The attenuation coefficient (μ) represents how easily a material can be penetrated by a beam of energy E. This difference allows distinguishing bones in radiology due to their strong attenuation. In the radiotherapy range (X-rays ~0.5 MeV upward, and ^{60}Co 1.17 MeV and 1.33 MeV), the attenuation coefficients are not so different, avoiding selective absorption and facilitating deeper penetration of ionizing radiation in the body.

The main application of our dosimeter is to experimentally map the 3D dose distribution of a radiotherapy session as an estimation of the dose distribution in the patient. Since organs and human tissue are mainly composed of water (most organs and tissues contain more than 70% water), the dosimeter material should have characteristics as close to water as possible.

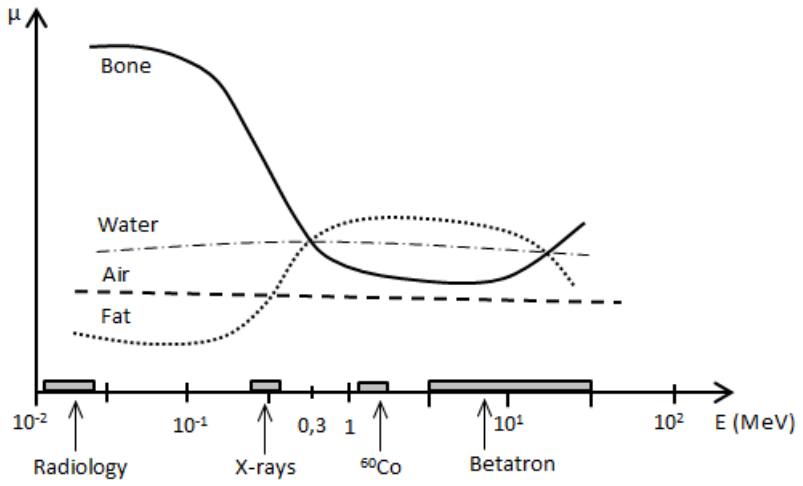

Figure 1.9: Absorption coefficient of tissue compounds of different densities (bone, water, air and fat) as function of the energy (adapted from *Zaragoza, 1992*).

Water equivalence is a desirable characteristic of any dosimeter, also 1D and 2D, since the current protocols used in radiotherapy departments, such as the International Atomic Energy Agency (IAEA) TRS-398 (*IAEA, 2000*) or the American Association of Physicists in Medicine (AAPM) TG-51 (*AAPM, 1999*) are based on reporting the absorbed dose to water, and the QA measurements are usually performed in water tanks. If a dosimeter is water equivalent, its perturbation in the water tank is minimized.

Three parameters are often used to quantify the water equivalence of a dosimeter material: mass density (ρ), electronic density (ρ_{el}) and effective atomic number (Z_{eff}). The electronic density is expressed by equation 1.13, where N_A (= $6.022 \cdot 10^{23}$ mol^{-1}) is Avogadro´s number, ρ_m is the mass density, and N_i, Z_i and A_i are respectively the number of atoms, the atomic number and the mass number of atoms of specie i.

$$\rho_{el} = N_A \rho_m \frac{\sum N_i Z_i}{\sum N_i A_i} \quad (1.13)$$

Z_{eff} can be calculated by equation 1.14 (*Johns and Cunningham, 1983*), where a is the element-specific ratio of the number of electrons to the total electronic number, Z is the atomic number of each element, and m is an energy-dependent number. The exponent m is usually 3.5 for the kilovoltage (kV) range used in diagnostic radiology, and 1 for the megavoltage (MV) range used in radiotherapy.

$$Z_{eff} = \sqrt[m]{a_1 Z_1^m + a_2 Z_2^m + \cdots} \quad (1.14)$$

However, since the dominant interaction in radiotherapy is the Compton effect as seen previously, and for low Z_{eff} materials (such as carbon, air, water and tissue) this region is very broad (see figure 1.7), the cross section for Compton effect varies only slowly with Z. Therefore, it is preferable to compare other parameters, like the mass attenuation coefficients and the stopping powers. They are directly related to the

absorbed dose in the medium, as seen in equations 1.7 and 1.8. The water equivalence of the dosimeter presented in this thesis is discussed in detail in chapter 4.7.

1.2.2. Non-ionizing radiation

The way light interacts with the dosimeter is important for this thesis since the dosimeter is cured by UV light and measured by obtaining its absorbance and fluorescence spectra.

Light interacts with matter in many different ways that can be classified into (figure 1.10): reflection, refraction, absorption, luminescence, scattering and transmission. First, light may be reflected on the surface of the solid (also on the back surface once it is inside the solid). When light enters into the medium, the medium´s refractive index may be different, so light´s velocity changes (refraction), which produces bending of the beam at the interface without changing intensity. During propagation, light may be attenuated if light frequency and transition frequencies of the atoms in the medium are resonant (absorption). Spontaneous emission of light from excited atoms, in all directions and with a different frequency, may also be possible (luminescence). Light can also interact with the medium by redirecting the beam, either with or without a change in frequency (inelastic or elastic scattering respectively). Finally, light that was not attenuated along the pathway is transmitted (*Fox, 2007*).

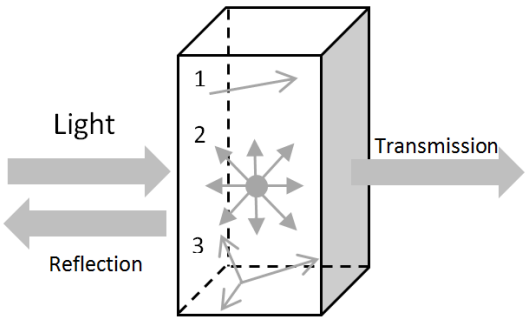

Figure 1.10: Processes that occur when light interacts with matter (adapted from *Fox, 2007*).

Focusing on a molecular level, when a molecule AB absorbs a photon, it is excited to a higher electronic state AB*. The primary processes in which the excited species loses its excess energy are presented in figure 1.11 (*Wayne and Wayne, 2005*). Absorption of light can therefore promote a chemical change (routes i to iii), but also the unstable excited molecule may be deactivated by physical processes where the excess energy is not used for a chemical change (routes iv to viii). The photophysical processes are the following:

- Intra- and inter- molecular energy transfer: excitation energy populates a new energetic level in the same or in a different molecule respectively.
- Luminescence: emission of light. It is classified into fluorescence or phosphorescence depending on the nature of the excited state (singlet and triplet respectively). If the species AB* was originated from a chemical reaction instead of absorption of light, then the emission is called chemiluminescence.
- Quenching: loss of energy by collision with another molecule M. It competes with emission, reducing the fluorescence or phosphorescence intensity. Quenching is very important in the liquid phase, where collisions are very frequent. In the solid state, collisions may be hindered by the rigidity of the structure.

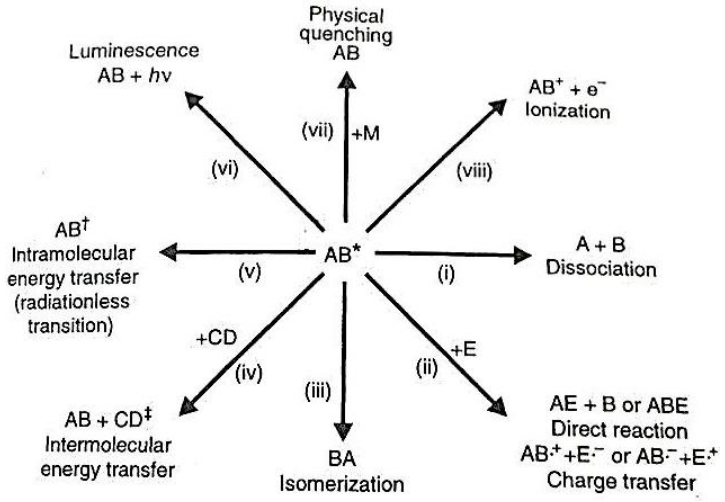

Figure 1.11: Routes of loss of electronic excitation (*Wayne and Wayne, 2005*).

The most common measurement method used in 3D dosimetry is optical CT, which consists on measuring the absorbed light. The absorbed intensity follows Beer-Lambert law (equation 1.15), where I_0 is the intensity of the incident light, I is the intensity of the transmitted light, ε is the molar extinction coefficient ($cm^{-1}mol^{-1}$), c the concentration of absorbing species and d is the optical path length. The absorbance or optical density is defined as $A = -\log(I/I_0)$, therefore $A = \varepsilon cd$ (*Drobny, 2010*).

$$I = I_0 10^{-\varepsilon cd} \quad (1.15)$$

However, fluorescence is much more sensitive than absorbance (*Lakowicz, 2006*), and that is the reason for developing a radiofluorogenic dosimeter.

1.2.2.1. Fluorescence

Particular emphasis has thus far been put on those dosimeters that change their optical properties as function of the absorbed dose. Optical CT is used to reconstruct the pattern of delivered doses by measuring the transmitted light intensity in different directions and for different sections. The transmitted light intensity is corrected to

obtain the absorption, which contains information about the absorbed dose. For solid 3D dosimetry, the scanning process is as follows: for a particular section of the dosimeter the transmitted light is measured for one direction, then the solid is rotated and the transmitted light is measured for a different direction; this process is repeated for different sections. Besides the time consuming scanning process, the use of complex algorithms like the inverse Radon transform (*Radon, 1917*), used to reconstruct the image given the projection data, makes the process very long. A way to increase the scanning speed is by using scanners based on charged-couple device (CCD) or scientific complementary metal-oxide-semiconductor (sCMOS) cameras that measure the fluorescence and allow obtaining a complete 2D image in one go. In that way it is not necessary to scan different directions for each section. Measuring fluorescence could also provide higher sensitivity and spatial resolution, which is crucial for 3D dosimetry.

In figure 1.12 (*Lakowicz, 2006*) the Jablonski diagram illustrates the electronic states of a molecule. The states are grouped by spin multiplicity, singlet (S) and triplet (T), and arranged by increasing energy (S_0, S_1, S_2). At each energy level, vibrational levels may exist (depicted by 0, 1, 2 in S_0). When a molecule absorbs a photon of energy $h\nu_A$ it is excited to a higher state ($S_0 + h\nu_A \rightarrow S_1$). From there, non-radiative transitions may happen such as internal conversion ($S_1 \rightarrow S_0 + heat$) and intersystem crossing ($S_1 \rightarrow T_1$). These processes compete with the luminescent processes of fluorescence ($S_1 \rightarrow S_0 + h\nu_F$) and phosphorescence ($T_1 \rightarrow S_0 + h\nu_P$) . The lifetime of fluorescence is extraordinarily short, typically near 10 ns, while the lifetime of phosphorescence is milliseconds to seconds. After the excitation light ceases, phosphorescence continues for up to a few seconds, while fluorescence not.

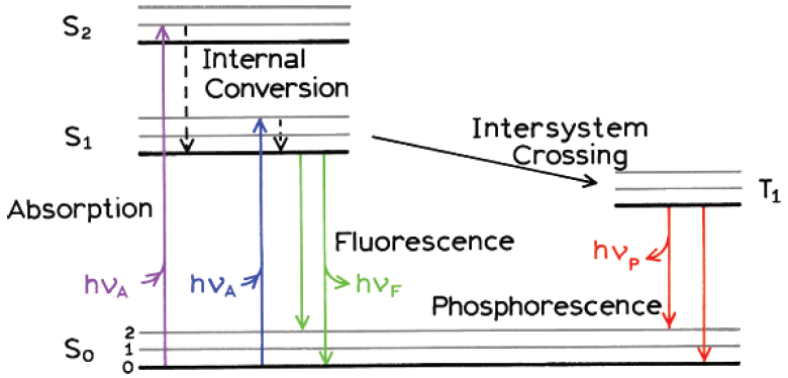

Figure 1.12: Jablonski diagram (*Lakowicz, 2006*).

Fluorescence, therefore, occurs when an excited molecule that has absorbed photons emits light while returning to its ground state. Usually the molecule is excited to a high vibrational level of S_1. From there, it decays quickly (10^{-12} s) by internal conversion to the lowest vibrational level of S_1. Fluorescence emission starts generally from that level, and decays typically to a high vibrational level of S_0, which again quickly decays by internal conversion to its lowest vibrational level . Some characteristics of fluorescence emission derived from this are discussed below (*Lakowicz, 2006*).

Stokes shift

Fluorescence typically occurs at lower energies (longer wavelengths) than absorption. The difference between absorption and emission energy is the Stokes shift (figure 1.13), and the ratio of emitted to absorbed photons is the quantum yield. This is usually due to the energy loss by internal conversion, from a high vibrational level to the lowest vibrational level of both S_1 and S_0. In that way, fluorescence is emission from the $S_1 \rightarrow S_0$ transition. Environmental factors may also contribute to this loss, such as quenching, pH, and solvent polarity.

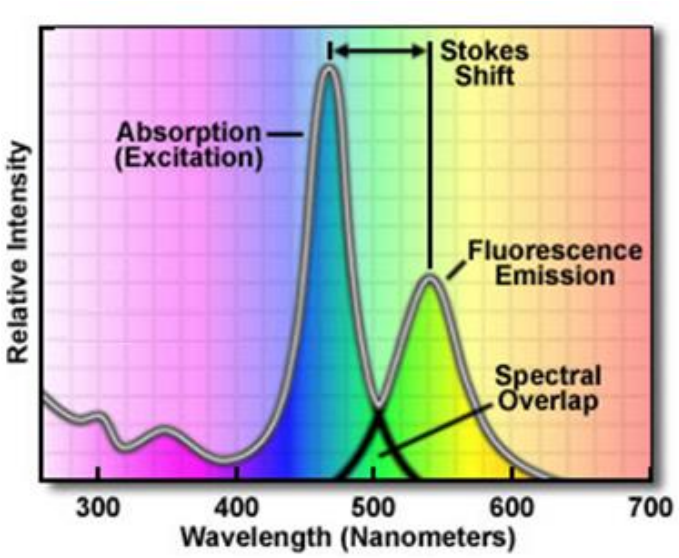

Figure 1.13: Excitation and emission spectra showing the Stokes shift (*Abramowitz and Davidson, 2017*).

Mirror image

Generally, the fluorescence spectrum $(S_1 \rightarrow S_0)$ is the mirror image of the $(S_0 \rightarrow S_1)$ absorption, since they involve the same transition. It may be the mirror image of the total absorption spectrum or not, depending whether there are transitions involving vibrational energy levels and if their spacing is similar in both levels, S_1 and S_0, or not. For example, the shoulder that appears in the absorption spectrum in figure 1.13 may be due to excitation to the second excited state S_2, which relaxes rapidly to S_1 and therefore emission from S_2 is not observed. Exceptions to this mirror-image rule occur also due to environmental factors, like changes in the pH or quenching by the formation of charge-transfer complexes with other molecules or with themselves (excimers).

Independence on excitation wavelength

Another consequence of the quick dissipation of the excess energy upon excitation, leaving the fluorophore in the lowest vibrational level of S_1, is that the fluorescence emission spectrum is generally independent of the excitation wavelength (Kasha's rule) (*Turro, 1978*). Exceptions to this rule are molecules that exist in two ionization states and therefore present different absorption and emission spectra, and molecules that emit from S_2.

Exceptions to these rules are due to the environment of the molecules that emit fluorescence. These environmental factors that decrease the fluorescence intensity will be discussed in chapter 1.4.

1.3. Polymers

Polymers are organic compounds of high molecular weight formed by small molecules, monomers, linked together. As we saw in chapter 1.1, one of the characteristics of a good 3D dosimeter is being solid. The hardening of a polymer is called curing. This term includes polymerization (link of monomers) and cross-linking (link of polymer chains) (*Drobny, 2010*).

Conventionally, polymers are cured by applying heat (and pressure to prevent bubble formation). For instance, the solid dosimeter Presage™, whose main component is polyurethane, is cured at temperatures below 80 °C, usually at room temperature, at a pressure of 60 psi for 6-48 h. Other polymers were also tested as dosimeter matrices (*Adamovics and Maryanski, 2006*) but showed some problems: acrylates, polyesters, polystyrenes and polycarbonates produce high heat (> 100 °C) during curing, causing the color change of the leuco dye; polyvinylchlorides are not water equivalent ($Z_{eff} = 14.2$); and epoxies are low radiation sensitive.

The long curing times required for Presage™ of several days for big samples (*Bache et al., 2015*) and the lack of control of the curing process leads to consideration of another way to obtain a solid polymer matrix. UV light curing is widely used in industry, for example in tissue engineering for the fabrication of polymeric scaffolds from hydrogels (*van Blitterswijk et al., 2008*). Electron beam curing is also highly used in industrial applications, like curing of coatings and adhesives, but with this method the radiochromic leuco dye would be exposed to ionizing radiation, causing its color change.

By UV light it is possible to obtain time- and space- controlled curing. This is the method used in this thesis. In this chapter, the photocuring of polymers is explained, and also some important characteristics of the polymer matrix for its application as a dosimeter, such as its glass transition temperature and its dielectric constant.

1.3.1. Photocuring of polymers

Polymers may degrade and change their properties when exposed to UV radiation from sunshine. However, artificial UV radiation is used to convert a liquid into a solid almost instantaneously. This process of hardening a monomeric, oligomeric, or polymeric substrate using UV light is called UV curing or photocuring (*Roffey, 1997*).

UV lamps

UV light comprises a range of the electromagnetic spectrum from 10 nm to 400 nm and it can be generated by different types of lamps: mercury lamps, electrodeless lamps, excimer lamps, xenon lamps, continuous wave and pulse lasers, and light-emitting diodes (LEDs).

The three lamps used in this thesis are LED because of the significant advantages of semiconductor technology. Conventional old-fashioned UV lamps require warming up to reach operative conditions. LED lamps do not need a warm-up time, light comes on instantly when turned on, the light output remains constant over time and they are highly efficient. LEDs are solid-state light sources that emit a narrow quasi-monochromatic spectrum at a specific wavelength. Therefore, LED UV curing allows using a particular wavelength for curing that does not stimulate the leuco dye. Also, it is possible to select a LED lamp whose emission spectrum overlap with the absorption band of the photoinitiator, a compound required for the fast transformation from liquid to solid (*Drobny, 2010*).

Photoinitiators

A photoinitiator is a molecule that absorbs photons from the UV source by its chromophoric site in a single event, and generates reactive species (radicals or ions) that will initiate polymerization or cross-linking. Photoinitiators are classified depending on the type of reactive species generated (*Green, 2010*):

- Free radical photoinitiators (type I and type II)
- Cationic photoinitiators

The photoinitiators used in this project are free radical photoinitiators, since cationic photoinitiators require the use of shortwave UV, which would expose the radiochromic dye accidently. Cationic photoinitiators (commonly iodonium and sulfonium salts) release an acid catalyst upon UV exposure. The release of this acid catalyst would also trigger the radiochromic process unintentionally. Consequently, cationic photoinitiators are not used in this project.

Free radicals initiate the UV curing of acrylates and methacrylates, which are the polymers used in this thesis; and therefore, free radical photoinitiators are used. When a free radical photoinitiator absorbs a photon, it is excited to a singlet state. Radicals are formed via a triplet state by two possible reactions, Norrish type I and type II.

Type I photoinitiators undergo a unimolecular reaction, hence the suffix I. When the chromophore (usually an aromatic carbonyl) absorbs radiation, it produces the bond cleavage or homolytic decomposition (chemical bond dissociation where each of the fragments retains one of the originally bonded electrons) of the carbonyl group and the adjacent carbon, and generates two radicals capable of initiating polymerization.

Examples of type I photoinitiators are benzoin ether derivatives, benzyl ketals, hydroxyl-alkylphenones, α-aminoketones, and acylphosphine oxides.

Type II photoinitiators undergo a bimolecular reaction where the excited state of the photoinitiator interacts with a second molecule (co-initiator). Aromatic ketones (benzophenone, substituted benzophenone, benzyl fluorenone, camphorquinone, xanthone, and thioxantone) are used with tertiary amines as co-initiators. Triplet states of ketones possessing an α-hydrogen react with hydrogen-donating compounds by hydrogen abstraction. The resulting radical pair is generated by a homolytic cleavage of the R-H bond or by an intermediate charge transfer complex followed by proton transfer.

The main problem of free radical photoinitiators is that radicals are formed in the triplet state, which is the most stable state of molecular oxygen, O_2. Molecules of triplet oxygen contain two unpaired electrons (oxygen is paramagnetic) and this electronic configuration prevents its reaction with molecules that are in the singlet state; however, it readily reacts with radicals. Oxygen, therefore, decreases the efficiency of free radical photocuring by quenching the triplet states and by reacting with radicals before they initiate polymerization. Radicals can also decay back to the original state with emission of light or heat, but if they are capable of initiate polymerization, the following steps occur:

1. Initiation: $AB^* \rightarrow \bullet R_1 + \bullet R_2$ and $\bullet R_1 + \bullet R_2 + M \rightarrow \bullet P_1$
2. Propagation: $\bullet P_n + M \rightarrow \bullet P_{n+1}$
3. Termination $\bullet P_n + \bullet P_m \rightarrow P_n - P_m$ or $\rightarrow {P'}_n - P_m$ (chain transfer)

First, the excited photoinitiator molecule (AB^*) produces two free radicals in the triplet state $(\bullet R_1, \bullet R_2)$, who react with the monomer (M) to produce the first polymer chain (P_1). Then, the monomer is consumed during the chain propagation, and finally the chain terminates by combination or disproportionation of polymer radicals.

Free radicals initiate polymerization and also cross-linking of the polymer chains. Only relatively few cross-links per chain are needed, since too many would produce a brittle powder under internal stress. The photo-cross-linkability of a polymer depends on its chemical structure, molecular weight and ordering of the polymer segments. Photo-cross-linking and photodegradation are competing processes, so it is important to select a polymer that does not degrade with UV light (neither with ionizing radiation for its application as a dosimeter). The components used for the dosimeter matrix will be explained in chapter 3. Figure 1.14 shows the general UV curing mechanism.

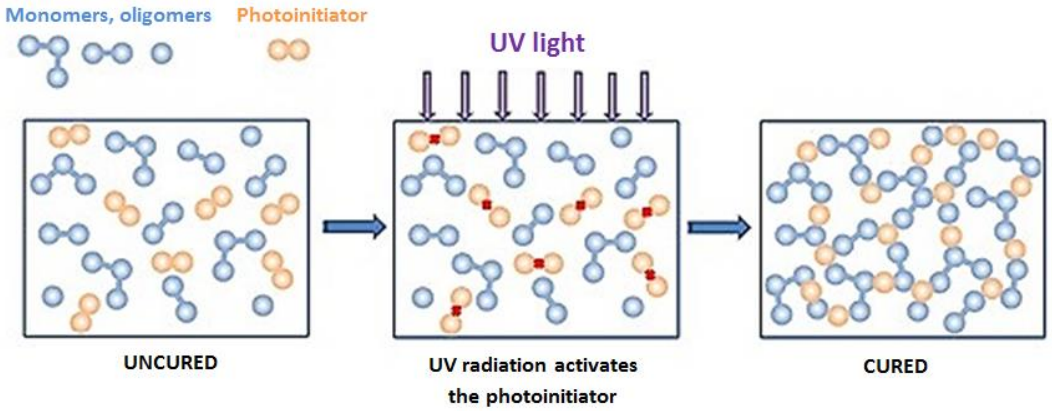

Figure 1.14: UV curing mechanism. The mixture of monomers and oligomers is cured thanks to the activation of the photoinitiator by UV light (*Gotro, 2016*).

To conclude, UV LED curing for the fabrication of the 3D dosimeter improves productivity by accelerating the process from days to minutes. The equipment, consisting of a LED lamp, is simple, small, and easy to operate. The process is environmentally friendly, reducing volatile organic compound (VOC) emissions and eliminating the use of flammable and polluting solvents. The photocuring of the polymer matrices studied in this thesis require the use of a free radical photoinitiator. Several photoinitiators, of both types I and II, are analyzed in chapter 4.2.4, and a study of the photocuring parameters is presented in chapter 4.4.

1.3.2. Glass transition and mechanical properties

Polymer 3D networks consist of polymer chains linked together in all directions generally by covalent bonds. The structure of these networks may present amorphous and crystalline regions (figure 1.15a). The degree of order or crystallinity affects the mechanical properties of the polymer, being harder, stiffer, and less ductile for a higher crystallinity. The dye used in this thesis needs a rigid environment in order to fluoresce. The physical constraint associated with space limitation restricts the intramolecular rotations and vibrations of the dye molecule and, therefore, it blocks the radiationless pathway and opens the radiative decay channel, allowing fluorescence (*Mei et. al, 2014*). This is schematically illustrated in figure 1.5b, where the dye fluoresces when it is constrained by the polymer chains. Therefore, a rigid polymer matrix would allow more dye molecules to fluoresce.

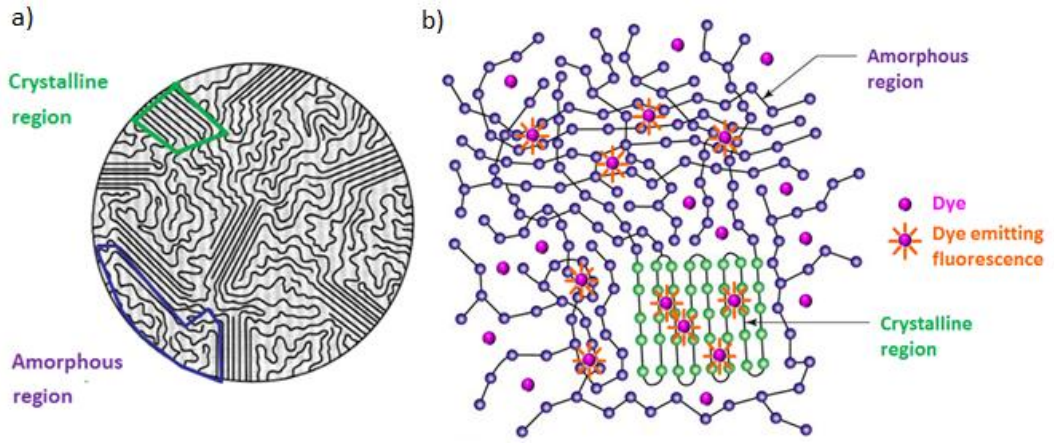

Figure 1.15: a) Crystalline and amorphous regions in a polymer (*Noels, 2015*). b) Schematic drawing to show that dye molecules need to be constrained in order to emit fluorescence (adapted from *Gotro, 2017*).

The glass transition is a reversible transition from a hard glassy state into a viscous rubbery state, characterized by the glass transition temperature (T_g). At temperatures above T_g the polymer material is soft and flexible, while below T_g it behaves as a hard solid, although in both cases is structurally amorphous.

Regarding the mechanical properties, when a stress is applied, the rubbery state is easily deformable and capable of withstanding more strain before failure than the glassy state, which is brittle and can lead to a fracture surface.

The T_g of the material can be modified by changing structural factors. T_g increases when increasing chain rigidity, for example by introducing stiff chemical groups as benzene rings that obstructs bond rotation. Also by steric hindrance, for instance methyl groups in some positions restrict rotation, or by increasing the size of the side group without increasing flexibility. An increase in polarity increases T_g since strong bonding restricts rotation about the backbone and atomic movements; on the contrary, an increase in symmetry lowers T_g since free-volume allows chain rotation.

In the case of a copolymer, its T_g can be calculated by equation 1.16, where V_1, V_2 and T_{g1}, T_{g2} are the volume fractions and glass transition temperatures (in Kelvin) of both polymers (*Walton and Lorimer, 2005*).

$$T_g = V_1 T_{g1} + V_2 T_{g2} \quad (1.16)$$

To conclude, the relevance of T_g with respect to the dosimeter response is to ensure that the dye has a rigid environment, which is necessary for fluorescence emission. The mechanical properties of the dosimeter polymer matrix can be modified by changing the T_g and this can be done by adding a secondary polymer to the main polymer of the matrix. It is important to design the proper polymer matrix for the dosimeter that allow the dye to fluoresce. The polymers used in this thesis are discussed in chapter 3.

1.4. Triphenylmethane dyes

Triphenylmethane dyes are synthetic organic compounds based on the triphenylmethane structure (figure 1.16) that have been used since the late 19th century in textiles and medicine. They present an intense color and good stability (*Morrison and Boyd, 1973*). They are mainly used today for dyeing of textiles, inks for printers, staining and dyeing of histological samples, pH-indicators, and saturable absorbers for mode-locking of lasers. Its application as dosimeters was first introduced by Weyde and Frankenburger in 1931 for UV radiation, and in 1965 by McLaughlin and Chalkley for ionizing radiation (*McLaughlin et.al, 2011*).

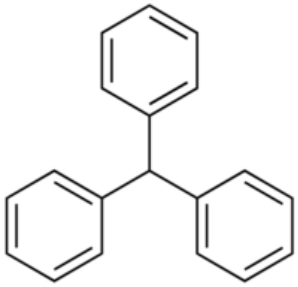

Figure 1.16: Chemical structure of triphenylmethane, basis of the skeleton of triphenylmethane dyes.

Currently, there are two commercially available dosimetry systems based on triphenylmethane dyes: the Risø B3 radiochromic film that uses pararosaniline, and Presage™ that uses malachite green. These dyes are radiochromic, so they are transformed from its colorless leuco form into a color form (magenta and green respectively) by effect of ionizing radiation (figure 1.17). Ionizing radiation breaks the bond of the central carbon with the nitrile group[1] $(-C \equiv N)$ in pararosaniline leuco dye and with the hydrogen atom in malachite leuco dye, and a double bond is formed, which produces a deeply colored dye. This phenomenon is utilized for dosimetry, since the absorbed dose can be determined by measuring the color change either spectrophotometrically or by a scanner (RisøScan) (*Helt-Hansen and Miller, 2004*).

[1] "Nitrile" is the term used in organic chemistry, while "cyanide" is used in inorganic chemistry.

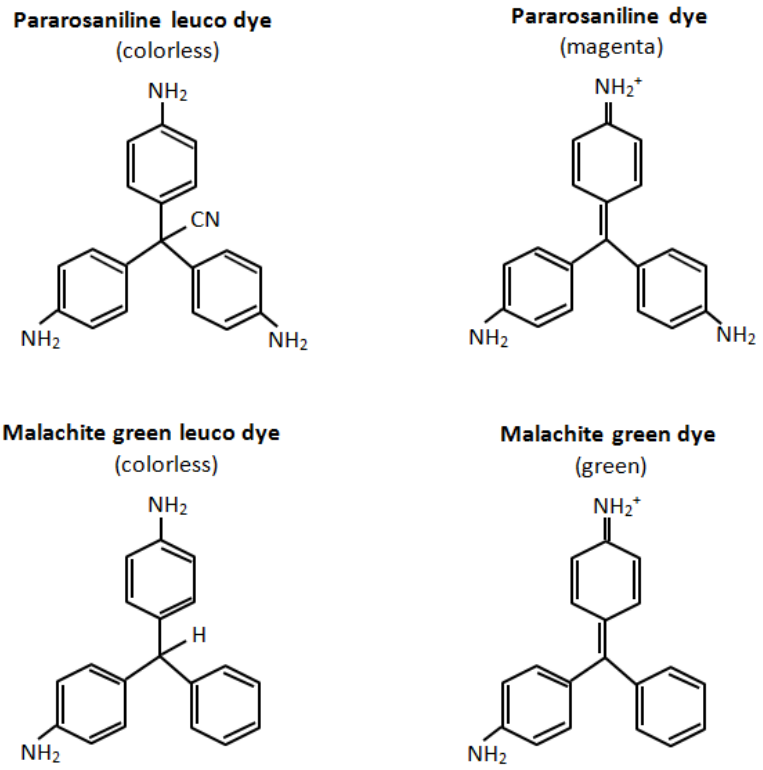

Figure 1.17: Chemical structure of pararosaniline and malachite green in their leuco dye and dye forms.

1.4.1. Optical properties of triphenylmethane dyes

Organic compounds can be classified according to the type of bonding of the valence electrons into saturated or conjugated. In saturated compounds, the valence electrons are tightly held in localized σ bonds and therefore they only respond (electronic transitions) at high UV frequencies. They also absorb in the IR due to vibrational transitions, but they are transparent in the visible region. Some examples of saturated compounds are the polymers cyclic olefin co-polymer, polypropylene and polyethylene. Conjugated compounds, on the contrary, alternate single and double bonds in their structure and the electrons from the *p*-like atomic states of the carbon atoms form large delocalized π orbitals. The two main examples are conjugated polymers and aromatic hydrocarbons. Optical properties of conjugated molecules are particularly interesting because electronic transitions of π electrons occur usually in the visible region of the electromagnetic spectrum, where they present a strong absorption band (*Fox, 2007*).

The main component of triphenylmethane dyes is benzene (C_6H_6), which is an aromatic hydrocarbon, and therefore contains conjugated double bonds. Benzene is traditionally drawn as a hexagon with alternating single and double carbon bonds (figure 1.18a), although in reality the electronic cloud spreads out across the whole molecule. In benzene, the 4 valence electrons of each carbon atom ($1s^2 2s^2 2p^2$) are arranged into three sp^2 hybridized orbitals and one p_z orbital. Three σ bonds at 120° with the

hydrogen and the two adjacent carbon atoms result from the electrons in the sp^2 orbitals, while the remaining electron in the p_z forms a π orbital perpendicular to the bond axis (figure 1.18b). Due to the planar structure of benzene, π orbitals are close enough to overlap above and below the plane (figure 1.18c), resulting in large delocalized π orbitals (figure 1.18d) (*Fox, 2007*).

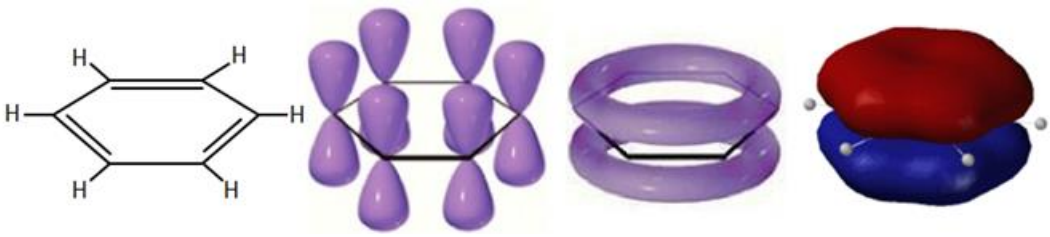

Figure 1.18: Representations of benzene. a) Traditional representation with alternating single and double bonds. b) π orbitals of the carbon atoms. c) Delocalized π orbitals (*Kshitij, 2015*). d) Electron density. Bonding (red) and antibonding (blue) orbitals (*Iverson Lab, 2016*).

This electronic spreading in the molecule due to delocalized π orbitals reduces the energy difference between the bonding and antibonding orbitals (in figure 1.18d, red and blue orbitals respectively), which corresponds to the energy needed to carry out an electronic transition (excitation energy). This is a $\pi \rightarrow \pi^*$ transition from the HOMO (highest occupied molecular orbital) to the LUMO (lowest unoccupied molecular orbital), which occurs at a lower energy than the $\sigma \rightarrow \sigma^*$ transition because electrons in σ bonds are more tightly bound to the nucleus and more energy is required to break these bonds. That is the reason why conjugated compounds have an optical absorption spectrum at lower frequencies than saturated compounds. Benzene absorbs at 260 nm, in the UV region (*Fox, 2007*).

As it was discussed in chapter 1.2.2, when a molecule absorbs a photon, it is excited to a higher electronic state and the excess of energy can be released by several mechanisms. The mechanism that interests us for our dosimeter is fluorescence, but phenolphthalein (a triphenylmethane dye used as pH indicator) is a well-known example of a non-fluorescent molecule. However, the introduction of an oxygen bridge confers stiffness to its structure as observed in fluorescein, which is known for its fluorescence. The difference is caused by the mobility of the benzene groups that can rotate around the central carbon atom in the case of triphenylmethane dyes while they are rigid in fluorescein (figure 1.19). Rigidity favors fluorescence since it suppresses the energy release by other ways such as vibrations and rotations (*Schäfer, 1972*).

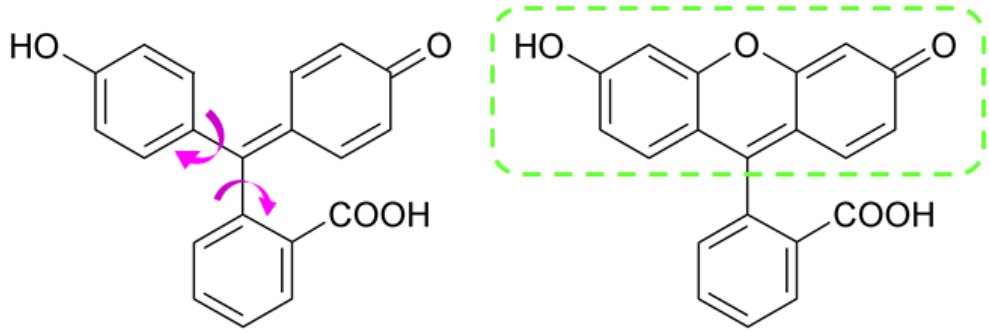

Figure 1.19: Phenolphthalein (left) and fluorescein (right) dye molecules, showing mobility vs. stiffness. Fluorescein is fluorescent in solution while phenolphthalein is not.

The dosimeter presented in this thesis is based on pararosaniline, which is non-fluorescent in solution. However, this dye shows fluorescence when it is inside a solid state matrix, as it will be shown along chapter 4. The solid matrix is essential to provide rigidity to the dye molecule and allow fluorescence emission. Some challenges related to how the matrix affects the dye fluorescence will be discussed below.

1.4.2. Influence of environmental factors on fluorescence emission

As it was discussed in chapter 1.2.2.1 about fluorescence measurements, fluorescence is the result of a three-step process: excitation of a molecule due to absorption of a photon, vibrational relaxation to the lowest energy level of S_1, fluoresce emission of a longer wavelength photon, and return of the molecule to the ground state S_0. It is desirable that the dye molecules remain in the S_1 level until they are called for fluorescence emission. However, there are many non-radiative processes that compete and reduce fluorescence efficiency. These processes may be due to a direct relaxation to the ground state ($S_1 \rightarrow S_0$) (internal conversion) or to the intersystem crossing to the triple state ($S_1 \rightarrow T_1$), and related not only to the dye molecule but also to surrounding molecules (*Schäfer, 1972*). In this section, some important effects on the fluorescence emission from the dye due to its environment are discussed: photobleaching, quenching, dimer formation and solvent polarity.

Photobleaching

Photobleaching (or fading) is relevant for the read-out and it occurs when the fluorophore permanently loses the ability to fluoresce. This happens when the fluorophore molecule is in the triplet state. Since the triplet lifetime is very long with respect to the singlet, it allows the dye molecules to react with surrounding molecules that can produce irreversible covalent modifications and being photochemically altered (*Herman et. al, 2017*). This effect is accentuated if the dye is embedded in a solid matrix because the triplet lifetime is very long (in some cases up to several seconds) (*Schäfer, 1972*). It is possible to reduce photobleaching by decreasing the exposure time or by lowering the excitation energy, although these methods also reduce the measurable fluorescence signal (*Herman et. al, 2017*).

Quenching

Quenching is another process contributing to fluorescence decrease or elimination and, contrary to photobleaching, often reversible. It comprises a variety of processes that induce non-radiative relaxation of excited state electrons to the ground state, which may be either intramolecular or intermolecular in nature. A common mechanism of quenching is collisional quenching, in which the excited fluorophore is deactivated by collision with a non-fluorescent molecule. It is very common in solution, and in most cases the molecules are not chemically altered. Quenching can also occur as a result of a complex formation between the fluorophore and the quencher that returns immediately to the ground state without emission. This non-fluorescent complex is reversible and does not rely on molecular collisions (*Herman et. al, 2017*).

One of the best-known quenchers is molecular oxygen, whose stable state is the triplet, and who quenches almost all known fluorophores by a combination of different mechanisms. An encounter with molecular oxygen mainly causes the excited singlet state S_1 of the fluorophore to become an excited triplet T_1 and from there, the fluorophore returns to the ground state by non-radiative decay (*Lakowicz, 2006*). Another quenching mechanism is the energy transfer, which happens if the quencher has a state (singlet or triplet) of energy equal or lower than that of the state to be quenched. In the case of molecular oxygen, it has low-lying excited singlet states.

A different mechanism of quenching is due to anions, such as iodine (I^-), bromide (Br^-) or chloride (Cl^-). This is known as the heavy atom effect. In some cases, the π electrons of the dye make a loop when oscillating between the end groups, creating an orbital magnetic moment that can couple with the spin of the electron; this is the spin-orbit coupling effect. The triplet yield is higher than in a case where this loop is blocked. Heavy atoms increase the spin-orbit coupling, enhancing the rate of intersystem crossing. This effect occurs independently if the heavy atoms are in the dye structure itself or in the surrounding molecules (*Schäfer, 1972*).

Dimer formation

Organic dyes have a tendency to form dimers (combination of two dye molecules in their ground state) when they are in an aqueous solution. Dimers present an absorption band at shorter wavelengths than the monomers and they are weakly fluorescent or non-fluorescent. Dimerization increases with increasing dye concentration and decreasing temperature. This effect does not occur if organic solvents, like ethanol, are used instead of water. However, in organic solvents and with high dye concentrations, there is usually a strong interaction between dye molecules in the ground state and dye molecules in the excited state, resulting also in non-fluorescent dimers. Therefore, dimers decrease fluorescence emission. But, if these dimers exist only in the excited state (excimers) or if an excited complex (exciplex) is formed by an excited dye molecule and a molecule of a different compound, new fluorescence bands may appear. In these

cases the compounds decay to the ground state by emission and decompose immediately into the two components (*Schäfer, 1972*).

Solvent polarity

The ground and excited electronic states of a molecule may be perturbed by the environment. Solvent effects can be interpreted in terms of dipole-polarization, where the fluorophore is considered a dipole and the solvent a continuous dielectric medium with uniform dielectric constant.

The wavenumber (cm^{-1}) difference of the absorption ($\bar{\nu}_A$) and emission ($\bar{\nu}_F$) is given by the Lippert-Mataga equation (equation 1.17), where h ($6.6256 \cdot 10^{-27}$ ergs) is Planck´s constant, c ($2.9979 \cdot 10^{10}$ cm/s) is the speed of light, ε and n are respectively the dielectric constant and the refractive index of the solvent, a is the radius of the cavity in which the fluorophore resides, and μ_E, μ_G are the dipole moments of the fluorophore in the excited and ground states respectively.

$$\bar{\nu}_A - \bar{\nu}_F = \frac{2}{hc}\left(\frac{\varepsilon - 1}{2\varepsilon + 1} - \frac{n^2 - 1}{2n^2 + 1}\right)\frac{(\mu_E - \mu_G)^2}{a^3} + constant \quad (1.17)$$

Solvent dipoles can reorient or relax around μ_E after excitation, lowering the excited state energy and resulting in emission at lower energies (or higher wavelengths). This solvent relaxation effect increases with increasing solvent polarity and it is more sensitive for polar fluorophores than for nonpolar (figure 1.20) (*Lakowicz, 2006*).

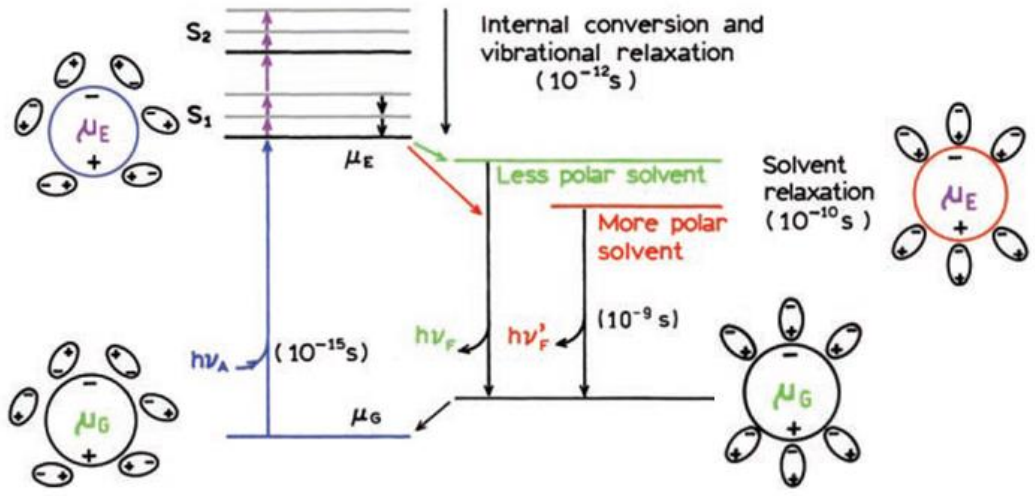

Figure 1.20: Jablonski diagram for fluorescence with solvent relaxation. Schemes of the dipole (fluorophore) surrounded by a dielectric medium (solvent) that can reorient its dipoles (*Lakowicz, 2006*).

The implication of this effect is that Stoke's shift changes. A higher dielectric constant of the solvent (polymer) will increase the Stoke's shift leading to a smaller spectral overlap of the absorption and emission spectrum. This would in turn lower the self-absorption and thereby improve the fluorescence efficiency. Furthermore, it has been proposed by Holmes and McLaughlin independently, that an increase in dielectric constant of the solvent of radiochromic dye would improve radiochromic response based on the photoionization of the leuco-dye (*Holmes, 1965*) (*McLaughlin and Kosanić, 1974*).

1.4.3. Radiation chemistry in pararosaniline leuco dye

The dosimeter presented in this thesis is based on pararosaniline leuco dye. Figure 1.21 shows how this molecule is transformed from its colourless leuco dye form into its magenta dye form by effect of ionizing radiation.

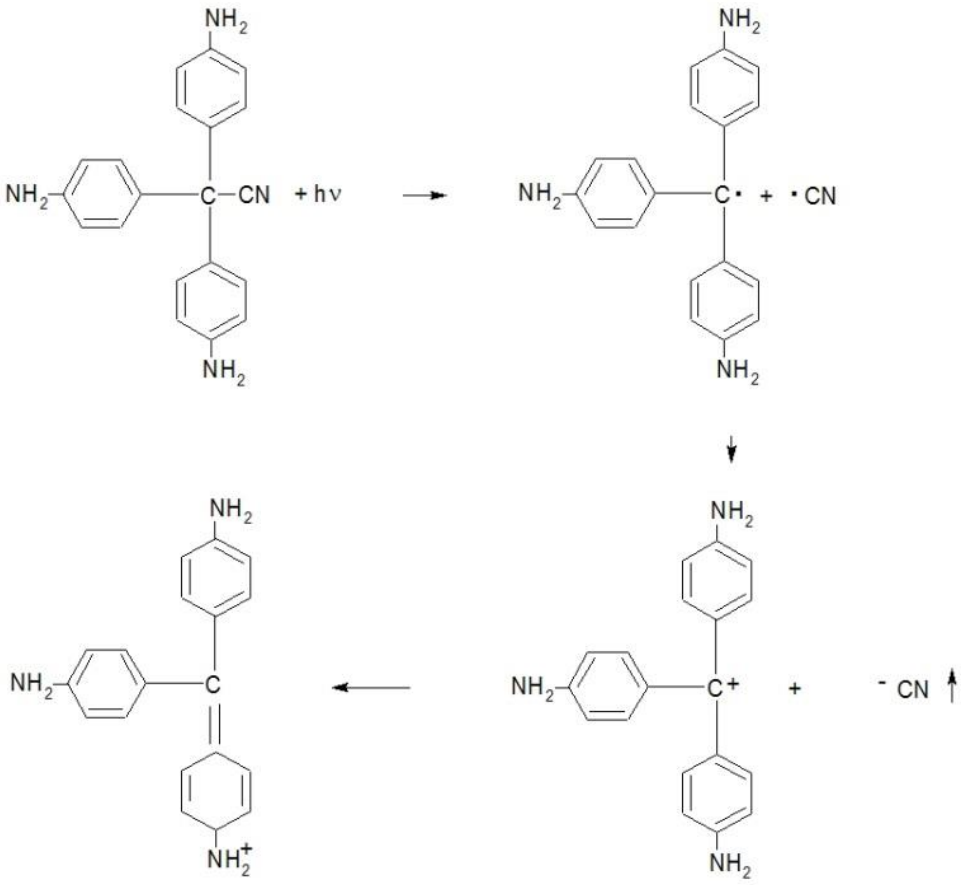

Figure 1.21: Effect of ionizing radiation in pararosaniline leuco dye.

In the first step, when the leuco dye molecule absorbs ionizing radiation ($h\nu$), radiolysis occurs. That is the cleavage of the bond of the nitrile group (CN) with the central carbon atom. This results in a couple of free radicals (molecules with an unpaired valence electron): the nitrilee radical (CN•) and a short-lived intermediate free radical on the central carbon atom (C•).

In the second step, the nitrilee anion (CN^-) is quickly scavenged by hydrogen ions (H^+). This is important to prevent the reaction from being reversible. Finally, in the third step, the stable free radical is formed by formation of the C=C double bond, which is the chromophore (part of the molecule responsible for its color) and presents a characteristic absorption band in the visible spectrum (*ICRU, 2008*).

To summarize, three factors have to be present (*McLaughlin and Kosanić, 1974*) (*Miller and McLaughlin, 1980*):

- Ionizing radiation: below 330 nm (UV) produces radiolysis of the molecule.
- Oxygen: required to facilitate the formation of free radicals.
- Hydrogen ions: scavenge the nitrile anions liberated from the leuco dye during the radiolysis.

1.5. The Risø B3 radiochromic dosimeter film

The effect of ionizing radiation on the absorption spectrum of pararosaniline has been used in a commercial dosimeter film, the Risø B3 radiochromic film. In this chapter its characteristics are discussed.

The Risø B3 radiochromic dosimeter film is a result of the research carried out at Risø (Center for Nuclear Technologies, Technical University of Denmark) between 1978 and 1980, and it has been used since then for high dose industrial dosimetry and sterilization of medical devices. These films stand out for their pre- and post- irradiation stability, dose rate independence and wide dose range (from 300 Gy to 160 kGy) (*TIR 100-205, 2010*).

This material is based on the radiochromic response of pararosaniline leuco dye (originally developed by NIST and Risø), contained in polymeric films of 20 µm nominal thickness of polyvinyl butyral (PVB). Due to the color change with ionizing radiation, the dose response is determined by measuring the absorbance. The fluorescence of these films was studied by Abdel-Fattah (*Abdel-Fattah et al., 2001*), showing a decrease in the fluorescence intensity with the absorbed dose.

To illustrate the radiochromic response, an experiment was performed, where 28 films were irradiated at different doses in a Gammacell with a dose rate of approximately 140 Gy/minute. They were irradiated at 6 dose levels (0.5, 1, 5, 10, 20 and 30 kGy) (figure 1.22) with 4 films for each dose, and their absorbance spectra were measured with a spectrophotometer (figure 1.23a). The peak of the absorbance spectrum, around 554 nm, is represented for each film as function of the dose in figure 1.23b, where it can be seen the linear relationship between the increase of absorbance and the absorbed dose.

Figure 1.22: Risø B3 radiochromic dosimeter films. The first film is unirradiated for reference, the others are irradiated at 0.5, 1, 5, 10, 20 and 30 kGy (from left to right).

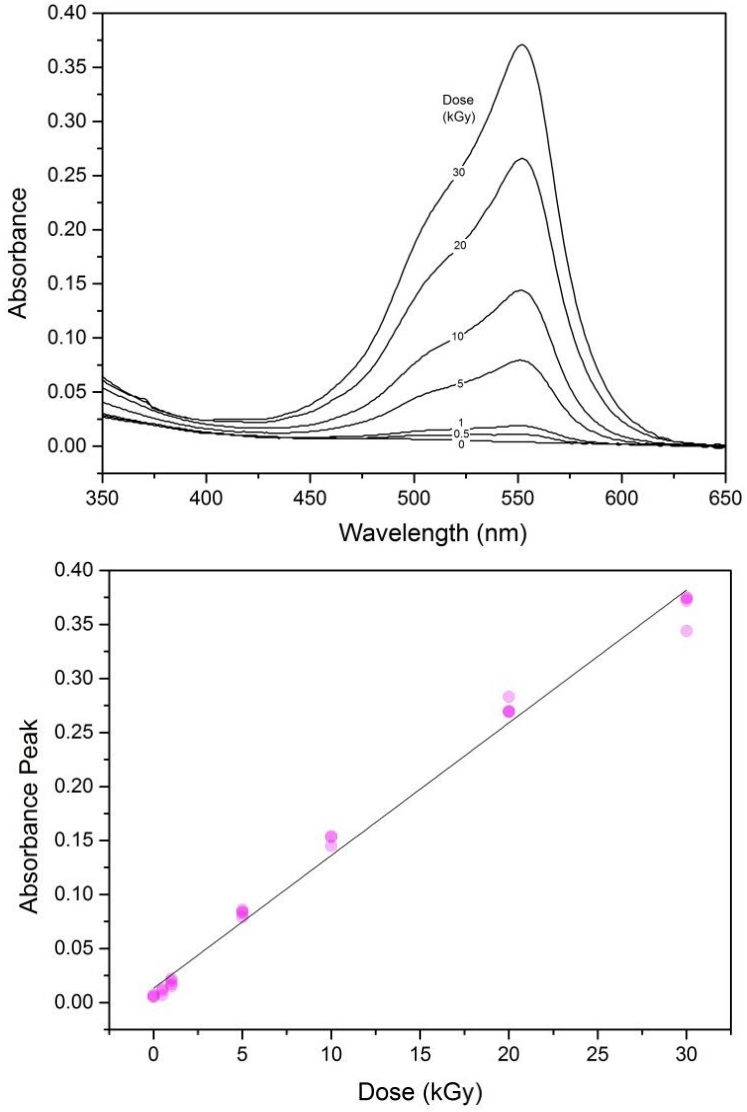

Figure 1.23: a) Absorbance spectra of some films. b) Absorbance peak as function of the dose for all the films.

The objective of this thesis is to develop and characterize a solid-state polymer dosimeter based on the radiochromic Risø B3 dye. The challenge of this objective is that a solid polymer material with a typical thickness of 10 mm has to provide the same diffusion properties as a thin (20 micron) polyvinyl butyral (PVB) film.

Chapter 2

Aim

The aim of this PhD project is to develop a new 3D solid state polymer dosimeter that is radiochromic and radiofluorogenic, and which can be used to ascertain that the radiotherapy treatment is delivered as intended by mapping the 3D dose distribution through optical fluorescence tomography.

The motivation for this thesis is that combining the advantages of a solid polymer dosimeter together with optical fluorescence tomography measurement process might provide higher spatial resolution, higher accuracy and a faster measurement, facilitating the use of 3D dosimetry in a clinical basis.

The objective of this project is the development of the dosimeter and its characterization.

Chapter 3

Materials & Methods

This chapter contains a description of the chemicals, equipment and methods used for fabrication and characterization of the dosimeter.

3.1. Pararosaniline leuco dye

Pararosaniline, also known as paramagenta or parafuchsin, it is classified with the C.I (color index) generic name Basic Red 9, the C.I constitution number C.I. 42500, and the CAS (Chemical Abstracts Service) registry number 569-61-9 (*Duxbury, 1993*) (*Gessner and Mayer, 2012*). It is an organic compound of the family of the triphenylmethane dyes, among the first synthetic dyes developed. It can be in the leuco dye form or in the dye form (figure 3.1). The chemical formulas, names, and molecular weights for both structures are collected in table 3.1. Pararosaniline leuco dye was supplied by Niels Clauson-Kaas A/S (NCK, 2016), in the form of white powder.

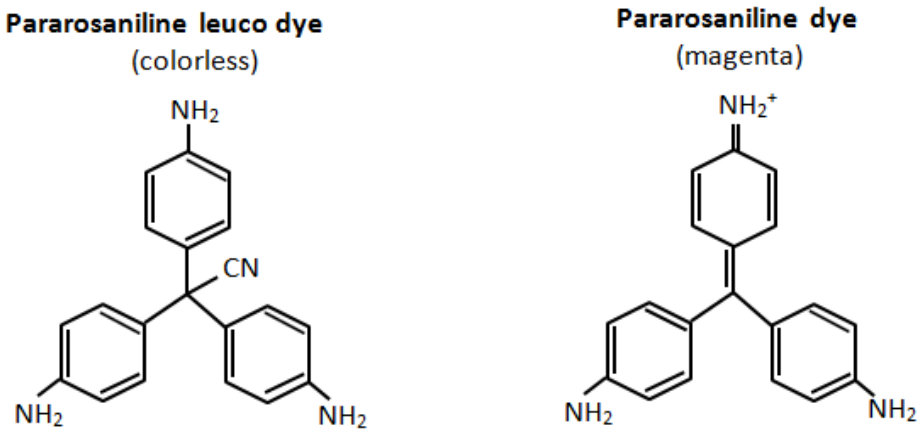

Figure 3.1: Pararosaniline in its leuco dye and dye forms.

Table 3.1: Chemical formulas and names for pararosaniline.

	Pararosaniline leuco dye	Pararosaniline dye
Formula	$(H_2NC_6H_4)_3C_2N$ or $C_{20}H_{18}N_4$	$(H_2NC_6H_4)_3C$ or $C_{19}H_{18}N_3$
IUPAC name	4,4',4''-tri(aminophenyl) acetonitrile	[4-[Bis(4-aminophenyl)methylidene]-1-cyclohexa-2,5-dienylidene]dianiline
$M_w(g/mol)$	323.82	287.36

The leuco dye can undergo transformation to its colored state either by exposure to UV light below 330 nm or by ionizing radiation, as explained in chapter 1.4.3 (figure 1.21). The leuco dye is oxidized (loss of electrons) by free radicals and the nitrile anion is scavenged by hydrogen ions, resulting in a stable dye.

3.2. Polymer matrix

The polymer matrix is formed, as pointed out in chapter 1.1.2, by: host polymer, secondary polymer, hydrogen donor, solvent and photoinitiator. Specifications about the chemicals appear in Annexe I.

Host polymer

The host polymer is poly(ethylene glycol) diacrylate (PEGDA) (figure 3.2), which provides the main physical properties to the dosimeter. PEGDA-575 g/mol is used in this work, but it was also tested (chapter 4.2.3) with different molecular weights (250 g/mol and 700 g/mol), all supplied by Sigma-Aldrich (*Sigma-Aldrich, 2017*).

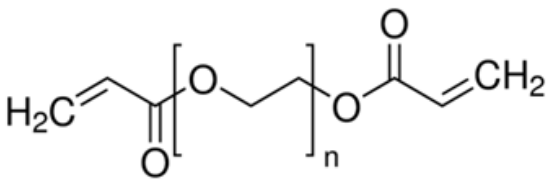

Figure 3.2: Poly(ethylene glycol) diacrylate (PEGDA) (*Sigma-Aldrich, 2017*). Chemical formula: $(C_3H_3O)(C_2H_4O)_n(C_3H_3O_2)$.

PEGDA is a biocompatible hydrogel (high water content polymer) commonly used in dental compounds and in artificial scaffolds for tissue engineering (*van Blitterswijk, 2008*). It is considered biomimetic because it possesses tissue-like elasticity and bio-functionality, emulating the permeability and transport properties of the extracellular matrix (intricate network of macromolecules present in all living tissues) (*Lin, 2015*).

Another advantage of PEGDA is that it is curable by using UV light and a photoinitiator, enabling temporal and spatial control of the curing. Besides, it provides good diffusion properties to the dosimeter, and good optical properties, since it is transparent. Optical clarity is an important requirement for the polymer matrix to facilitate the dosimeter measurement.

Secondary polymer

The secondary polymer used in this thesis is 2-hydroxyethyl methacrylate (HEMA) (figure 3.3), supplied by Sigma-Aldrich. It is used to further the mechanical stability of the host polymer by cross-linking.

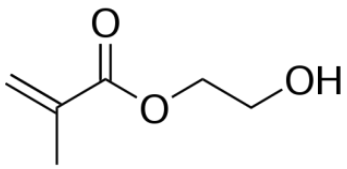

Figure 3.3: 2-hydroxyethyl methacrylate (HEMA). Molecular weight: 130.14 g/mol. Chemical formula: $C_6H_{10}O_3$ (*Sigma-Aldrich, 2017*).

Poly(2-hydroxyethyl methacrylate) (poly-HEMA) is a polymer that, due to its high swelling, forms a hydrogel in water. It was used in the 1950s by Otto Wichterle to produce the first soft contact lenses. Poly-HEMA can be achieved by crosslinking HEMA with an acrylate. These acrylate/methacrylate systems have been widely used in biomedical applications, as soft contact lenses, drug delivery systems, and implants (*Kopeček, 2009*). One of the acrylate/methacrylate systems is the PEGDA/HEMA, formed by polymerization of HEMA with PEGDA as cross-linker (*Figueiredo et al., 2013*), which has also been produced by UV photocuring for cell immobilization (*Hsue et al., 2017*).

For these applications, HEMA is the host polymer while PEGDA is added as secondary polymer to increase hydrophilicity. In this thesis, however, PEGDA is used as host polymer and HEMA as secondary polymer in order to ensure a highly diffusive matrix to facilitate high mobility of free radicals, caused by ionizing radiation, through the whole dosimeter volume, allowing a homogenous radiochromic and radiofluorogenic response and not just a change in the surface in contact with oxygen. HEMA is used to make the dosimeter mechanically more stable after curing.

In the compositions studied in this thesis, PEGDA comprises 94.6 vol% (*Compositions 1*, *2* and *4*) and 86.5 vol% (*Compositions 3* and *5*); while HEMA comprises 0.5 vol% and 9 vol% respectively (the remaining is the solvent).

Hydrogen donor (additives)

In order to avoid reversibility of the reaction from the dye to the leuco dye, it is necessary to scavenge the nitrile anions (CN^-) leaving from the leuco dye (chapter 1.4.3, figure 1.21). Since they are quickly scavenged by hydrogen ions (H^+), a hydrogen donor compound is necessary. In chapter 4.2.3 the effect of two solid additives that act as hydrogen donors is analyzed (figure 3.4): bis(2,4,6-trichlorophenyl) oxalate (TCPO) and 2,2,2-Trichloroethane-1,1-diol (Chloral Hydrate), both supplied by Sigma-Aldrich. When they are exposed to ionizing radiation they liberate chlorine and subsequently hydrogen from the polymer.

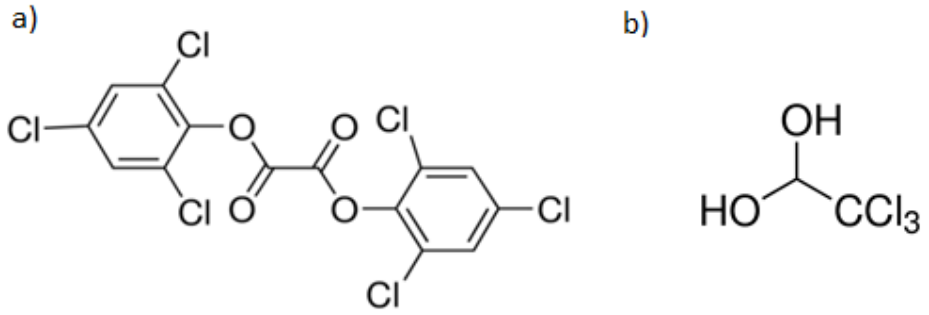

Figure 3.4: a) Bis(2,4,6-trichlorophenyl) oxalate (TCPO). Molecular weight: 448.90 g/mol. Chemical formula: $C_{14}H_4Cl_6O_4$. b) 2,2,2-Trichloroethane-1,1-diol (Chloral Hydrate). Molecular weight: 165.40 g/mol. Chemical formula: $C_2H_3Cl_3O_2$ (*Sigma-Aldrich, 2017*).

Solvent

The solvent, used to dissolve the dye, is ethanol 96 vol% in water (figure 3.5), supplied by CCS Healthcare AB (*CCS, 2017*). In chapter 4.5, citric acid 20 vol% in water, and pentaerythritol tetrakis(3-mercaptopropionate) (Mercapto) (both supplied by Sigma-Aldrich) are studied for the dosimeter stability.

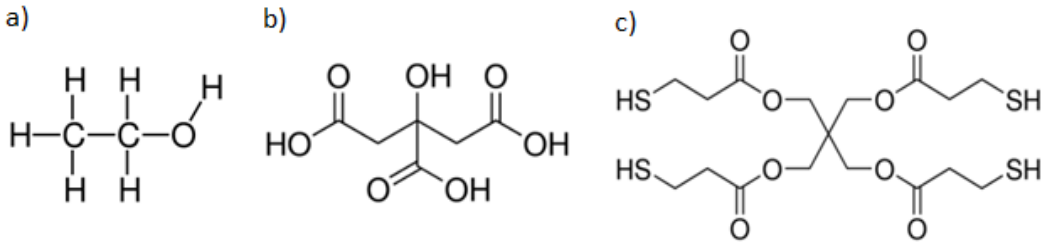

Figure 3.5: a) Ethanol. Molecular weight: 46.07 g/mol. Chemical formula: C_2H_6O. b) Citric acid monohydrate. Molecular weight: 192.12 g/mol. Chemical formula: $C_6H_8O_7$. c) Pentaerythritol tetrakis(3-mercaptopropionate) (Mercapto). Molecular weight: 488.66 g/mol. Chemical formula: $C_{17}H_{28}O_8S_4$ (*Sigma-Aldrich, 2017*).

Photoinitiator

The acrylate/methacrylate (PEGDA/HEMA) system is photocurable by free radical photoinitiators, as discussed in chapter 1.3.1. Since pararosaniline leuco dye is sensitive to radiation below 330 nm (*McLaughlin and Kosanić, 1974*) (*Miller and McLaughlin, 1980*), the wavelength of the UV light used for photocuring must be higher. It is also necessary that the emission spectrum of the LED lamp used for photocuring overlaps with the absorption band of the photoinitiator. Therefore, the chosen photoinitiators must absorb above 330 nm (table 3.2).

Table 3.2: Photoinitiators used in the thesis.

	TPO	ITX	CQ	CPTX	Irgacure 819 + Darocur 1173
Free radical photoinitiator	Type I	Type II	Type II	Type II	Type I
Absorbance band (nm)	~ 380	~ 380	~ 470	~ 390	~ 370 and ~ 240

The main photoinitiator used in this thesis is diphenyl(2,4,6-trimethylbenzoyl)phosphine oxide (TPO), supplied by Sigma-Adrich. The reaction with PEGDA is shown in figure 3.6. In the first step, the TPO molecule absorbs UV radiation and decomposes into two free radicals. In the second step, these free radicals react with PEGDA by opening its C=C bond and therefore allowing crosslinking (*Yang et al., 2015*).

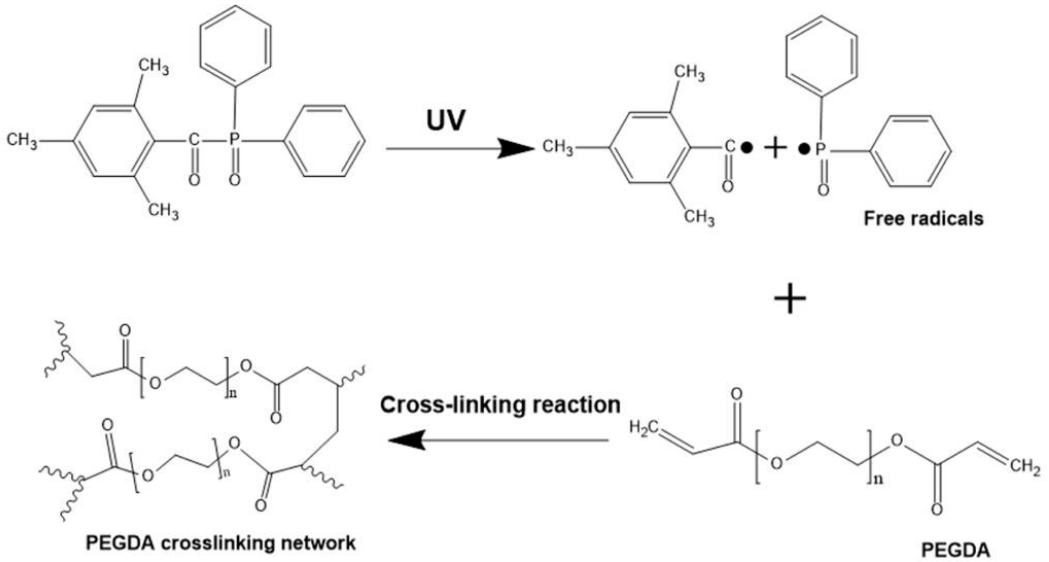

Figure 3.6: Diphenyl(2,4,6-trimethylbenzoyl)phosphine oxide (TPO). Molecular weight: 348.37 g/mol. Chemical formula: $C_{22}H_{21}O_2P$. Crosslinking reaction of PEGDA induced by TPO photoinitiator (*Yang et al., 2015*).

Other photoinitiators a tested in chapter 4.2.4, suplied also by Sigma-Aldrich (figure 3.7): isopropyl-9H-thioxanthen-9-one (ITX), camphorquinone (CQ), 1-chloro-4-propoxy-9H-thioxanthen-9-one (CPTX), phenylbis(2,4,6-trimethylbenzoyl)phosphine oxide (Irgacure 819), and 2-hydroxy-2-methylpropiophenone (Darocur 1173). The last two were mixed in 20 vol% -80 vol% respectively.

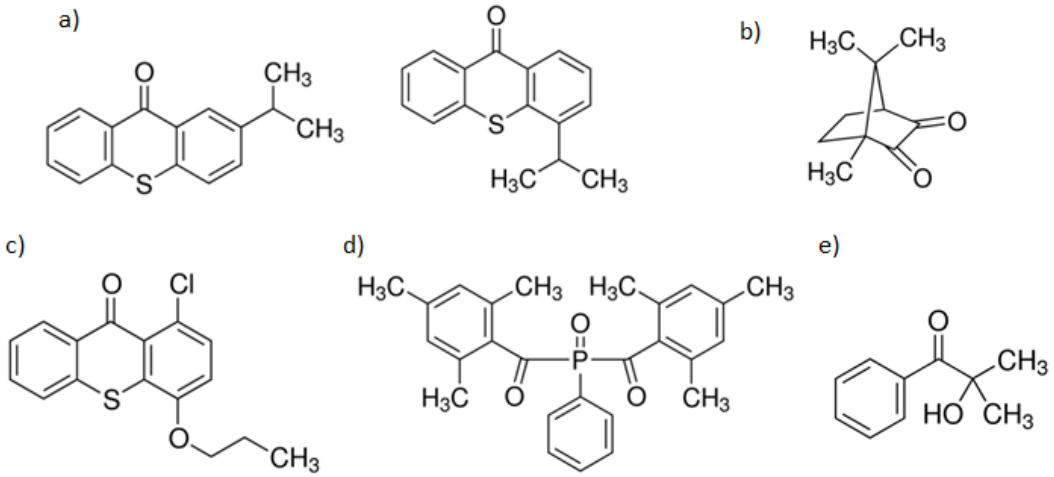

Figure 3.7: a) ITX (2- and 4- isomers). b) CQ. c) CPTX. d) Irgacure 819. e) Darocur 1173. (*Sigma-Aldrich, 2017*).

TPO, Irgacure 819 and Darocur 1173 belong to type I, while ITX, CQ and CPTX belong to type II and therefore require the use of a co-initiator as discussed in chapter 1.3.1. The co-initiators that were used are (figure 3.8) ethyl 4-(dimethylamino)benzoate (EDB) and 2-(dimethylamino)ethyl methacrylate (DMAEM), both supplied by Sigma-Aldrich.

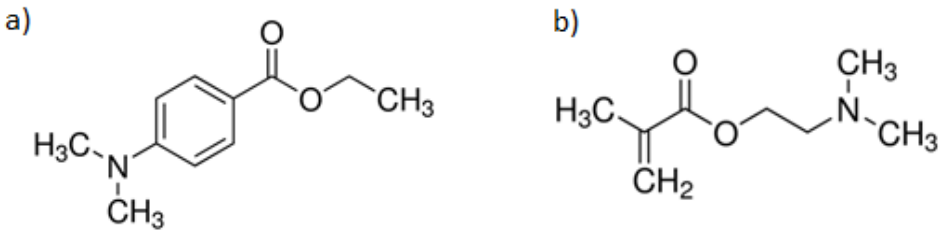

Figure 3.8: a) EDB. b) DMAEM. (*Sigma-Aldrich, 2017*).

3.3. Manufacturing. Main compositions

Solids (leuco dye and additives in some cases) were weighed in a Secura balance by Sartorius (*Sartorius, 2017*) (figure 3.9a). Then, liquids were added to the glass vials containing the solids by using 100–1000 µl and 500–5000 µl Pipet-Lite LTS pipettes by Rainin (*Rainin, 2017*) in the following order: solvent (ethanol), host polymer (PEGDA) and secondary polymer (HEMA). After agitation, solutions of the photoinitiator in PEGDA at 0.5 m/v% (14.35 mM) were added.

At the beginning, magnetic stirrers and 50 ml dark glass flasks (to avoid UV light) were used (figure 3.9b). Mixtures were agitated at 600 rpm for 1.5 hours before adding the photoinitiator, and then for a further 2 hours.

Subsequently, UV protection films were placed on the windows and the manufacturing process was accelerated by using a vortex rotor by Heidolph Instruments (*Heidolph, 2017*) with capacity for 12 small screw cap 10 ml glass vials (figure 3.9c). Mixtures were agitated at 1600 rpm for 30 min before adding the photoinitiator, and then for a further 30 min. Mixtures can be safely stored for periods up to several months, since they are stable in the liquid state, although samples are usually cured the same or the next day. Manufacturing, storage and measurements are made at room temperature and with UV protection.

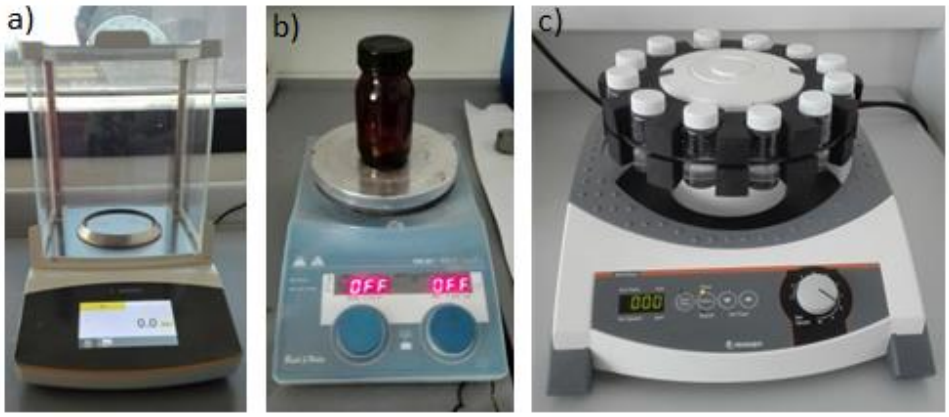

Figure 3.9: a) Secura balance. b) Single mixing system. c) Vortex rotor.

The main compositions that are used in this thesis appear in table 3.3. Variations have also been studied, for example by changing the molecular weight of PEGDA or changing the photoinitiator, but they are based on these 5 formulations. Changes will be explained in detail along chapter 4.

Table 3.3: Main compositions used along the thesis.

Composition 1

(high dye, TCPO)

leuco dye: 120 *mg* (60.85 *mM*)
TCPO: 3 *mg* (1.10 *mM*)
Ethanol: 0.3 *ml* (0.84 *M*)
PEGDA: 5.16 *ml* (1.84 *M*)
HEMA: 0.03 *ml* (40.61 *mM*)
TPO: 0.6 *ml* (1.41 *mM*)

Composition 2

(high dye)

leuco dye: 120 *mg* (60.85 *mM*)
Ethanol: 0.3 *ml* (0.84 *M*)
PEGDA: 5.16 *ml* (1.84 *M*)
HEMA: 0.03 *ml* (40.61 *mM*)
TPO: 0.6 *ml* (1.41 *mM*)

Composition 3

(high dye, high HEMA)

leuco dye: 120 *mg* (55.6 *mM*)
Ethanol: 0.3 *ml* (0.77 *M*)
PEGDA: 5.16 *ml* (1.68 *M*)
HEMA: 0.6 *ml* (0.74 *M*)
TPO: 0.6 *ml* (1.29 *mM*)

Composition 4

(low dye)

leuco dye: 12 *mg* (6.09 *mM*)
Ethanol: 0.3 *ml* (0.84 *M*)
PEGDA: 5.16 *ml* (1.84 *M*)
HEMA: 0.03 *ml* (40.61 *mM*)
TPO: 0.6 *ml* (1.41 *mM*)

Composition 5

(low dye, high HEMA)

leuco dye: 12 *mg* (5.56 *mM*)
Ethanol: 0.3 *ml* (0.77 *M*)
PEGDA: 5.16 *ml* (1.68 *M*)
HEMA: 0.6 *ml* (0.74 *M*)
TPO: 0.6 *ml* (1.29 *mM*)

In all previous compositions, PEGDA-575 g/mol was used, and photoinitiator solutions were also made in PEGDA-575 at 0.5 m/v%. Volumes (0.6 ml) correspond to the photoinitiator solutions, while molarities correspond to the photoinitiator itself. Molarities of PEGDA include also the molarity correspondent to the photoinitiator solutions.

3.4. Photocuring process

Three different LED lamps have been used for photocuring along the thesis (table 3.4, figure 3.10). They emit UV light above 330 nm to avoid the reaction of the leuco dye. The LEDs were all tested on Risø B3 radiochromic films to determine if they were safe to use.

Table 3.4: Characteristics of the lamps used for photocuring.

	Lamp 1	***Lamp 2***	***Lamp 3***
Type of lamp	LED	LED	LED
Emission wavelength	407 nm	460 nm	385 nm
Surface power density (at 9 cm)	4.5 mW/cm^2	25 mW/cm^2	15 mW/cm^2

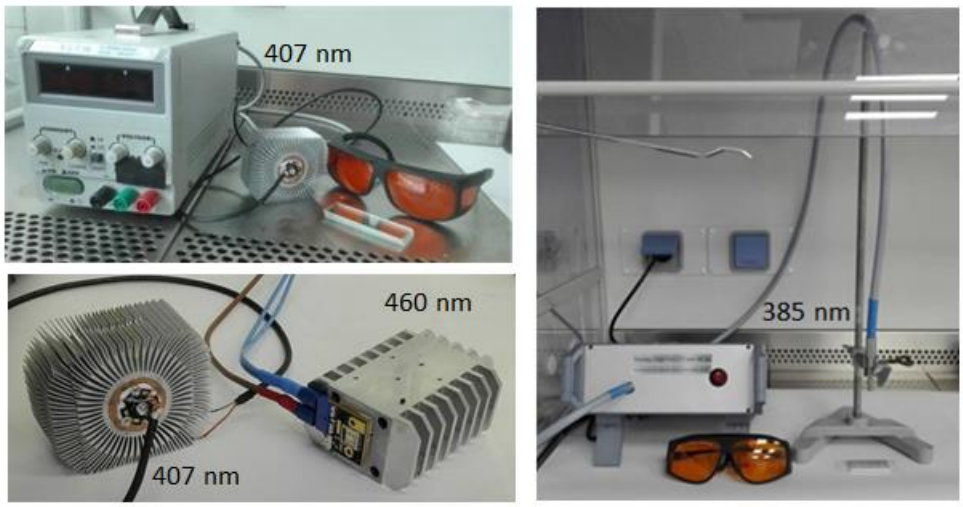

Figure 3.10: Lamps used for photocuring. a) *Lamp 1*. b) *Lamp 1* and *Lamp 2*. c) *Lamp 3*.

The polymer solid-state was photocured in different shapes: cuvettes, slides, pellets and larger 3D shapes. Samples were usually cured from a distance of 9 cm to the lamp. Specifications about the lamps are shown in Annexe 1.

Cuvettes (1 cm thickness) were made for measurement of the specific absorbance, and thereby enable optimization of the composition (chapter 4.1). They were illuminated with *Lamp 1* from one side while rotating the cuvette. In some cases, they were cooled in iced water while curing due to the high temperatures reached.

Tests on slides and pellets form the main part of the work described in this thesis (chapters 4.2 to 4.6) since they were used for the dosimeter´s characterization by acquiring also fluorescence and EPR measurements. They are more convenient than cuvettes for characterization because their smaller thickness avoids self-absorption of the emitted fluorescence. Both were cured from the top.

Slides (1 mm thickness) were made by using 5 glass plates to form a mould (figure 3.11a). The liquid was poured into the middle and another glass plate was placed on top to ensure the best surface quality. The thicknesses of the slides, nominally 1 mm, were measured with an electronic caliper.

Pellets (4.75 mm diameter, 2.78 mm thickness) were made to improve the fabrication and measurement processes, and to allow EPR measurement. Two aluminium molds were made, one for fabrication and another for absorbance and fluorescence measurements (figure 3.11b). The fabrication mold, which allows curing of 15 pellets at once, is placed between two glass plates to ensure the best surface quality.

Larger 3D samples were made to test the dosimeter in real application shapes (chapter 4.1). They were made by using plastic molds as the sphere shown in figure 3.11c. They were cured by moving *Lamp 1* around the mold, and from the top in the case of *Lamp 3*.

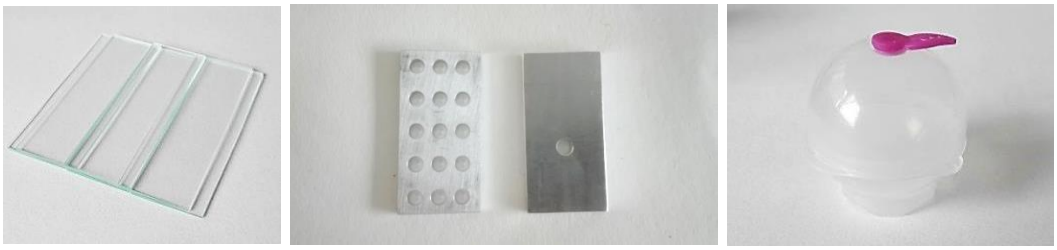

Figure 3.11: a) Fabrication mold for slides made with glass plates. b) Fabrication mold for pellets (left) and holder for optical measurements (right). c) Spherical plastic mold of 3.5 cm diameter.

Characterization of *Lamp 3*

The best sample quality was obtained when curing with *Lamp 3*, obtaining a hard sample with a dry surface, and needing a short curing time. The problem of not having a dry surface was observed when curing with *Lamp 1*, and that is the reason samples were measured the next day after curing. This is due to oxygen inhibition in the curing process, which manifests by surface tack of the cured samples. Adding mercapto to the composition resulted in a dry sample surface immediately after curing. However, this problem was not observed when using *Lamp 3*.

The surface power density of *Lamp 3* was measured with a power meter for different lamp to mold distances (figure 3.12).

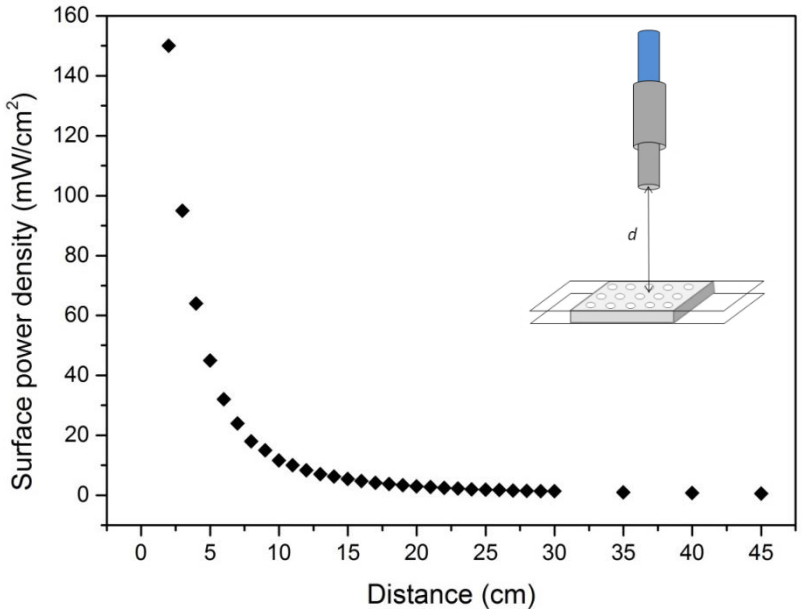

Figure 3.12: Surface power density as function of the lamp to mold distance for *Lamp 3*. Detail of the mold used for fabrication of pellets between two glass plates, where the measured distance is from the lamp to the first glass plate.

3.5. Irradiations

Samples were irradiated with a ^{60}Co source at DTU Risø. Two gammacells were used, called "*Gammacell 1*" and "*Gammacell 3*", with dose rates of approximately 5 Gy/min and 140 Gy/min respectively (figures 3.13a and 3.13d). ^{60}Co rods are circularly distributed, giving a uniform radiation field in the center, where samples are placed. A detail of the open *Gammacell 1* is shown in figure 3.13b (*Gammacell 3* presents a similar structure). Samples are contained in a steel cylinder with polyether ether ketone (PEEK) inside (figure 3.13c). Cuvettes and slides are placed directly, while pellets are first placed on acrylonitrile butadiene styrene (ABS) holders that go inside the PEEK cylinder shown in figure 3.13c. This geometry allows fulfilling the charge particle equilibrium (CPE) conditions required to calculate the absorbed dose in the medium, as discussed in chapter 1.2.1.1. In both gammacells the uncertainty of the delivered dose is 1.3%.

Figure 3.13: a) *Gammacell 1* (dose rate: 5 Gy/min). b) Open *Gammacell 1*. c) Steel and PEEK cylinders containing the samples. d) *Gammacell 3* (dose rate: 140 Gy/min).

3.6. Absorbance and fluorescence measurements

Absorbance measurements were performed with the UV-VIS spectrophotometer UV-2600/2700 by SHIMADZU (*Shimadzu, 2017*) (figure 3.14a). This equipment has a holder for cuvettes and another for films, the latter was used to measure slides by placing them directly, and pellets by placing them in the aluminum holder designed for that purpose (figure 3.11b). Fluorescence measurements of slides and pellets were performed with the setup developed in a parallel PhD project (*Sanders, 2017*) (figure 3.14b). This fluorescence setup consists on a power meter connected to a green laser to excite fluorescence, an optical mount to focus the laser light to the sample, an Ocean Optics QE6500 spectrometer (*Ocean Optics, 2017*) to measure the fluorescence from the sample, and a software to process the signal. A reference stick was used to ensure stable conditions.

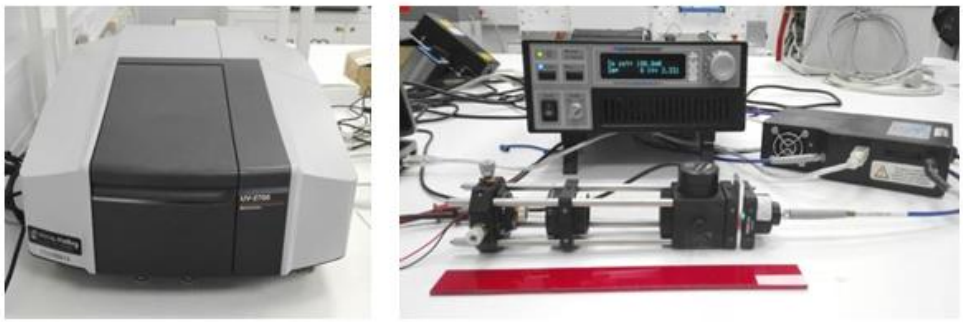

Figure 3.14: a) UV-VIS spectrophotometer UV-2600/2700. b) Fluorescence setup.

Two green lasers were used to excite fluorescence, a 532 nm neodymium-doped yttrium aluminium garnet (Nd:YAG) laser first, and a 520 nm diode laser later. The change was due to the superior stability of the diode laser, increasing reproducibility of fluorescence measurements.

Two software systems were used, the Ocean Optics SpectraSuite software and an in-house LabVIEW-based software, also developed in the parallel PhD project (*Sanders, 2017*).

3.7. Electron Paramagnetic Resonance (EPR) measurements

Electron Paramagnetic Resonance (EPR), also known as Electron Spin Resonance (ESR), is a spectroscopy technique based on the interaction of electromagnetic radiation with intrinsic magnetic moments in the sample. It is used to study paramagnetic systems, which have unpaired electrons and are therefore attracted by magnetic fields also known as paramagnetism. Applying a magnetic field to the unpaired electron creates an energy difference between the two spins which can be detected by absorption of microwave radiation.

When an external magnetic field is applied, the unpaired electrons can either orient in a parallel or antiparallel direction to the magnetic field, resulting in two distinct energy levels (magnetic spin quantum number: $m_s = \pm 1/2$) (Zeeman effect) (figure 3.15). An unpaired electron can move between the two energy levels by absorbing or emitting a photon of energy $\Delta E = h\nu = g_e \mu_B B_0$, where g_e (2.0023) is the Landé factor, μ_B ($9.274 \cdot 10^{-24}$ J/T) is the Bohr magneton, and B_0 is the applied magnetic field. To find the energy difference between the two states, the sample is excited to a specific microwave frequency while varying the magnetic field. When the energy difference between the energy levels matches the microwave energy, the unpaired electrons can move between their two spin states and there is a net absorption. The microwave absorption as function of the magnetic field is the EPR spectrum (*Chechik et al., 2016*).

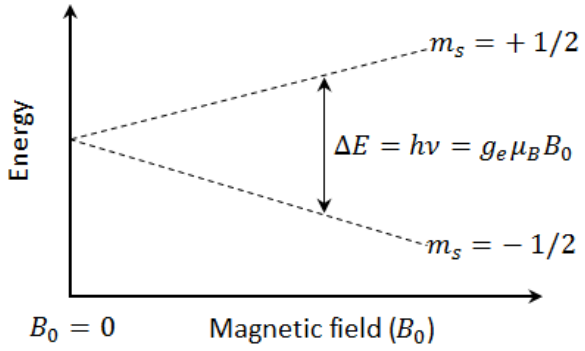

Figure 3.15: Energy levels of an electron spin in an applied magnetic field.

An example of application for this technique is alanine dosimetry, used at DTU Risø (secondary standard dosimetry laboratory), where the EPR signal of alanine serves as reference to calibrate industrial irradiations. The peak-to-peak amplitude of the first derivative of the EPR spectra as function of the dose can be fitted to equation 3.1 (*Waldeland et al., 2011*). $N(D)$ is the number of free radicals as function of the dose, N_∞ is the number of radicals at saturation, and D_0 is the characteristic saturation dose of the dosimeter.

$$N(D) = N_\infty(1 - e^{-\frac{D}{D_0}}) \quad (3.1)$$

The equipment necessary to measure the EPR signal consists on the components shown in figure 3.16a (*Chechik et al., 2016*). The external magnets generate a homogeneous magnetic field across the sample that is inside a resonant cavity (to amplify weak signals from the sample). The microwave bridge supplies continuous microwave radiation of a fixed frequency to the resonant cavity, inducing spin transitions. The console records the EPR spectra, which is the absorbed microwave energy as function of the magnetic field. The variable temperature (VT) unit allows recording the signal at a desired temperature.

A Bruker EMX-micro spectrometer (figure 3.16b) was used to measure the EPR signal of our dosimeter (chapter 4.3), by placing pellets in a quartz tube inside the resonant cavity. The microwave frequency used was 9.75 GHz. More details can be found in Paper III.

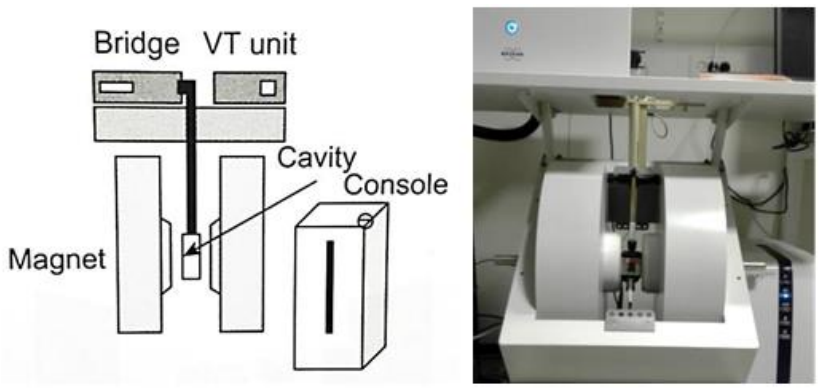

Figure 3.16: a) Components of an EPR spectrometer (*Chechik et al., 2016*). b) Bruker EMX-micro spectrometer used in this thesis.

3.8. Fourier Transform Infrared (FTIR) spectroscopy

Fourier Transform Infrared (FTIR) spectroscopy is a technique based on the absorption of infrared (IR) radiation by a sample (either in liquid or solid state). The resulting transmission or absorbance spectrum peaks correspond to the vibration frequencies of the molecular bonds, presenting a unique fingerprint of the sample. By identifying functional groups, this technique allows to determine the amount of components, the quality or consistency of a sample, and to identify unknown materials (*McMurry, 2016*).

In this project a PerkinElmer Spectrum 100 FT-IR Spectrometer with a ZnSe crystal plate (figure 3.17) was used. The resolution that was set at 16 cm^{-1}. A thin layer of the liquid dosimeter composition was place on the plate and following light cured in several steps, taking respective spectra (chapter 4.4.1).

Figure 3.17: PerkinElmer Spectrum 100 FT-IR Spectrometer and detail of the ZnSe flat plate.

To probe the composition of the liquid dosimeter composition prior to photocuring, attenuated total internal reflection (ATR-FTIR) method was used. The IR beam enters into the crystal and it is reflected at the sample-crystal interface. However, a fraction of light penetrates a few micrometers into the sample, known as an evanescent wave (figure 3.18). In the spectral regions where the sample absorbs energy, the evanescent wave is attenuated. Finally, the IR beam exits the crystal and it is directed to the detector, which measures the amount of energy at each frequency which has passed through the sample, obtaining therefore a transmission spectrum.

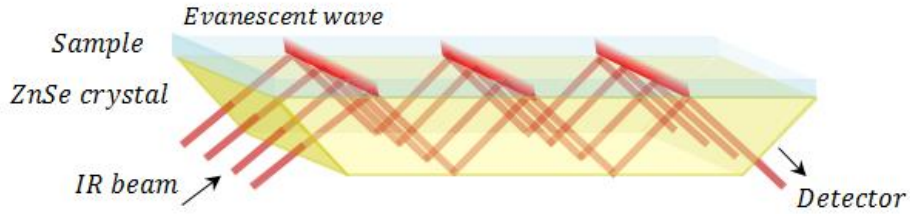

Figure 3.18: Mechanism of FTIR spectroscopy. The IR beam enters into the crystal and reflects at the sample-crystal interface. In those points the evanescent wave penetrates through the sample and it may be absorbed.

This method is used to quantify the photocuring of the liquid dosimeter composition during the photocuring process by measuring the double conversion of the acrylates in the composition as discussed in section 4.4.1.

3.9. Monte Carlo simulations

Monte Carlo is a computational method that provides a numerical solution to a macroscopic system by simulating the dynamics of its microscopic interactions, which are processed randomly and repeatedly (*Bielajew, 2013*). It is therefore useful for solving complex probabilistic problems, like the radiation transport in matter, where the individual trajectory of each particle is simulated by using random number sequences and probability distributions of the interactions that may occur.

The first Monte Carlo-like method was proposed by Comte de Buffon in 1777 to determine the probability of a needle, thrown on a ruled sheet of paper, of crossing one of the lines. Later in 1886, Laplace used this method to determine the value of π. The name "Monte Carlo method" was first coined in 1947 in a paper from Ulam, who had the idea of using stochastic sampling methods for the neutron transport calculation required for the thermonuclear bomb design. Since then, the development of Monte Carlo methods has growth dramatically, especially in the field of medical physics (*Bielajew, 2013*). Some examples of Monte Carlo codes for radiation transport are EGS (*Nelson et at., 1985*), MCNP (*Brown, 2003*), GEANT4 (*Agostinelli et al., 2003*) and PENELOPE (*Salvat et al., 2011*).

In this thesis, the EGSnrc code (Electron Gamma Shower - Canadian National Research Council) (*Kawrakow, 2000; Kawrakow et al., 2011*), which is one of the most widely used in medical physics, was used to analyze the water equivalence of the dosimeter.

PEGS4 (*Kawrakow et al., 2011*), a data preparation package that is part of the EGSnrc Monte Carlo based software system, was used to create the materials shown in table 3.5. Compositions, mass densities, and energy ranges (electrons from 512 keV to 50 MeV and photons from 1 keV to 50 MeV) were inserted in the software EGSnrc GUI – PEGS Data. The user code EXAMIN (*Kawrakow et al., 2011*) provides easy access to the underlying material data sets produced by PEGS4. EXAMIN is a straightforward code which obtains dosimetric quantities, such as photon interaction probabilities and electron mass collisional stopping powers, by examination of the PEGS4 data files. The user code DOSRZnrc (*Rogers et al., 2010*) was used for simulation of the gammacell, and the user code EGS_CHAMBER (*Kawrakow et al., 2005*) was used for chamber simulations.

Table 3.5: Materials used in Monte Carlo simulations.

	Dosimeter	PEGDA-575	Water
Composition	$C_{76}H_{101}O_{19}PN_4$	$C_{26}H_{46}O_{13}$	H_2O
Mass density (g/ cm^3)	1.12	1.12	1.00

Chapter 4

Results

4.1. Making the dosimeter

Hypothesis: Pararosaniline leuco dye dissolved in a photocurable polymer matrix results in a solid that responds to ionizing radiation with fluorescence. The host polymer provides rigidity to the matrix while at the same time allowing oxygen and radicals' diffusion.

Rigidity is necessary for two purposes: to avoid artifacts introduced by refractive and scattering effects as in polymer gel dosimeters (*Oldham, 2006*); and to enable fluorescence from the dye, which is not fluorescent in solution (*Oster et al., 1959*). Oxygen and radicals' diffusion is needed to obtain a homogeneous radiation response, since oxygen facilitates the radiochromic response of the leuco dye by free-radical formation. Oxygen diffuses freely in gels and in solid thin films including the 20 µm Risø B3 radiochromic film. However, in a 1 cm rigid solid cuvette, oxygen transfer only takes place at the surface of the dosimeter. The kinetics of the polymer matrix should allow oxygen and radicals' diffusion, such as lithium polymer batteries and polymer fuel cells allow ion transport (*Wegner, 2006*). The choice of the host polymer (PEGDA) is therefore crucial to obtain a solid and diffusive matrix.

Design of experiments

A design of experiments (DoE) (*Telford, 2007*) approach was used with 35 different samples (figure 4.1b) to find the optimal composition. The quantities of different components were changed while maintaining the amount of host polymer and solvent constant. Cuvettes were cured with *Lamp 1* (surface power densities of 3.5 and 8.2 mW/cm^2) for times varying from 5 to 40 min, depending on the composition. They were irradiated to 1 kGy in the laboratory Gammacell 220 irradiator *Gammacell 3* at an approximate dose rate of 140 Gy/min. The following characteristics were confirmed for all the samples:

- Phase after photocuring: gel or solid.
- No presence of inhomogeneities after irradiation (figure 4.1a).
- Existence of a fluorescent response by laser stimulation (figure 4.1c).
- Absorbance peak difference between unirradiated and irradiated.

Absorbance peak values for the different compositions were analyzed with MODDE 9.0 software (*MODDE, 2014*) by fitting to the partial least squares (PLS) model to find the most influential factors in the response. Figure 4.1d displays the scaled and centered regression coefficients of the fitted model. Terms are significant when they are far from zero and their uncertainties do not cross zero. Therefore, the most influential factors in the increase of the absorbance peak are the dye and the dose, as expected, but also the photoinitiator (TPO) and its interaction with the dose (TPO*Dose). A summary of the basic model statistics is shown in figure 4.1d. The model fitting is good when the four parameters (R^2, Q^2, model validity and reproducibility) are higher than the values appearing in the figure, which is the case.

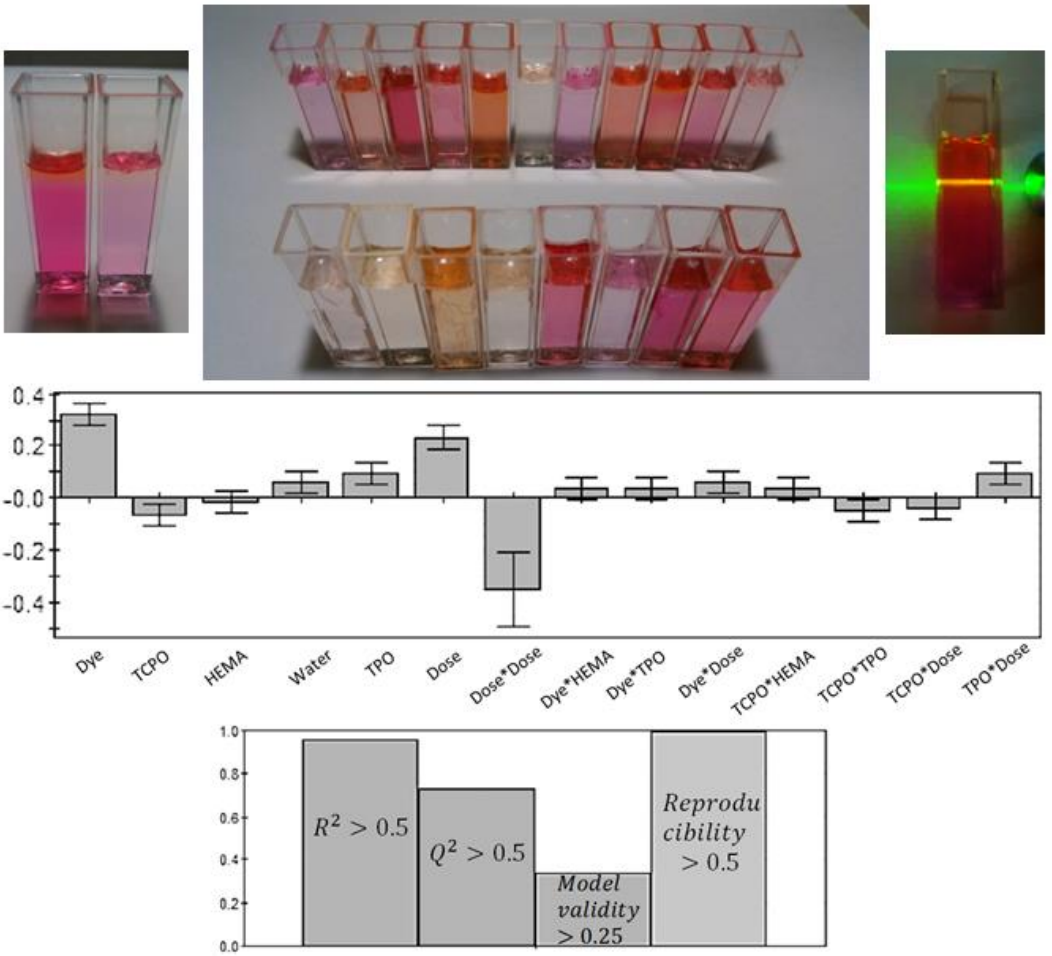

Figure 4.1: a) Samples with gradient color. b) Some of the samples used in DoE. c) Testing if green laser stimulation originates orange fluorescence in the material. d) Scaled and centered regression coefficients from the PLS model obtained with MODDE 9.0. e) Summary of the basic model statistics.

The composition that was chosen from the 35 samples as a starting point is called *Composition 1*. This composition is solid when photocured with *Lamp 1* (surface power density 3.5 mW/cm^2) for 5 min, it is fluorescent when irradiated, and it has the highest absorbance peak difference between the unirradiated and irradiated states.

Figure 4.2 shows the absorbance spectrum of this composition in the liquid state, with the characteristics peaks from the photoinitiator (378 and 400 nm), which disappear when photocured. For the solid cuvette, it can be seen how the peak from the dye at 556 nm clearly increases due to radiation.

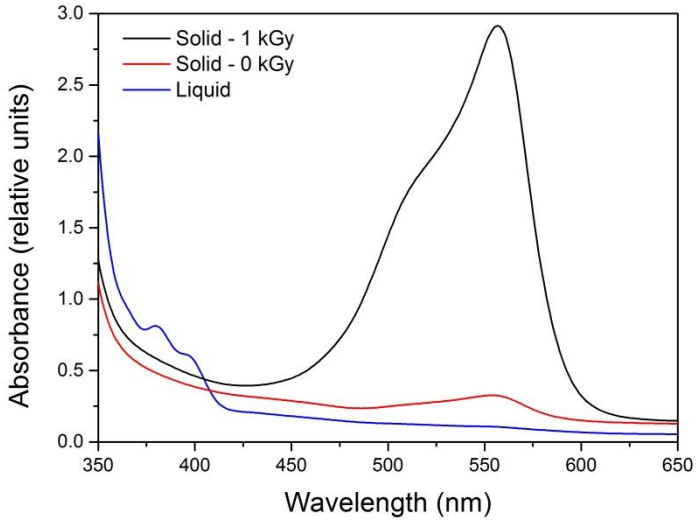

Figure 4.2: Absorbance spectra of a cuvette (path length 10 mm) of *Composition 1* in liquid and solid state (unirradiated and irradiated to 1 kGy).

3D shapes

The good consistency of this material allows making the dosimeter in any 3D shape. Some physical characteristics of the dosimeter are: flexibility of slides (figure 4.3a), which opens up their application in radiotherapy QA; reproducibility of small details from the mold (triangular prism with irregular surface in figure 4.3b), allowing tumor-shape printing; and transparency (figure 4.3c), facilitating optical measurements.

Figure 4.3: a) Slide irradiated to 1 kGy, demonstrating flexibility. b) Unirradiated sphere and prisms. Unirradiated and irradiated pellets. c) Unirradiated slides and pellets.

For large 3D samples, smaller amounts of dye and the shorter curing time obtained using *Lamp 3* are preferred. *Lamp 1* requires more curing time and the heat evolved in the process (as this process is exothermic) promotes the leuco dye reaction, as it happened with the fabrication of the 5 cm diameter sphere shown in figure 4.4a. The long 90 min curing with *Lamp 1* (surface power density: 4.5 mW/cm^2) and the high amount of dye (*Composition 2*) resulted in a red sphere. A 3.5 cm diameter sphere was made with one tenth less dye and cured with *Lamp 3* (surface power density: 15 mW/cm^2) for just 2 min, resulting in a lower background color sphere. Detail of the fluorescence from this sphere is shown in figure 4.5.

Figure 4.4: a) Sphere of 5 cm diameter, with high dye concentration, and cured with *Lamp 1* for 90 min. b) Sphere of 3.5 cm diameter, with low dye concentration, and cured with *Lamp 3* for 2 min. Both spheres are unirradiated.

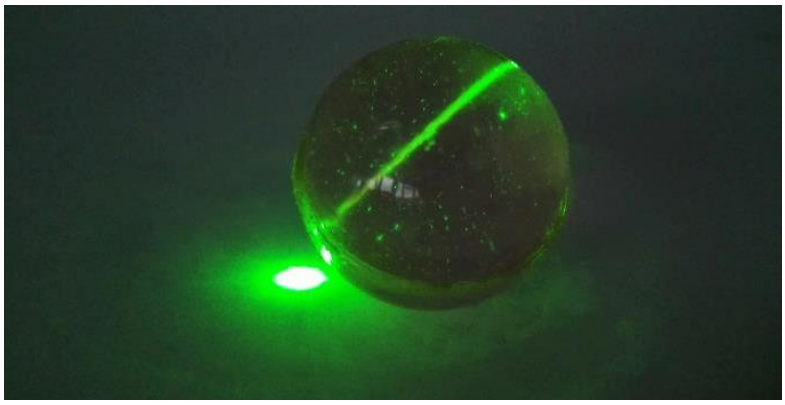

Figure 4.5: Fluorescence of the unirradiated 3.5 cm diameter sphere.

Conclusion: The initial hypothesis was accomplished. A composition was identified in which the dosimeter is solid when photocured, the rigidity of the matrix allows the dye to fluoresce, and there is oxygen diffusion through the whole volume when is irradiated. The dosimeter can be made in any 3D shape.

4.2. Dose response by absorbance and fluorescence signals

In this chapter, the dose response of the dosimeter is analyzed by measuring the absorbance and fluorescence spectra of slides and pellets.

4.2.1. Initial results for high doses (Paper I)

Paper I - Radiochromic and radiofluorogenic 3D solid polymer dosimeter; initial results for high doses.

Hypothesis: The dosimeter responds to ionizing radiation by increasing its absorbance and fluorescence.

Experiment: A slide of *Composition 1* was cured with *Lamp 1* (surface power density: 4.5 mW/cm^2) during 10 min, and consecutively irradiated in *Gammacell 3* (dose rate: 140 Gy/min) to the following dose levels: 100, 200, 30, 400, 500, 600, 700, 800, 900 and 1000 Gy. Fluorescence was excited with the 532 nm Nd:YAG laser. Absorbance and fluorescence spectra of the slide were measured after each irradiation.

Results: Figure 4.6 shows the normalized absorbance and fluorescence spectra for the different doses. We observe an increase in the fluorescence intensity when increasing the dose, contrary to the results shown in an earlier study with polymer films of the same dye (*Abdel-Fattah et al., 2001*). Both absorbance and fluorescence spectra were analyzed in different regions (figure 4.7). The absorbance response is linear with the dose while the fluorescence is exponential. The best fittings occur in the regions containing the peaks (530 - 575 nm for absorbance and 575 - 624 nm for fluorescence). Both signals respond linearly to the dose in the medical dose range.

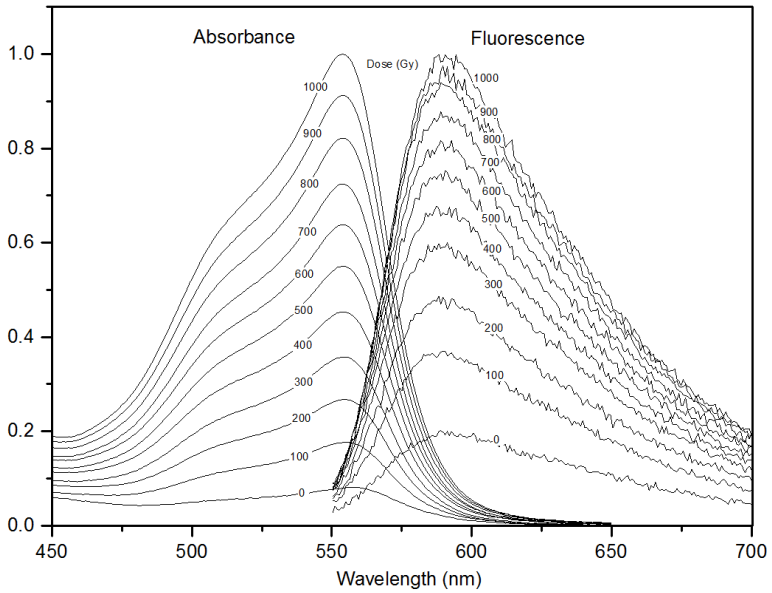

Figure 4.6: Normalized absorbance and fluorescence spectra of a slide of *Composition 1* irradiated consecutively. (Noisy fluorescence signal due to noise from the Nd:YAG laser.)

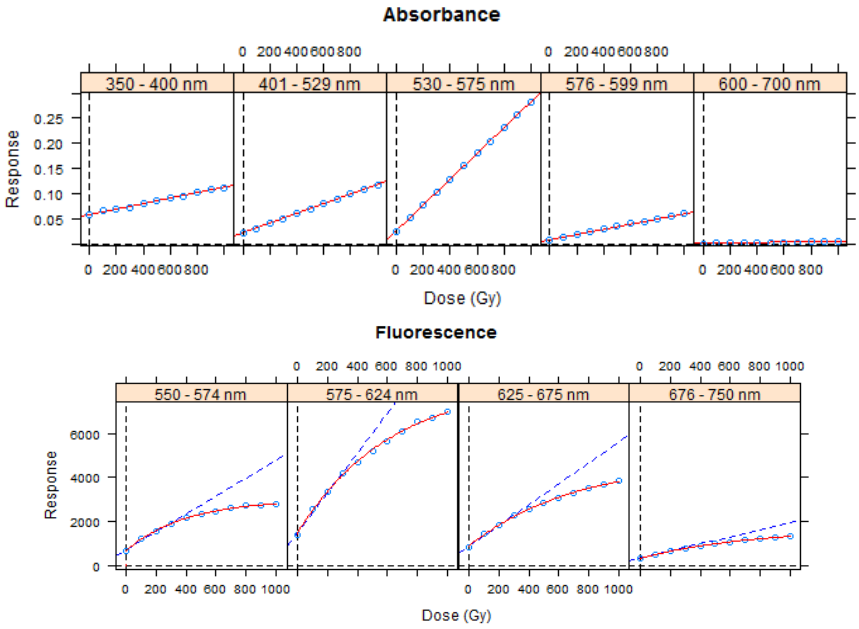

Figure 4.7: Analysis of the different regions of the spectra for both responses with RStudio.

Conclusion: Absorbance and fluorescence from the dosimeter increase with the dose, as expected. They increase linearly and exponentially, respectively. Both are lineal in the low dose range used in radiotherapy. The spectral regions analysis suggests that the peak amplitude is the best way to study the dose response.

4.2.2. Effect of dose fractionation

Hypothesis: The dosimeter response is independent on dose fractionation, and it is therefore the same if the dose has been accumulating by successive irradiations (fractions) or if otherwise, it has been directly irradiated to a specific dose.

Experiment: Five slides of *Composition 1* were cured in the same way than the slide from the previous chapter: *Lamp 1* (surface power density: 4.5 mW/cm^2) for 10 min. Each slide was irradiated in *Gammacell 3* (dose rate: 140 Gy/min) to a specific dose: 200, 400, 600, 800, and 1000 Gy. Fluorescence was excited with the 532 nm Nd:YAG laser.

Results: Absorbance and fluorescence peaks for each slide irradiated to a specific dose, were compared with the results shown in the previous chapter obtained by dose fractionation for a single slide. Figure 4.8 shows that the absorbance peaks perfectly agree, while for the fluorescence there is a difference in the last point at 1 kGy. What it is observed in the graph is the inner filter effect (*Lakowicz, 2006*). The cause of this effect is the fact that some of the dye molecules in the matrix either absorb the fluorescence emission or that some of the excitation light is absorbed by the dye.

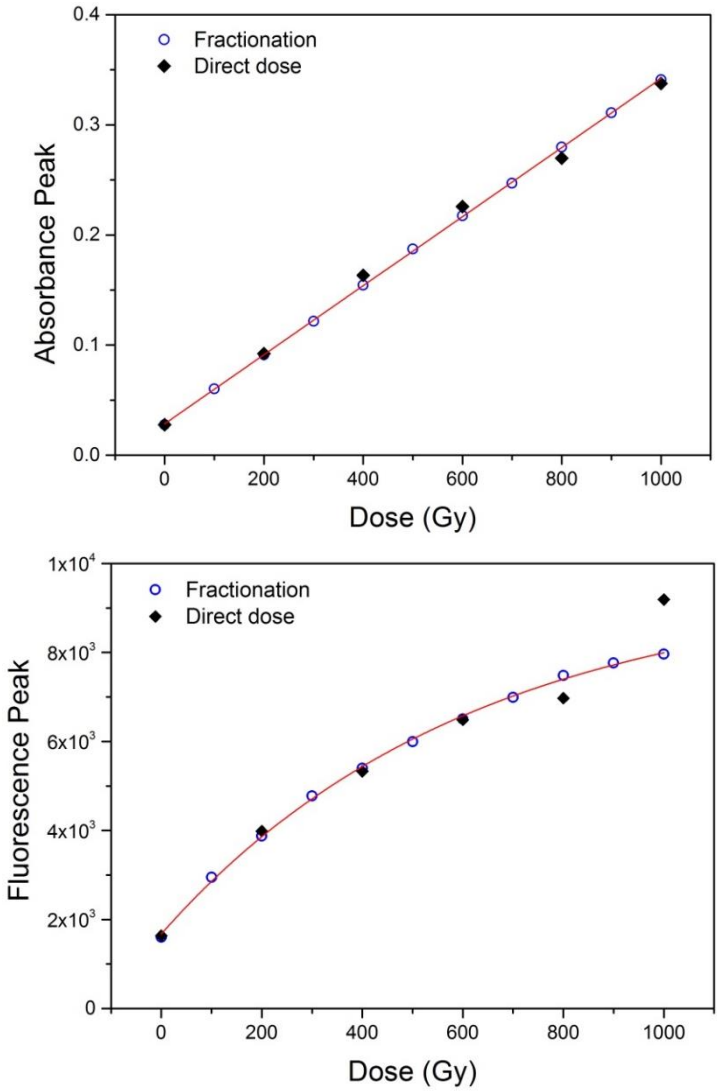

Figure 4.8: Analysis of dose fractionation in absorbance and fluorescence spectra.

Conclusion: The absorbance response of the dosimeter is independent of dose fractionation up to 1 kGy, while the fluorescence response differs at 1 kGy. In both cases the dosimeter is independent on dose fraction at the medical dose range.

4.2.3. Effect of the molecular weight of PEGDA

Hypothesis: The molecular weight of PEGDA influences the fluorescence response of the dosimeter. A more compacted polymer matrix is expected from a higher molecular weight of PEGDA, facilitating the fluorescence from the dye.

In order to analyze the results it is important to know that the desired characteristics for the fluorescence of the dosimeter are:

- High contrast between unirradiated and irradiated states.
- Low background (unirradiated state) to facilitate the measurement.

Experiment: Slides of *Composition 1* were made with PEGDA-575 g/mol (usual), PEGDA-250 g/mol and PEGDA-700 g/mol. They were cured with *Lamp 1* (surface power density: 4.5 mW/cm^2) for 10 min and irradiated in *Gammacell 3* (dose rate: 140 Gy/min) to 1 kGy. Fluorescence was excited with the 532 nm Nd:YAG laser.

Results: Normalized absorbance and fluorescence spectra are shown in figure 4.9. The response varies for the different molecular weights. PEGDA-250 has the highest fluorescence signal when irradiated, but it also has the highest fluorescence when unirradiated, resulting in an undesired high fluorescent background. Comparing PEGDA-575 and PEGDA-700, the first one shows higher fluorescent contrast and lower fluorescent background, and therefore PEGDA-575 is preferable.

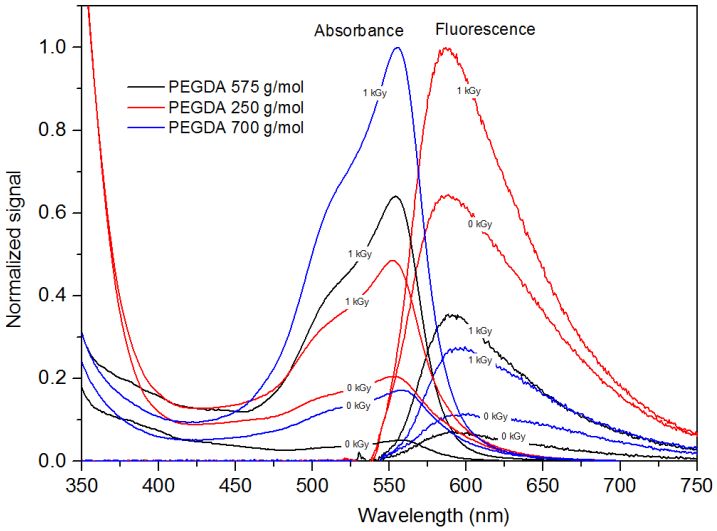

Figure 4.9: Normalized absorbance and fluorescence spectra at 0 kGy and 1 kGy for slides of *Composition 1* with different molecular weights of the host polymer, PEGDA.

It was observed that the three transparent polymers acquired color when adding the dye, and this color was different for each type: yellowish for PEGDA-575, pinkish for PEGDA-250, and slightly orange for PEGDA-700. In the polymers' compositions, variation in the amount of the inhibitors monomethyl ether hydroquinone (MEHQ) and butylated hydroxytoluene (BHT) was found:

- PEGDA-575: 400-600 ppm (parts per million) MEHQ
- PEGDA-250: 100 ppm MEHQ
- PEGDA-700: 100 ppm MEHQ + 300 ppm BHT

Therefore, it seems MEHQ prevents a reaction of the polymer with the dye. This idea was tested by adding MEHQ to PEGDA-250 before adding the dye, and the solution is less colorful than without extra addition of MEHQ.

Conclusion: PEGDA-575 is better for fluorescence measurements due to its high contrast and low background. The importance of the high amount of MEHQ inhibitor present in PEGDA-575 was demonstrated.

4.2.4. Effect of hydrogen donors (solid additives)

Hypothesis: The fluorescence response of the dosimeter improves (higher fluorescence contrast and lower fluorescence background) by using hydrogen donors.

Experiment: Slides of *Composition 1* without additives and with TCPO and Chloral Hydrate as additives (same molarity in both cases: 1.41 mM) were cured with *Lamp 1* (surface power density: 4.5 mW/cm^2) for 10 min and irradiated in *Gammacell 3* (dose rate: 140 Gy/min) to 1 kGy. Fluorescence was excited with the 532 nm Nd:YAG laser.

Results: Normalized absorbance and fluorescence spectra are shown in figure 4.10. Additives increase both background signals, more in the case of TCPO. It can be observed that both the highest contrast fluorescence and the lowest fluorescence background, occur for the case of no additives.

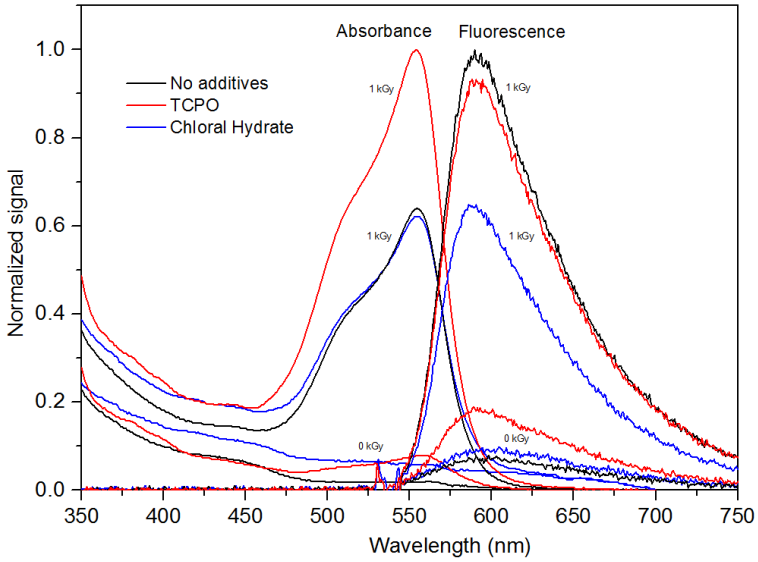

Figure 4.10: Normalized absorbance and fluorescence spectra at 0 kGy and 1 kGy for slides of *Composition 1* without additives, with TCPO and with Chloral Hydrate.

Conclusion: The initial hypothesis about the use of hydrogen donors was not correct. On the contrary, it was observed that it was preferable to avoid the use of any additive, so the TCPO was removed, changing to *Composition 2*.

4.2.5. Effect of the photoinitiator (Paper II)

Hypothesis: The photoinitiator affects the dose response of the dosimeter. In chapter 4.1., it was observed from the DoE model that TPO and its interaction with the dose were influential factors in the absorbance peak increase. The dye fluorescence depends on the matrix rigidity, which at the same time depends on the photoinitiator used for curing.

Therefore, different fluorescence responses to dose are expected for different photoinitiators.

1. Radiochromic effect caused by radicals
2. Radiochromic effect caused by UV photolysis (photoionization)

Type I and Type II photoinitiators

Experiment: Fluorescence of slides of *Composition 2* with different photoinitiators (TPO, CPTX, CQ and ITX) was analyzed for 0 and 300 Gy. Except for TPO, which is a type I photoinitiator, a co-initiator was needed: EDB and DMAEM were used for that purpose. The photoinitiator to co-initiator ratio used was 1:2, by using concentrations of 14.35 mM for photoinitiators and 30 mM for co-initiators (*Neumann, 2006*). All photoinitiators were dissolved in PEGDA-575 and their concentration in the total solution was 1.41 mM. Slides were cured with *Lamp 1* (surface power density: 4.5 mW/cm^2) for 10 min, except samples with CQ which were cured with *Lamp 2* (surface power density: 25 mW/cm^2) for 20 min. The absorbance band of CQ at around 470 nm requires the use of *Lamp 2* whose emission wavelength is 460 nm. Slides were irradiated in *Gammacell 3* (dose rate: 140 Gy/min) to 300 Gy. Fluorescence was excited with the 532 nm Nd:YAG laser.

Results: Figure 4.11 shows the fluorescence of the unirradiated and irradiated slides. The use of the co-initiator DMAEM decreases the contrast in all cases. Samples with CPTX have a high fluorescence background, so they were also discarded. The highest contrast occurs for TPO and CQ+EDB, both with similar results. Although the result for CQ+EDB was observed to be better due to its lower background, its long curing makes it low desirable.

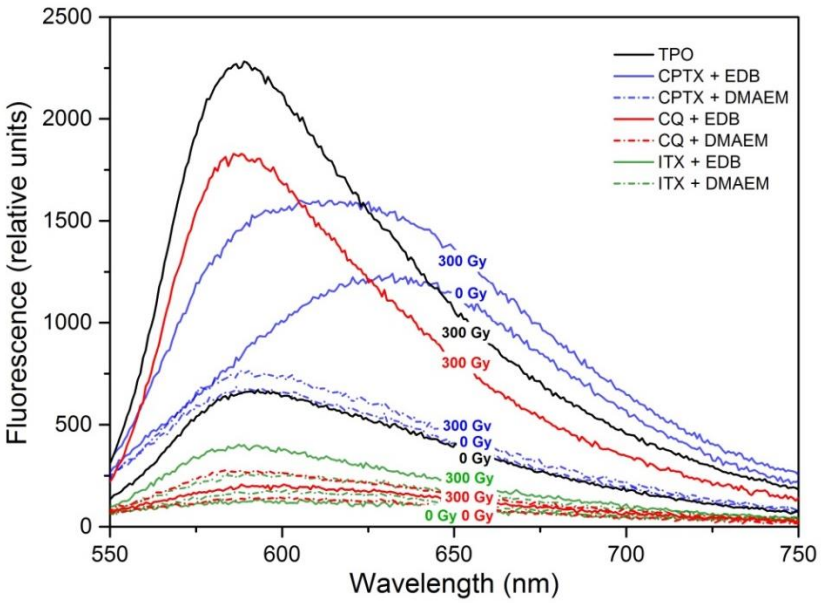

Figure 4.11: Fluorescence spectra of slides (unirradiated and irradiated to 300 Gy) with type I photoinitiator (TPO) and type II photoinitiators.

Paper II - Radiochromic and radiofluorogenic 3D solid polymer dosimeter; effect of the photoinitiator

Experiment: Slides of *Composition 2* were made with different photoinitiators: TPO at concentrations of 1.41 mM and 0.60 mM, ITX at 1.41 mM with EDB as co-initiator, and CQ at 1.41 mM also with EDB. Five slides per photoinitiator type were cured at once with *Lamp 1* (surface power density: 4.5 mW/cm^2) for 10 min. Slides of CQ were cured with *Lamp 2* (surface power density: 25 mW/cm^2) for 20 min each slide. They were studied for a large dose range: 2, 6, 8, 10, 20, 50, 100, 300, 600 and 1000 Gy. Irradiations were carried out in *Gammacell 1* (dose rate: 5 Gy/min). Fluorescence was excited with the 532 nm Nd:YAG laser.

Results: Paper II presents the results for TPO and ITX + EDB; the results for CQ + EDB are also included here. Figure 4.12 shows the normalized absorbance and fluorescence spectra of slides made with the different photoinitiators. Figure 4.13 shows the analysis of the peaks of both signals as function of the dose.

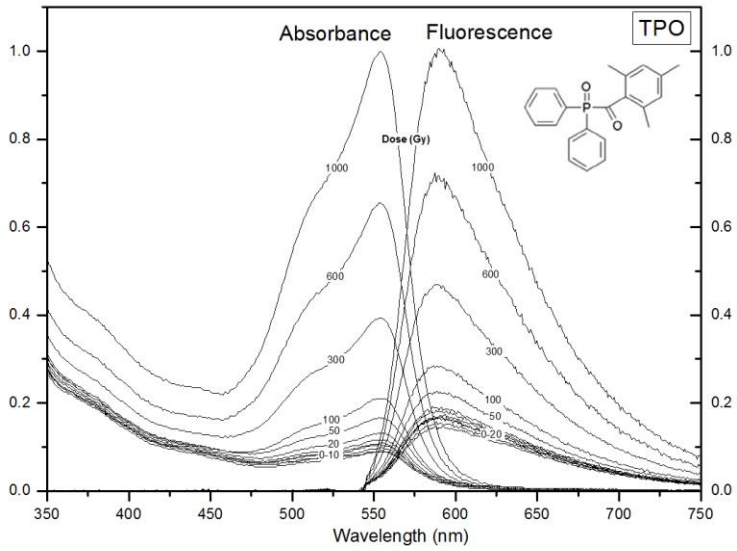

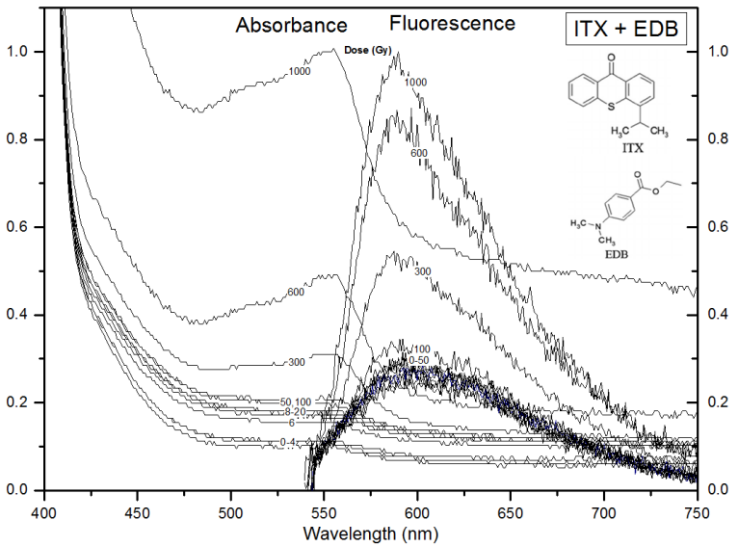

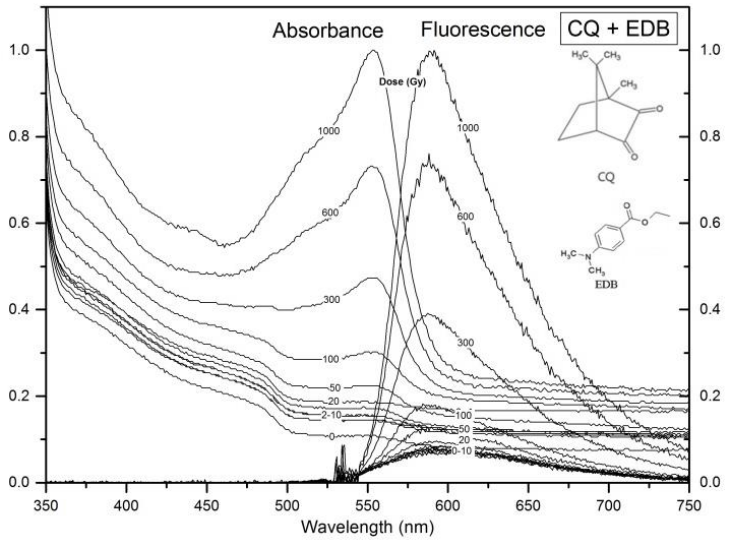

Figure 4.12: Normalized absorbance and fluorescence spectra for slides with TPO, ITX + EDB and CQ + EDB as photoinitiators.

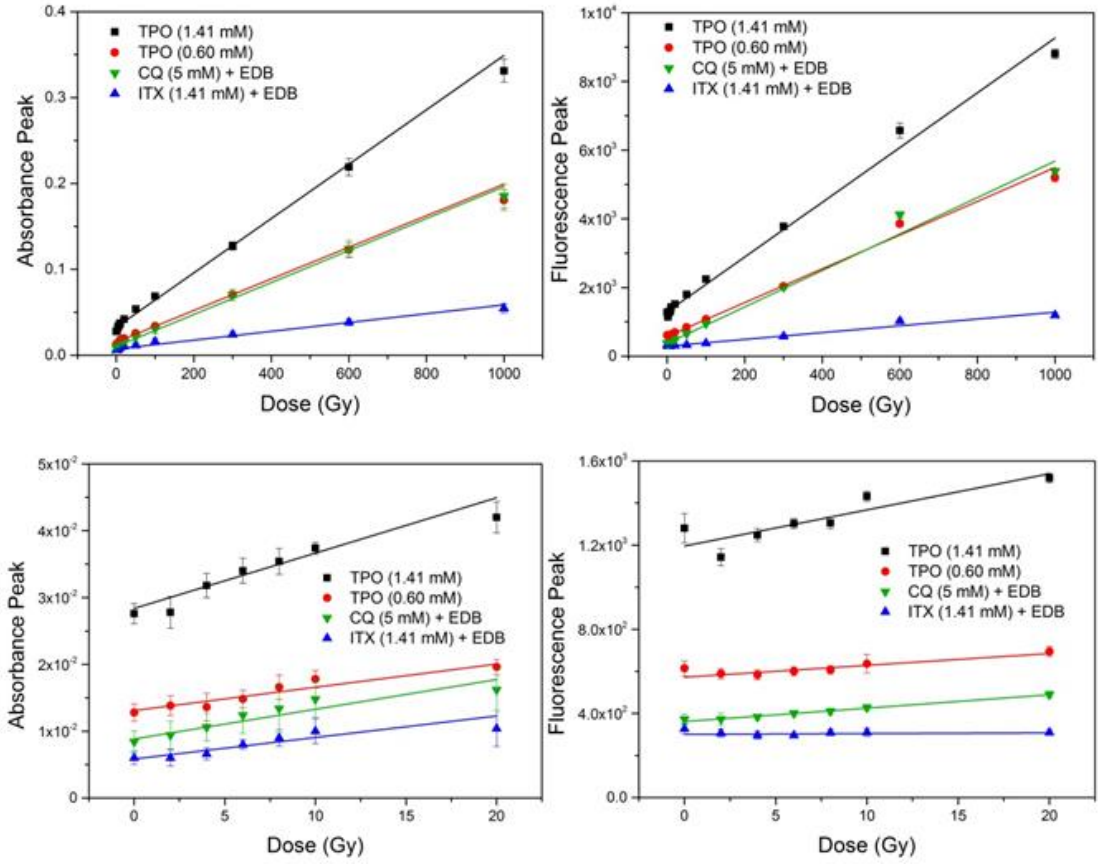

Figure 4.13: Absorbance and fluorescence peaks as function of the dose for slides with different photoinitiators (5 slides per type). Below: zoom in for low doses.

In figure 4.13 it can be seen that ITX has the lowest fluorescent response. This is due to the heavy atom effect (chapter 1.4.2; quenching) from sulfur. On the contrary, TPO (1.41 mM) presents the highest contrast. The problem of TPO is its high fluorescence background, which is even higher than when irradiated to 2 Gy afterwards. This is due to presence of secondary species from the photoinitiator after curing, which are fluorescent. When decreasing the amount of TPO, the fluorescence background decreases, but the fluorescence sensitivity to dose decreases too. Therefore, it is not only radiation that affects the dye, but also these species from TPO, which contain benzene groups that emit at 300-350 and therefore stimulate the dye.

Mixture of Type I photoinitiators

Experiment: The sensitivity to low doses was studied also for pellets of *Composition 5* (low dye, high HEMA) with TPO and with a mixture of type I photoinitiators: 20% Irgacure 819 and 80% Darocur 1173 in a concentration of 0.5 vol% in PEGDA-575. Four pellets of each type were cured with *Lamp 1* (surface power density: 4.5 mW/cm^2) for 10 min and irradiated in *Gammacell 1* (dose rate: 5 Gy/min) to 5, 10 and 20 Gy. Fluorescence was excited with the 520 nm diode laser.

Results: Figure 4.14 shows that the background is lower for the mixture of photoinitiators than for TPO. But in both cases the fluorescence is not sensitive to low doses, although the absorbance it is.

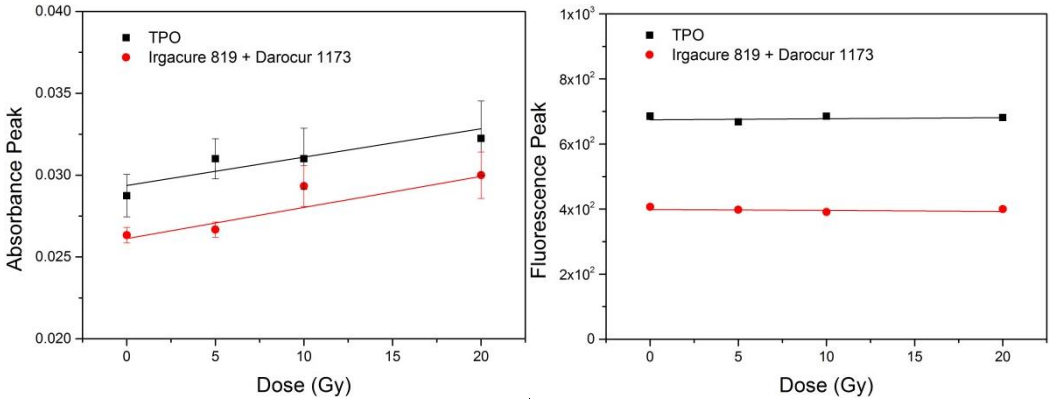

Figure 4.14: Absorbance and fluorescence peaks as function of the dose for pellets made with different photoinitiators. Error bars smaller than the markers in the case of the fluorescence response.

Conclusion: The starting hypothesis was accomplished: it was observed that the response is dependent on the type of photoinitiator. The type II photoinitiators CQ and CPTX and the co-initiator DMAEM, were discarded due to its long curing time, high fluorescence background, and low fluorescence contrast, respectively. The absorbance

and fluorescence responses of TPO and ITX + EDB for a large dose range were presented in Paper II. The use of ITX + EDB lowers the fluorescence background, but it is not sensitive to low doses. The same happens when using the mixture of type I photoinitiators: Irgacure 819 and Darocur 1173. Fluorescence sensitivity to low doses needs to be improved.

4.2.6. Effect of the secondary polymer

Hypothesis: Increasing the amount of secondary polymer results in a stiffer matrix that facilitates dye fluorescence and increases fluorescence sensitivity to low doses.

Experiment: A new composition with more HEMA was tested (*Composition 3*). Four pellets were cured with *Lamp 1* (surface power density: 4.5 mW/cm^2) for 10 min and irradiated in *Gammacell 1* (dose rate: 5 Gy/min) to 5, 10, 20, 30, 50, 75 and 100 Gy. They were compared with pellets made of *Composition 2*. Fluorescence was excited with the 520 nm diode laser.

Results: Figure 4.15 shows the results of *Composition 3* for low doses, which follow a straight line contrary to previous results. Irradiations were continued to higher doses and comparison of results with usual *Composition 2* (figure 4.16) show that, although both compositions have a similar fluorescence slope, the fluorescence sensitivity to low doses has successfully increased. Besides, the background fluorescence of *Composition 3* is lower due to the more diluted dye and the lower proportion of TPO. The latter may also be another reason for the improvement of the fluorescence sensitivity at low doses, since for a lower amount of photoinitiator there will be less remaining reactive species from TPO after photocuring.

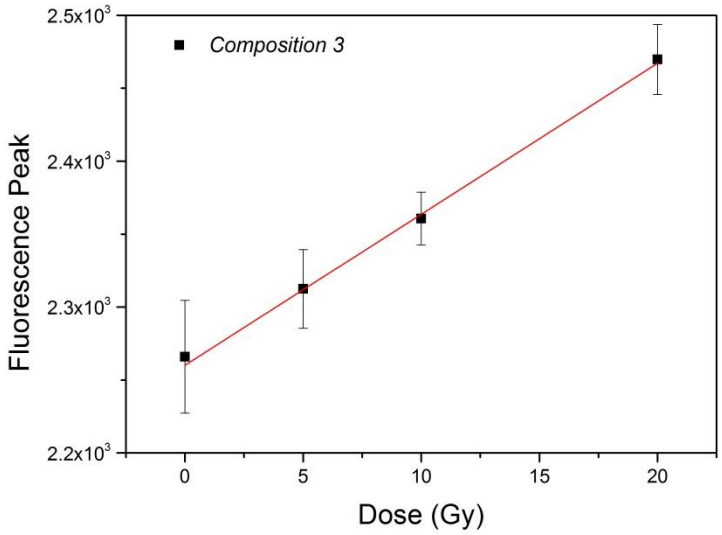

Figure 4.15: Fluorescence response for low doses for pellets made of *Composition 3*, characterized for a higher amount of HEMA. (Note the suppressed zero.)

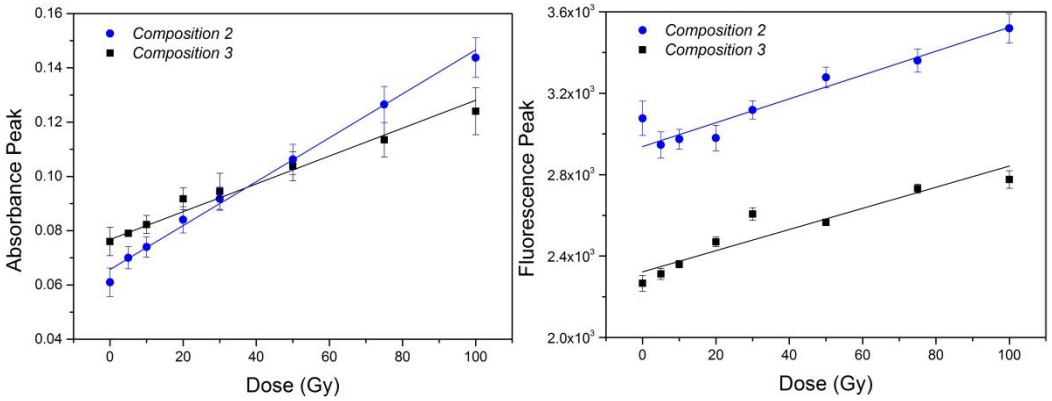

Figure 4.16: Absorbance and fluorescence responses to dose for the usual *Composition 2* and the new *Composition 3* with a higher amount of HEMA.

This result suggests that the local environment of the dye molecule is now more packed, which favors its fluorescence by restricting its vibrational and rotational movements. HEMA increases the stiffness of the polymer matrix by increasing its T_g. On one hand, HEMA increases the crosslinking density and therefore reduces the free volume, leading to an increase in T_g. On the other hand, its high polarity (measured in Annexe 2) also increases T_g since strong bonding restricts rotation and atomic movements. The T_g of the PEGDA/HEMA system can be calculated by equation 1.16. The volume fractions of HEMA and PEGDA, their T_g (*Galagan, 2010*), and the total T_g of each composition appear in table 4.1.

Table 4.1: Glass transition temperatures and volume fractions for each composition.

	T_g(℃)	***Composition 2*** **(vol. %)**	***Composition 3*** **(vol. %)**
HEMA	68	0.52	9.43
PEGDA	-25	99.48	90.57
PEGDA/HEMA T_g		-24.5 ℃	-16.2 ℃

Due to the good properties of HEMA, it was tested a composition with HEMA as the host polymer and PEGDA as the secondary. However, due to the low amount of MEHQ inhibitor in HEMA (50 ppm), it results a pink/magenta solution. Therefore, it is necessary adding MEHQ inhibitor.

Conclusion: Results show that the initial hypothesis is true: increasing the amount of HEMA increases the fluorescence sensitivity to low doses. Thanks to the high crosslinking density and the high polarity of HEMA, the T_g of the PEGDA/HEMA system increases, leading to a stiffer polymer matrix.

4.2.7. Effect of the dye

Hypothesis: The dosimeter dose response is due to the dye and not to the matrix.

Experiment: Pellets of *Composition 2* with and without dye (matrix) were cured with *Lamp 1* (surface power density: 4.5 mW/cm^2) for 10 min and irradiated in *Gammacell 1* (dose rate: 5 Gy/min) to 100 Gy. Fluorescence was excited with a 520 nm diode laser.

Results: Figure 4.17 shows the absorbance and fluorescence spectra for the dosimeter and its matrix (without dye). It can be observe how the peaks of both spectra for the matrix do not change much when irradiated. The increase with the dose is clear in the case of the dosimeter, due to the dye.

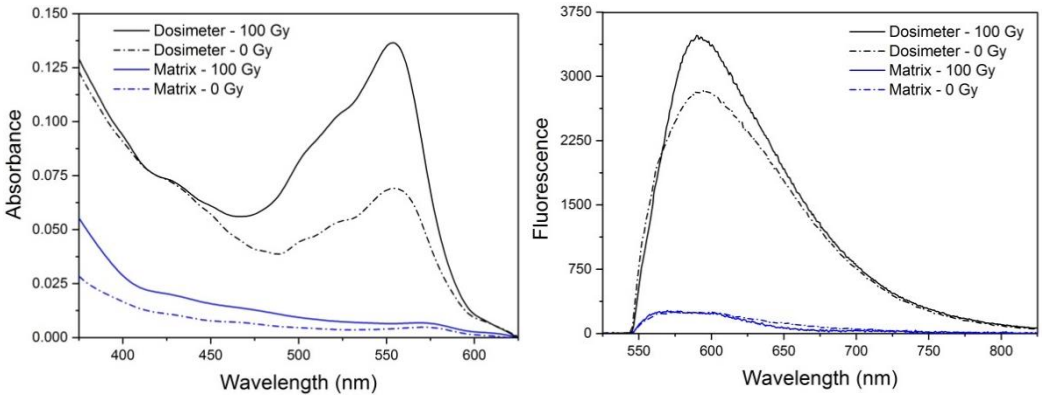

Figure 4.17: Absorbance and fluorescence spectra for the dosimeter and its matrix (without dye), unirradiated and irradiated to 100 Gy.

Conclusion: The dosimeter dose response is due to the dye. The polymer matrix facilitates the fluorescence from the dye but without contributing to its increase when irradiated. Further studies about this are presented in the next chapter about the EPR measurements.

4.3. Dose response by Electron Paramagnetic Resonance signal

Paper III - Radiochromic and radiofluorogenic 3D solid polymer dosimeter; a third signal: Electron Paramagnetic Resonance (EPR).

Hypothesis: Besides the optical signals, an EPR dose response from the stable free radicals originating from the radiochromic dye of the dosimeter is expected.

Experiment: To test this hypothesis, point detector experiments were performed with pellets (4 per type) made of *Composition 2* with and without dye (matrix), cured with *Lamp 1* (surface power density: 4.5 mW/cm^2) for 10 min and irradiated with *Gammacell 1* (dose rate: 5 Gy/min). They were analyzed for the following doses: 5, 10, 20, 30, 50, 75 and 100 Gy. Fluorescence was excited with a 520 nm diode laser.

Results: Figure 4.18 shows the EPR signal (first derivative of the EPR spectra), and the normalized absorbance and fluorescence spectra for the same pellet irradiated at different doses. Figure 4.19 shows the responses of the three signals (peak to peak amplitude for the EPR signal, and peaks for the optical signals) as function of the dose for the dosimeter and its matrix. The three signals were measured for the same pellets, 4 pellets for the dosimeter, and 4 pellets for the dosimeter´s matrix (without dye). The EPR spectra of alanine pellets was also measured for comparison. More details can be found in Paper III.

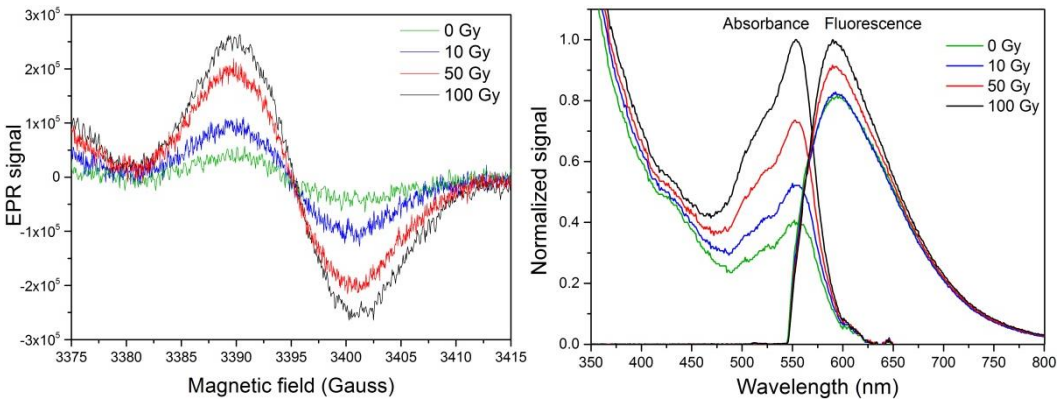

Figure 4.18: a) First derivative of the EPR spectra of a dosimeter pellet irradiated at several doses. b) Normalized absorbance and fluorescence spectra of a dosimeter pellet irradiated at several doses.

Conclusion: It was possible to measure an EPR signal from the dosimeter, which increases with the dose. Due to the EPR it has been observed that free radicals present in the dosimeter are the species that originate from the radiochromic dye and not from the matrix. Therefore, the matrix provides the required properties for the dosimeter, such as solid support, water equivalence, moldable, flexibility, optical clarity, good mechanical and optical properties, without interfering in the radiation response from the dye.

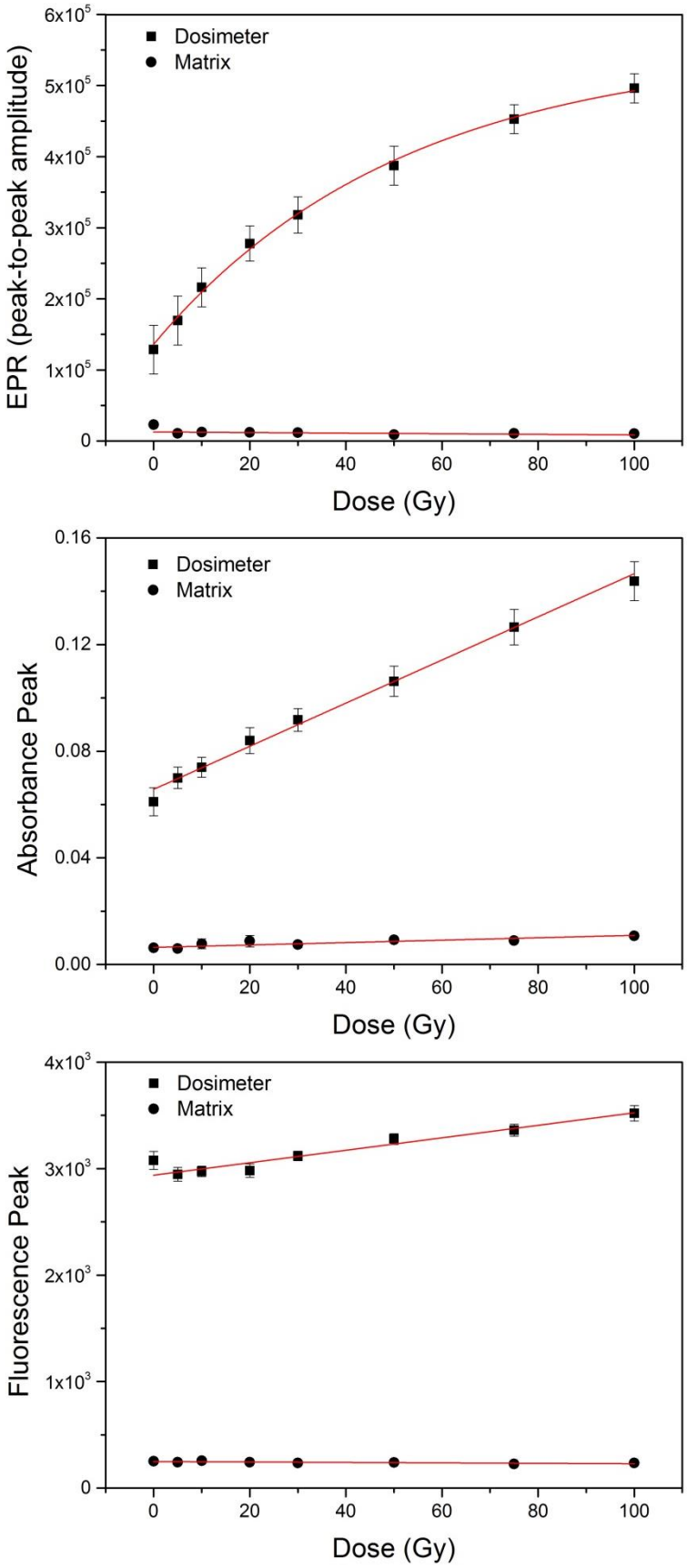

Figure 4.19: EPR, absorbance and fluorescence responses as function of the dose for the dosimeter and its polymer matrix.

4.4. Photocuring

In this chapter, the influence of the photocuring process on the dosimeter is analyzed.

4.4.1. Fourier transform infrared (FTIR) spectroscopy

FTIR spectroscopy is used to confirm photocuring efficiency. A thin layer of *Composition 2* is cured with *Lamp 3* (surface power density: 15 mW/cm^2) in three shots of 5 s, and a last shot of 20 s. After each irradiation the FTIR spectrum is recorded. In figure 4.20, the FTIR spectra of the initial and the final sample are shown, where the following functional groups can be identified: alcohol (O–H), alkane (C–H), carbonyl (C=O), alkene (C=C) with its stretching and twisting modes, and acrylate (CH_2=CHCOO$^-$) (*McMurry, 2016*).

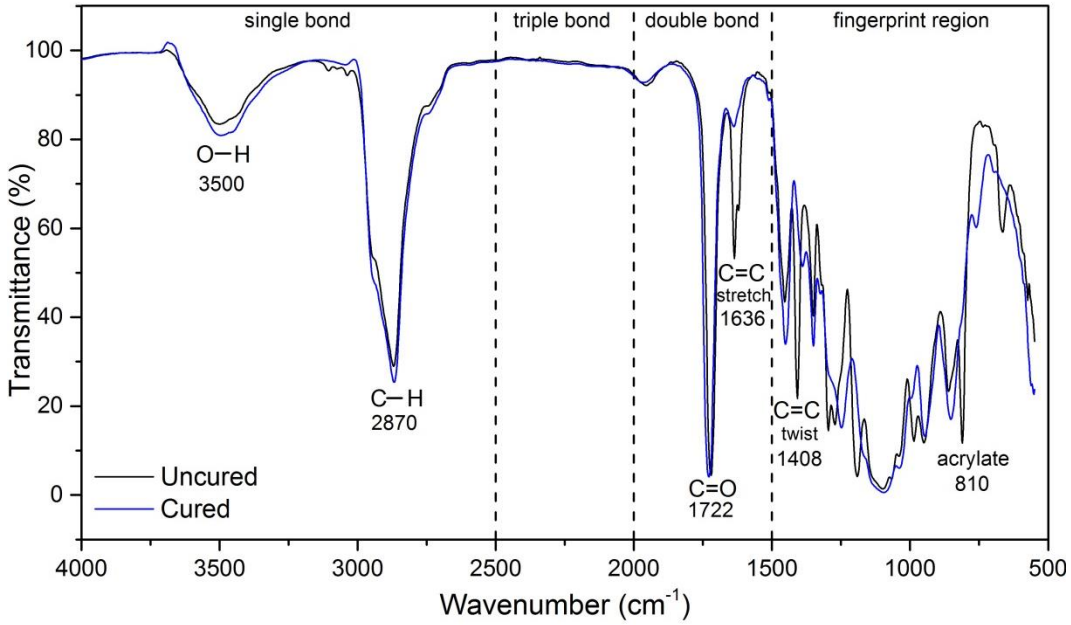

Figure 4.20: FTIR spectra of the uncured and cured sample.

The curing efficiency can be noticed by looking at the C=C bonds. As it was seen in chapter 3.2, the photoinitiator reacts with PEGDA by opening its C=C bonds allowing crosslinking. Therefore, a decrease in the number of C=C bonds (conversion) is expected after curing. The transmittance of this group increases after photocuring, and therefore its absorbance decreases. Absorbance spectra for the region of interest, calculated as $A = 2 - \log(T\%)$, are shown in figure 4.21. The peak at 1454 cm^{-1} could correspond to the aromatic ring (1450 – 1600 cm^{-1}) (*McMurry, 2016*).

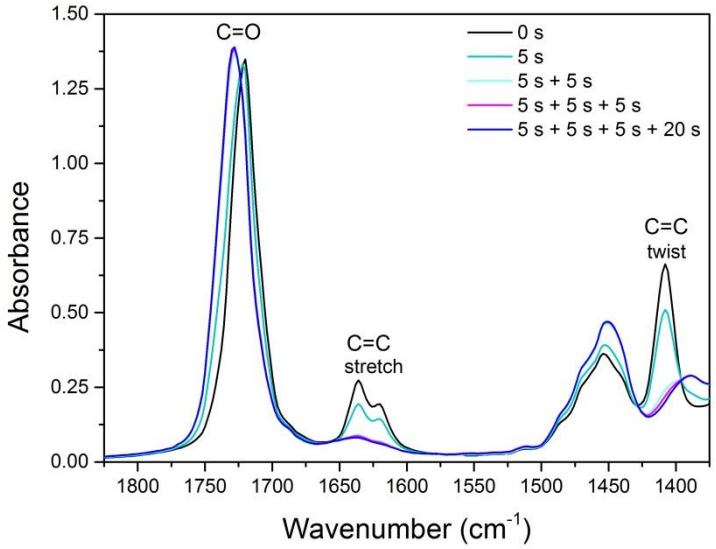

Figure 4.21: Absorbance spectra for the different curing times obtained from the FTIR.

The peaks that were used correspond to the C=C stretching and twisting modes; however, it could also have been used the acrylate peak at 810 cm^{-1} (*Glöckner et. al, 2008*). The percent conversion of the C=C bonds for each curing time (t) was calculated from the area of the absorption bands (A) and using the C=O peak as reference. The following equation (*Wu et. al, 2005*) was used:

$$Conversion(\%) = \frac{\left(\frac{A_{C=C(stretch)} + A_{C=C(twist)}}{A_{C=O}}\right)_0 - \left(\frac{A_{C=C(stretch)} + A_{C=C(twist)}}{A_{C=O}}\right)_t}{\left(\frac{A_{C=C(stretch)} + A_{C=C(twist)}}{A_{C=O}}\right)_0}$$

Figure 4.22 shows the conversion as function of the UV exposure. It can be observed that the solution was successfully photocured after the second exposure. The fitting reaches a 96% of conversion, suggesting that there is a rigid environment allowing the dye to fluoresce.

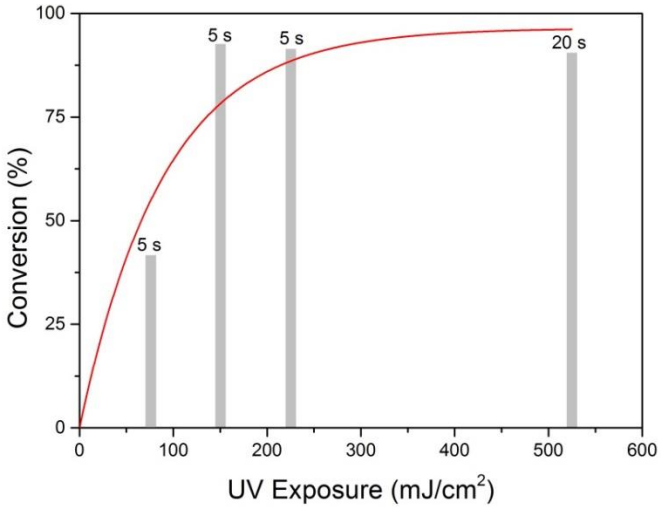

Figure 4.22: Conversion vs. UV exposure.

4.4.2. Reproducibility

Reproducibility can be divided into two: the photocuring reproducibility (measurements of different samples), and the measurement reproducibility (measurements of the same sample). Figure 4.23 shows the improvement of both along the project. All graphs are for unirradiated samples (slides and pellets) made of *Composition 2* and cured with *Lamp 1* (surface power density: 4.5 mW/cm^2) for 10 min.

Figures 4.23a and b show the importance of a proper photocuring. If there is remaining photoinitiator after curing (peaks at 378 and 400 nm in the absorbance spectrum), the fluorescence signal is higher (red and black curves) due to the fluorescence from the photoinitiator. This decreases photocuring reproducibility (compare with blue curve). Regarding measurement reproducibility, it improves by changing the Nd:YAG laser (figure 4.23c) to the diode laser (figure 4.23d). Finally both the photocuring reproducibility (figure 4.23e) and the measurement reproducibility (figure 4.23f), were improved by making pellets and measuring them with the diode laser.

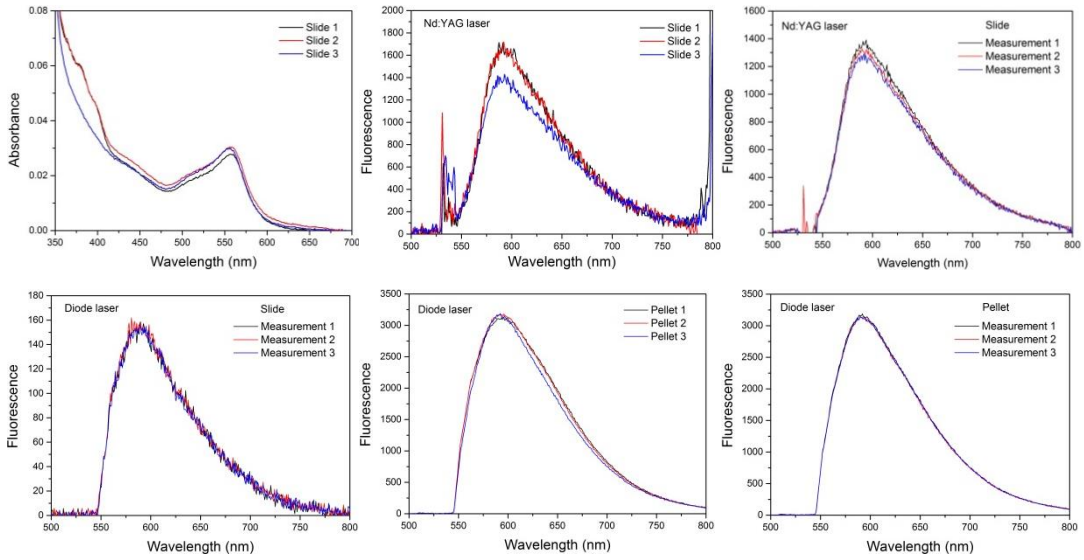

Figure 4.23: Evolution of the photocuring and measurement reproducibility along the project. a) Absorbance spectra of different slides. b) Fluorescence spectra of different slides. Excited with Nd:YAG laser. c) Fluorescence spectra of the same slide. Excited with Nd:YAG laser. d) Fluorescence spectra of the same slide. Excited with diode laser. e) Fluorescence spectra of different pellets. Excited with diode laser. f) Fluorescence spectra of the same pellet. Excited with diode laser.

4.4.3. Surface power density

Cuvettes of *Composition 1* were cured with *Lamp 1* for 10 min at different surface power densities: 3.5 mW/cm^2, 10.7 mW/cm^2 and 17.0 mW/cm^2. They were irradiated to high doses with *Gammacell 3* (dose rate: 140 Gy/min): 100, 200, 300, 400, 500, 600, 700, 800, 900 and 1000 Gy. Results are shown in figure 4.24.

It can be seen how the slope of the dose response decreases when increasing the surface power density. This may mean that samples cured for the same time at higher powers are harder and allow less diffusion, giving a lower response.

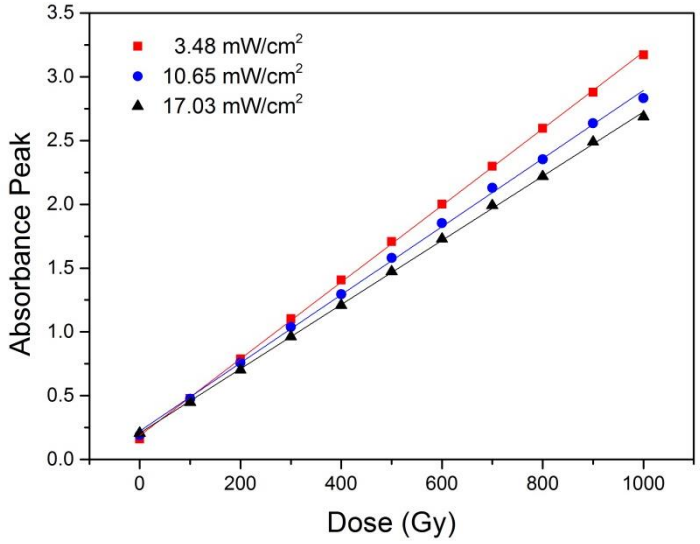

Figure 4.24: Absorbance peaks as function of the dose, for cuvettes of *Composition 1* cured with *Lamp 1* for 10 min at different surface power densities.

4.4.4. Surface power density and curing time

Pellets of *Composition 2* were cured with *Lamp 3* in four different ways (fast, medium and slow curing) by changing the surface power density and the curing time:

- Method 1 - Fast: 5.5 mW/cm^2, 1 min. Surface energy density: 330 mJ/cm^2.
- Method 2 - Medium: 0.4 mW/cm^2, 5 min. Surface energy density: 120 mJ/cm^2.
- Method 3 - Slow: 0.065 mW/cm^2, 50 min. Surface energy density: 195 mJ/cm^2.

Pellets were irradiated to 50 Gy with *Gammacell 1*. Fluorescence was excited with a 520 nm diode laser, and SpectraSuite software was used this time. Absorbance and fluorescence signals of the pellets were measured to analyze the dose sensitivity and the post-irradiation stability.

Figure 4.25 shows the results. For the dose response, the slope is similar for the different curing methods in both absorbance and fluorescence. Therefore, the curing method has no impact on the dose response. However, it is clearly affecting the background signal, being the lowest in the case of samples cured by method 1 (fast). Regarding post-irradiation stability, it seems that the most stable samples are the ones cured by method 1. However, due to the large uncertainties, it is not possible to confirm this to a high level of confidence and further investigation is required.

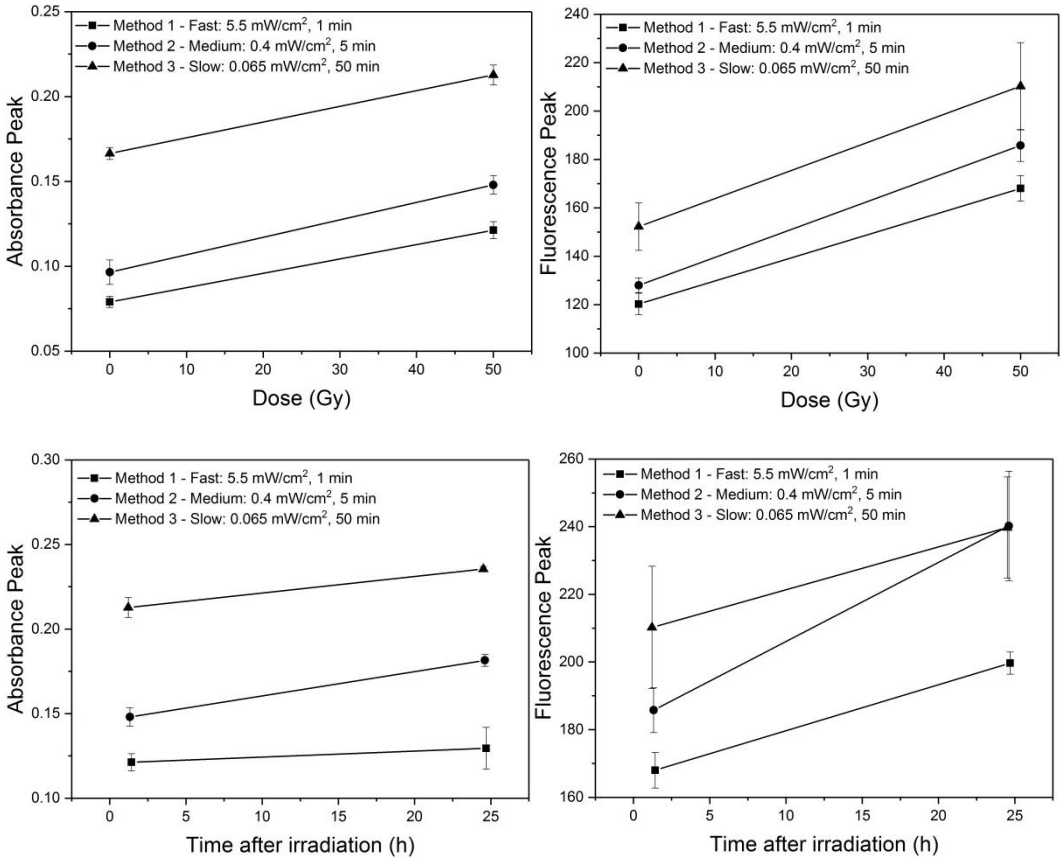

Figure 4.25: Absorbance and fluorescence peaks for pellets cured by different methods. Analysis of the dose sensitivity and post-irradiation stability.

Conclusion: In this chapter it has been ascertained by FTIR spectroscopy that the photocuring is effective; converting around 100% of PEGDA into solid, and therefore allowing the dye to fluoresce. It has been seen that reproducibility improves by making pellets and measuring them with a diode laser. It was also studied the effect of photocuring in the absorbance response at high doses, which decreases when increasing the surface power density. Finally, it was observed that photocuring with a high surface power density in a short time allows lowering the background signal (absorbance and fluorescence) and it seems to help with post-irradiation stability.

4.5. Stability

In this chapter, the pre- and post- irradiation stability of the dosimeter are analyzed.

4.5.1. Pre-irradiation stability

Slides of *Composition 2* made with different photoinitiators (5 slides per type) were cured with *Lamp 1* (surface power density: 4.5 mW/cm^2) for 10 min. Their absorbance spectra were measured after curing up to 40 days. A change in the absorbance peak over time was observed (figure 4.26). In the case of TPO, slides are stable at around 20 days after curing.

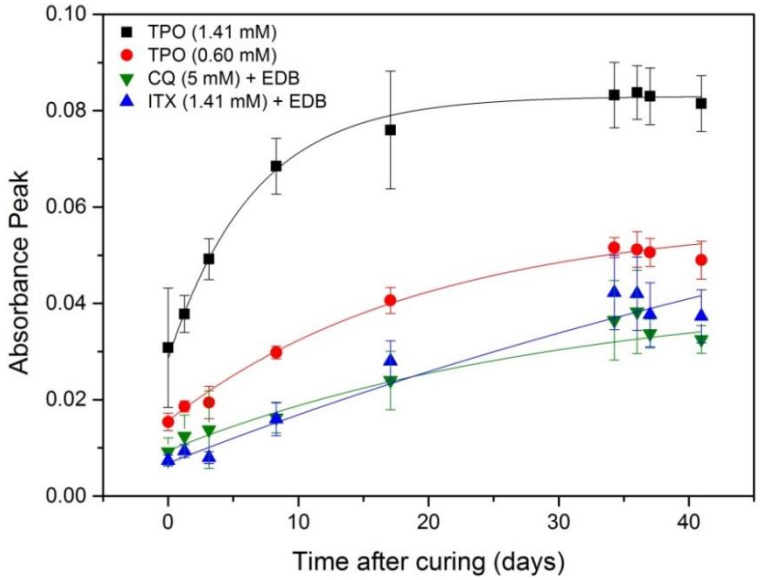

Figure 4.26: Pre-irradiation stability. Absorbance peaks for slides made with different photoinitiators measured over time after curing.

Stability of samples with different concentration of dye was analyzed by measuring absorbance and fluorescence signals over time for slides (three per type) made of *Composition 2* (dye 61 mM) and *Composition 4* (dye 6.1 mM). They were cured with *Lamp 1* (surface power density: 4.5 mW/cm^2) for 10 min. Fluorescence was excited with a 520 nm diode laser. Results (figure 4.27) show that the lower the dye concentration, the more stable is the dosimeter after curing.

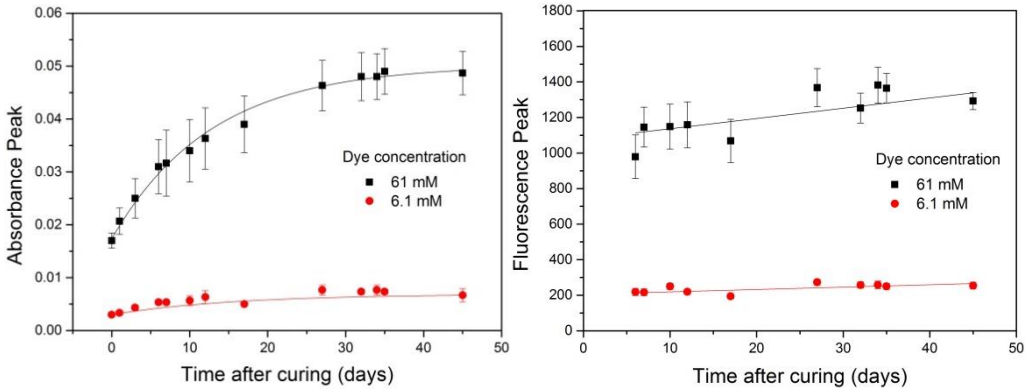

Figure 4.27: Pre-irradiation stability. Absorbance and fluorescence peaks for slides made with different dye concentration, measured over time after curing.

4.5.2. Post-irradiation stability

Pellets of *Composition 5* were cured with *Lamp 3* (surface power density: 15 mW/cm^2) for 2 min. Mercapto and citric acid were added to this composition in a concentration of 10 vol% and 5 vol% respectively, to study their effect in the post-irradiation stability. Pellets (4 per type) were irradiated to 50 Gy in *Gammacell 1* (dose rate: 5 Gy/min). Fluorescence was excited with the 520 nm diode laser, and the spectra were obtained with SpectraSuite software. Figure 4.28 shows that adding mercapto (alone or together with citric acid) decreases the background signal and helps with post-irradiation stability. However, when using mercapto, fluorescence sensitivity to dose decreases, which may be due to the heavy atom effect (chapter 1.4.2; quenching) from sulfur.

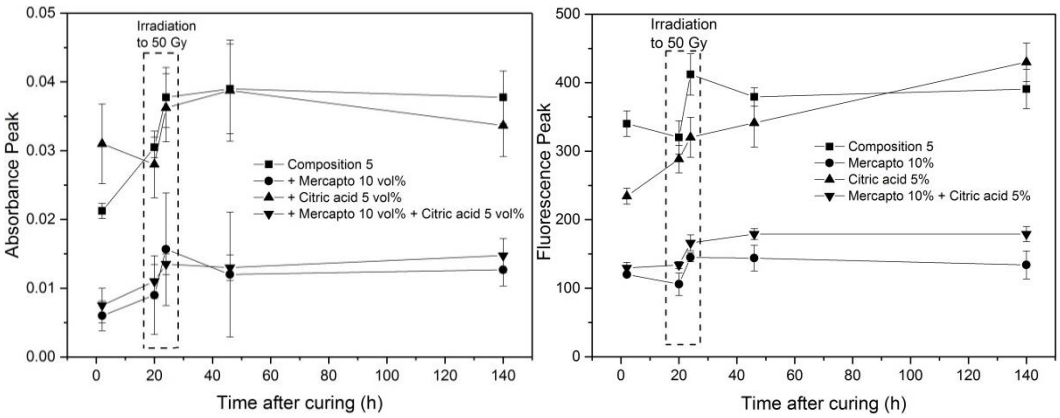

Figure 4.28: Pre- and post-irradiation stability. Absorbance and fluorescence peaks for slides made with mercapto and citric acid, measured over time.

Conclusion: In this chapter it was observed that the absorption and fluorescence response of slides with TPO are stable within approximately 20 days after curing; that lowering the dye concentration helps with pre-irradiation stability; and that adding mercapto helps with post-irradiation stability.

4.6. Dose rate dependence

In this chapter, the dose rate dependence of the dosimeter is analyzed.

Experiment: Pellets of *Composition 3* were cured with *Lamp 3* (surface power density: 15 mW/cm^2) for 2 min. They were irradiated (4 in each gammacell) in *Gammacell 1* (dose rate: 5 Gy/min) and *Gammacell 3* (dose rate: 140 Gy/min) at 100, 300, 600 and 1000 Gy. Fluorescence was excited with the 520 nm diode laser.

Results: Figure 4.29 shows the absorbance and fluorescence peaks as function of the dose for each gammacell. It can be observed how the absorbance is clearly not dose-rate dependent. For the fluorescence, there is a difference at 1 kGy. When 1 kGy is given to the dosimeter with *Gammacell 1* it takes approximately 3 hours, while with *Gammacell 3* it takes just 7 min. It may be then, that when the dose is deposited slowly, the matrix has time to relax by non-radiative processes, decreasing the fluorescence efficiency. But this difference could also be part of the uncertainty. Further investigation of the fluorescence dose-rate dependence at high doses could be convenient. For lower doses is not dose-rate dependent.

Conclusion: The dose rate dependence of the absorbance and fluorescence responses of the dosimeter requires further investigation.

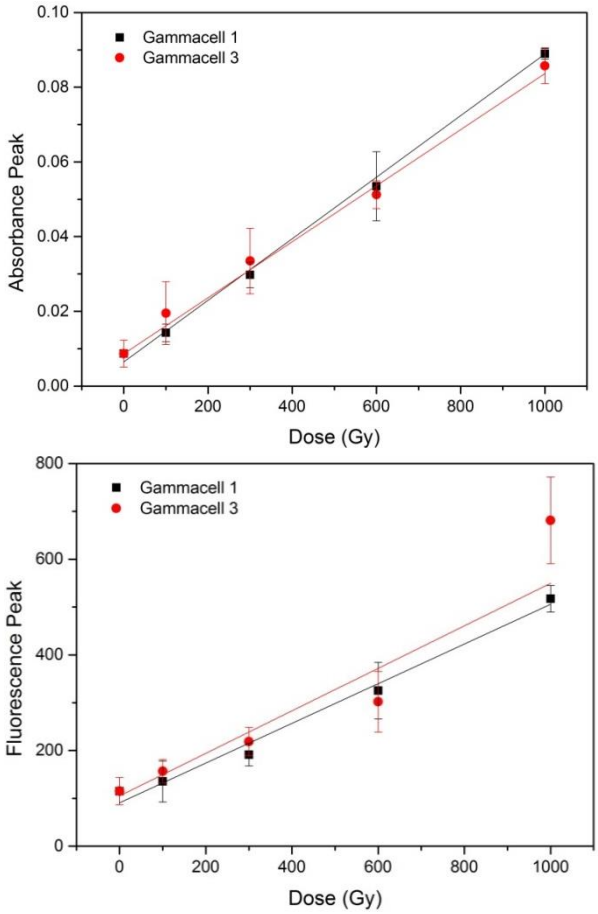

Figure 4.29: Absorbance and fluorescence peaks as function of the dose for pellets irradiated in *Gammacell 1* (5 Gy/min) and *Gammacell 3* (140 Gy/min).

4.7. Water equivalence and energy dependence

In this chapter, the water equivalence and energy dependence of the dosimeter were investigated in several ways: by calculating some physical parameters (Z_{eff}, ρ, ρ_{el}), by computing the mass attenuation coefficients and the stopping powers of the dosimeter with EXAMIN, and by comparing the dose delivered to the dosimeter with that delivered to water in similar geometries using Monte Carlo simulations.

4.7.1. Calculation of water equivalence parameters (Z_{eff}, ρ, ρ_{el})

As has been discussed in chapter 1.2.1.3, three parameters are often used to check whether a material has characteristics close to water: the effective atomic number (Z_{eff}), mass density (ρ) and electronic density (ρ_{el}). These parameters were calculated for the main component of our dosimeter (PEGDA-575), and for the whole dosimeter composition (with the dye in the leuco dye form). They were also calculated for common phantom materials, such as polystyrene and poly(methyl methacrylate) (PMMA). Equations 1.13 and 1.14 were used with m values of 3.5 and 1, for diagnostic radiology and radiotherapy respectively. Results (table 4.2) show good water equivalence of the dosimeter.

Table 4.2: Physical parameters to quantify water equivalence.

Material	Z_{eff} (m = 3.5)	Z_{eff} (m = 1)	$\rho(g/cm^3)$	$\rho_{el}(e^-/g)$ relative to water
Water	7.51	6.60	1.00	1.000
Polystyrene	5.74	5.29	1.04	1.007
PMMA	6.56	5.85	1.18	1.147
PEGDA-575	6.66	5.93	1.12	1.090
Dosimeter	7.00	5.95	1.12	1.079

4.7.2. Analysis of μ/ρ and L_Δ/ρ with EXAMIN

The mass attenuation coefficients (μ/ρ) and the restricted Spencer-Attix mass stopping powers (L_Δ/ρ) are both directly related to the absorbed dose in the medium, as it was previously seen. They are calculated for each material to test water equivalence. For the restricted mass stopping powers, the cutoff energy Δ = 1 keV was used, which means that tracking of electrons with kinetic energy below that value are stopped.

Results for energies ranging from 1 keV to 50 MeV are shown in figures 4.30 a and b in a logarithmic scale. Linear-logarithm scales for energies from 100 keV to 50 MeV are presented in figures 4.30 c and d to emphasize the close matching.

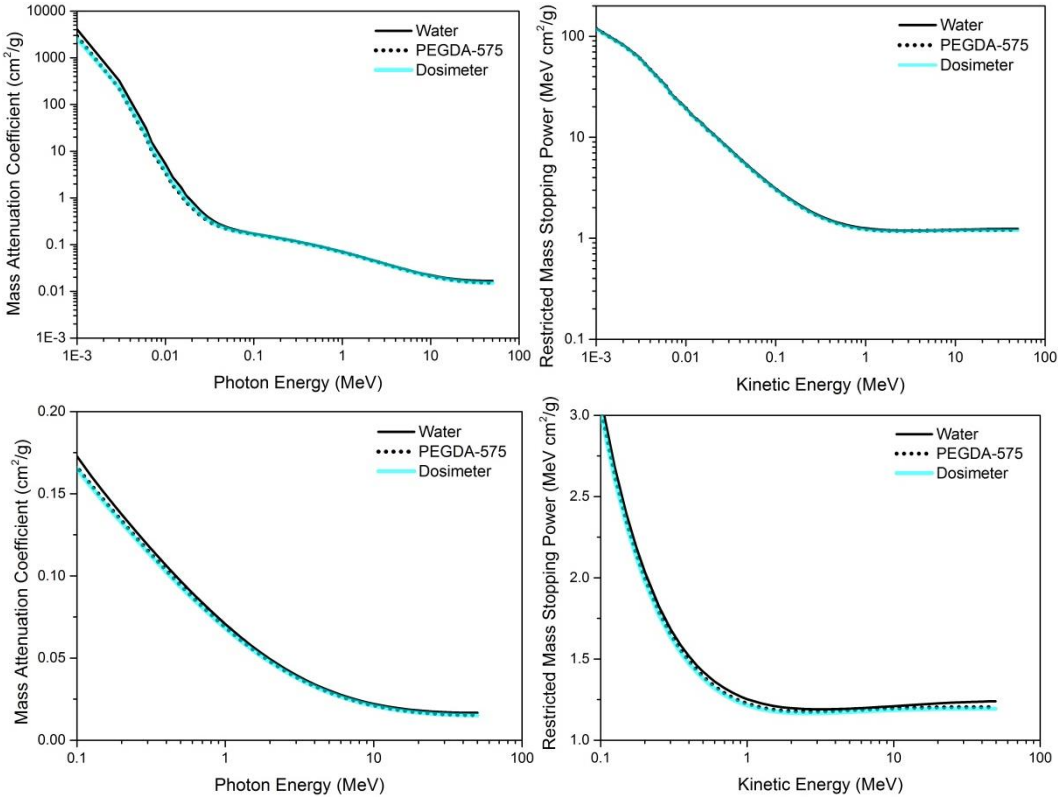

Figure 4.30: Results obtained with EXAMIN. a) Mass attenuation coefficients in a logarithm-logarithm plot. b) Restricted mass stopping powers in a logarithm-logarithm plot. c) Mass attenuation coefficients in a linear-logarithm plot. d) Restricted mass stopping powers in a linear-logarithm plot.

To analyze the water equivalence in more detail, figure 4.31 shows the difference compared with water, calculated as the difference divided by the value for water, as a percentage. Table 4.3 shows some values for the dosimeter deviation to water at specific photon energies: 100 keV (for radiology), 1.25 MeV (^{60}Co energy), 6 MeV and 15 MeV (LINAC energies equivalent to 6 MV and 15 MV, highly used in the clinic).

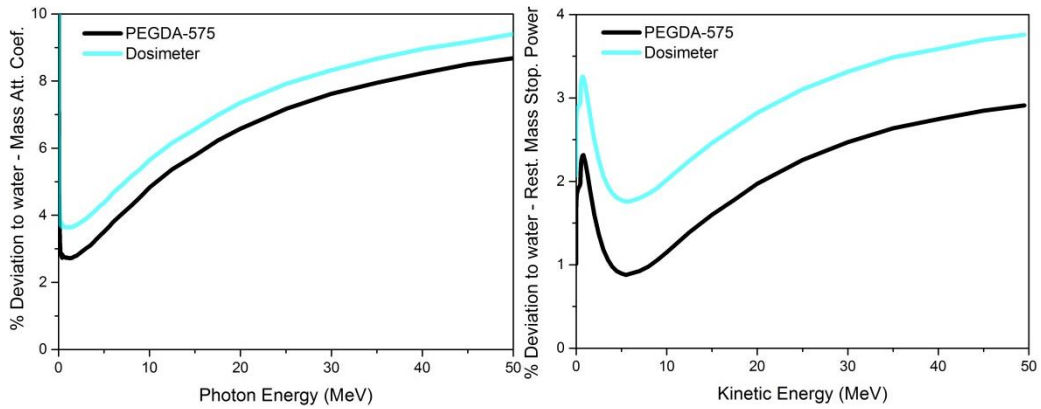

Figure 4.31: Deviation of the mass attenuation coefficients and the restricted mass stopping powers to water.

Table 4.3: Percentage deviation of the mass attenuation coefficient and the restricted stopping power of the dosimeter to water at specific energies.

Energy (MeV)	Mass attenuation coefficient	Restricted mass stopping power
0.1	4.46 %	2.85 %
1.25	3.64 %	2.99 %
6	4.67 %	1.76 %
15	6.56 %	2.46 %

4.7.3. Monte Carlo simulations of monoenergetic beams

The absolute magnitude of mass attenuation coefficients and restricted mass stopping powers is not of primary importance, what really matters is the behavior of the ratio of these magnitudes for the detector against water, and how constant that ratio is as function of energy. To analyze the water equivalence and energy dependence in such a way, the user code EGS_CHAMBER was used to calculate the dose ratio $D_{dosimeter}/D_{water}$ for different monoenergetic photon beams of energies ranging from 0.1 – 20 MeV.

The geometry that was used was a water cube of 50x50x50 cm^3 containing a 1 cm radius sphere in the middle (figure 4.32), which was made of the dosimeter material first and substituted by water afterwards.

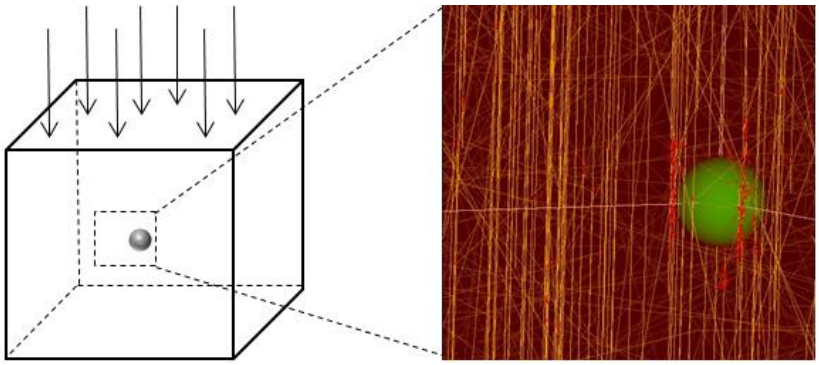

Figure 4.32: Geometry for the dose ratio calculations: water cube with a 1 cm radius sphere. Simulation of photon irradiation (yellow beams) with consequently formation of secondary electrons (red dots) when reaching the dosimeter (green sphere).

Results of the simulation are shown in figure 4.33. It can be seen how the dose ratio between the dosimeter and water is near constant, so the response does not exhibit energetic dependence, above 1 MeV. Below 1 MeV, the dose ratio is much more energy dependent due to the more rapid dependence with energy of the mass-energy absorption coefficient and the mass collisional stopping power.

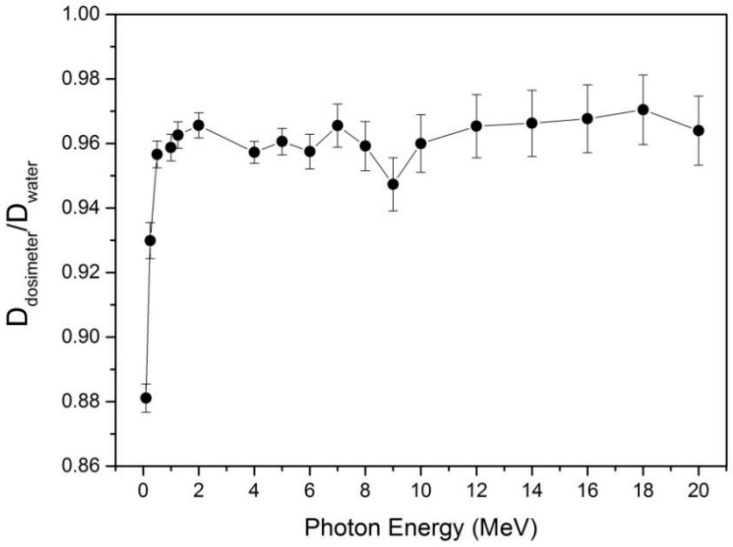

Figure 4.33: Results of the dose ratio calculations for different photon energies.

The same simulation was made for polystyrene (figure 4.34) to compare the dosimeter with a commonly used material in radiotherapy (polystyrene is the main component of the BC-60 scintillator). Results show a very good agreement for energies above 1 MeV, so they are equivalent. For lower energies, our dosimeter is closer to unity, so it is more equivalent to water and less energy dependent than polystyrene.

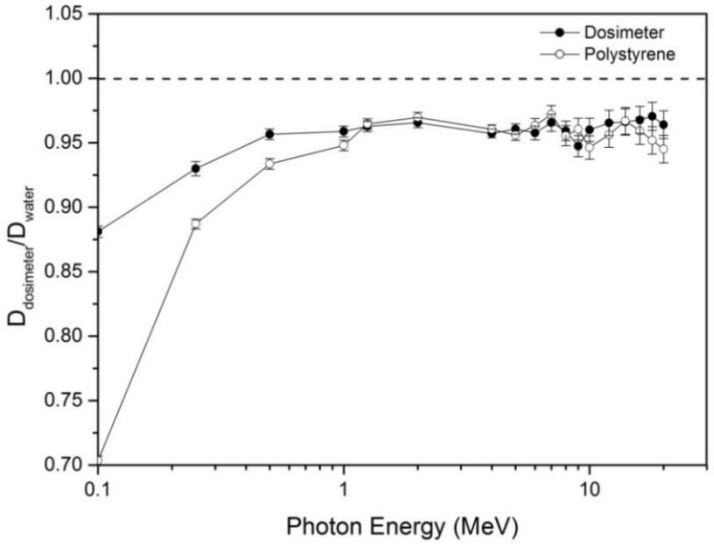

Figure 4.34: Comparison with polystyrene. Logarithmic scale in the x axis.

It was also compared with other dosimeters used in radiotherapy (*Beddar et al., 1992*) (figure 4.35). In this paper they simulate a cylinder of 1 mm radius and 4 mm high instead of a sphere. For our dosimeter, at 1 MeV the dose ratio is 0.953 ± 0.013 for the cylinder and 0.9587 ± 0.0041 for the sphere, which makes the results comparable despite the difference in geometry.

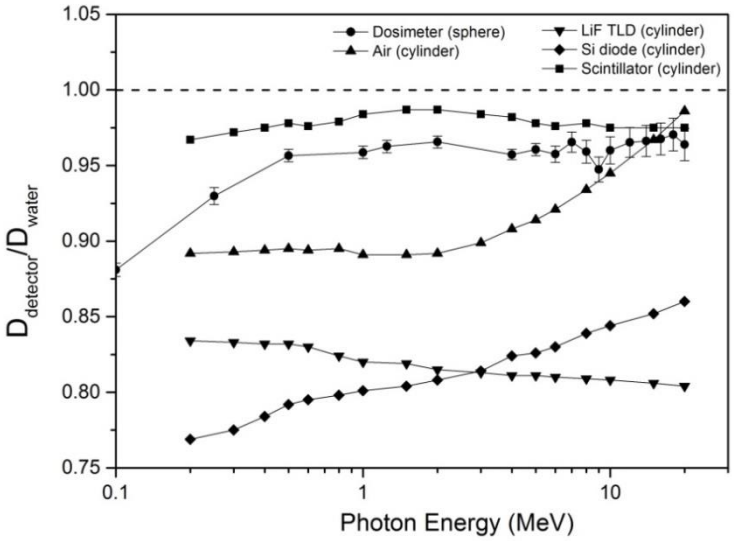

Figure 4.35: Comparison with other detectors. Logarithmic scale in the x axis.

4.7.4. Monte Carlo simulation of a gammacell

The geometry of *Gammacell 3* was simulated [by Mark Bailey] with the DOSRZnrc Monte Carlo user code in order to confirm the homogeneity and the magnitude of the doses delivered to the samples in this irradiator. The volume of the dosimeter that was studied was a cylinder of 7 cm height and 0.65 cm radius, in a region surrounded by air within the Gammacell irradiation volume. Figure 4.36 shows that the dose inside the dosimeter volume is very uniform; it is only slightly different at the bottom, but the rest of the volume receives a similar dose. The use of slides, cuvettes, or dosimeter pellets, will only change the magnitude of the dose very slightly, since these materials never exceeded *n* mm in thickness and cobalt-60 emits photons of energy 1.17 and 1.33 MeV, so the penetration is high: The presence of 3 mm water-equivalent material outside the dosimeter would be expected to change the fluence of photons inside the dosimeter by less than 2 %.

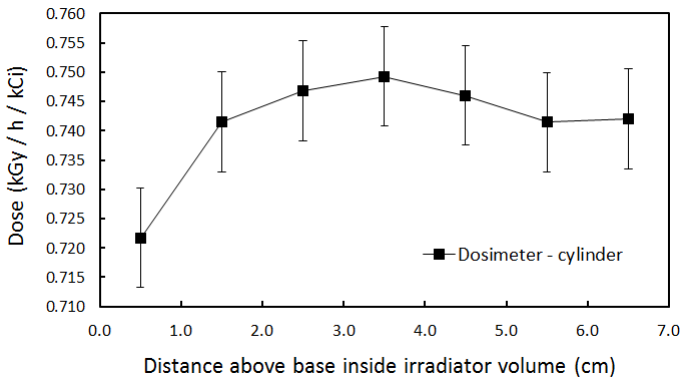

Figure 4.36: Dose in the dosimeter as function of the distance above the base.

4.7.5. Monte Carlo simulations with LINAC phase space files

Monoenergetic photon beams had been simulated for most of the calculations discussed earlier. However, the LINAC produces a continuous X-ray spectrum due to Bremsstrahlung interactions of the original electrons within the target. Since the main application of our dosimeter is to ascertain that the external radiotherapy treatment is delivered as intended by placing it in lieu of the volume targeted for treatment, a closer to laboratory conditions case was simulated, in which the dosimeter is irradiated by the Varian TrueBream™ LINAC (figure 1.1).

The geometry that was used is schematically illustrated in figure 4.37. A sphere of 1 cm radius was placed inside a water phantom at a depth of 10 cm from the surface. The sphere was made by the dosimeter material first, and substituted by water afterwards. The water phantom was a 50x50x50 cm^3 box placed in the source to surface distance (SSD) configuration, which means its surface is placed at the LINAC isocenter (that is at 100 cm from the target as commonly used). The field size is 10x10 cm^2, which is the commonly used reference size. The cutoff energy used for electrons was 512 keV (1 keV higher than the electron rest mass) and 1 keV for photons.

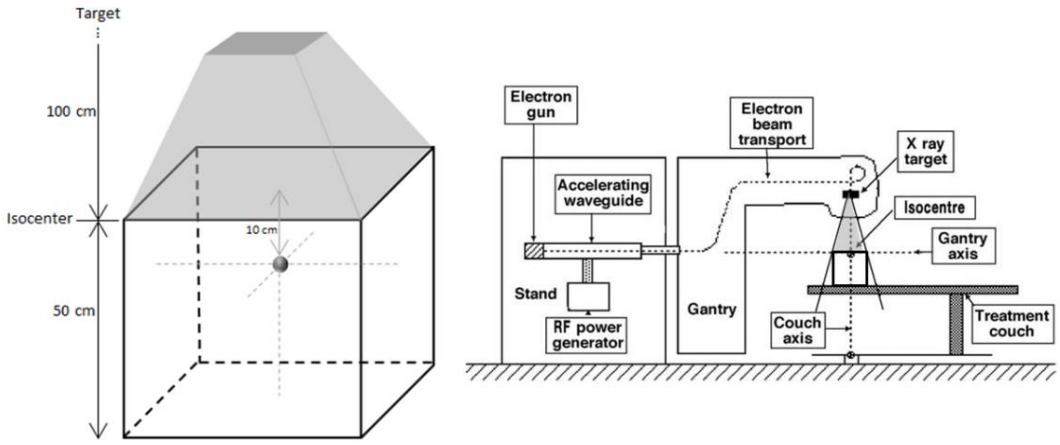

Figure 4.37: a) Geometry for the LINAC irradiation simulation. b) Scheme of the LINAC (adapted from *Podgorsak, 2005*) to show the position of the phantom.

Phase spaces were produced for the following photon energies: 4 MV, 6 FFF (6 MV flattening filter free beam), 6 MV, 10 FFF, 10 MV and 15 MV. The quality of the beam is represented by the tissue phantom ratio (TPR) for a field size of 10x10 cm^2, which is the ratio of the dose to water measured at 20 and 10 cm depths (TPR_{20_10}). The TPR_{20_10} parameter for each energy appears in table 4.4. The dose ratio was computed from the simulations, which is shown as function of the TPR_{20_10} in figure 4.38. The median value (0.9624 ± 0.0012) is very close to water. It can be seen that all the results are contained in the 0.4% deviation range from the median, so it is not very dependent on the beam quality.

Table 4.4: Beam-quality indicator for each photon energy.

Photon energy	TPR_{20_10}
4 MV	0.622
6 FFF	0.632
6 MV	0.666
10 FFF	0.707
10 MV	0.738
15 MV	0.763

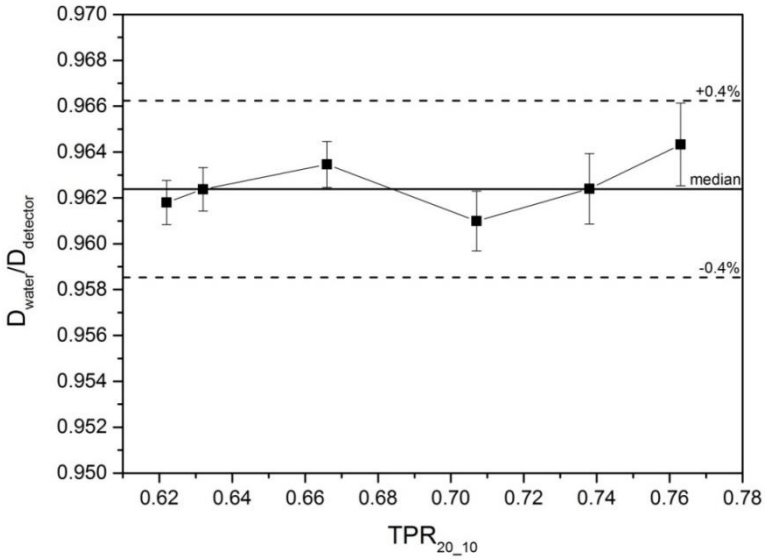

Figure 4.38: Dose ratio results for the LINAC irradiation simulation.

Conclusion: It can be concluded that the dosimeter is water equivalent. This was checked by calculating usual parameters like Z_{eff}, ρ and ρ_{el}; by analyzing μ/ρ and L_Δ/ρ with EXAMIN for a large range of energies; by simulating monoenergetic beams and obtaining the dose ratio to water; and by simulating LINAC phase spaces in laboratory-like conditions. For energies in the radiotherapy range, this dosimeter behaves very close to water and its energy dependence is almost negligible.

Chapter 5

Conclusions

Pararosaniline leuco dye dissolved in a photocurable polymer matrix resulted in a solid state dosimeter, which is radiochromic and radiofluorogenic. The dosimeter presents good optical and mechanical properties, it does not require a container and it can be made in any shape, being therefore a good candidate for use in 3D dosimetry. The fluorescence response is of particular interest as it facilitates detailed mapping of the absorbed 3D dose distribution by optical fluorescence tomography using laser stimulation.

The dosimeter responds to absorbed gamma radiation by an increase in its absorbance and fluorescence signals. Both radiation-induced responses are linear with dose and dose-rate independent for the medical dose range. Also for energies in the radiotherapy range, this dosimeter behaves very close to water and its energy dependence is almost negligible. This was determined by obtaining usual water equivalence parameters, by analyzing mass attenuation coefficients and stopping powers for a large energy range, and by obtaining the dose ratio to water with Monte Carlo simulations (both for monoenergetic beams and LINAC irradiations).

At least two stimuli are known to facilitate the leuco dye reaction: oxidation of the leuco dye caused by free radicals formed by radiolysis of solvent in the matrix due to ionizing radiation, and photoionization caused by short-wave UV photons (below 330 nm) created by secondary electrons formed during irradiation with gamma radiation. This was observed when analyzing the effect of the photoinitiator: the dose response is higher when using TPO as photoinitiator due to UV photolysis. When exposed to UV light, the TPO molecule absorbs UV radiation and decomposes into two free radicals: this is the mechanism used for photocuring of the polymer matrix. The same effect happens when the dosimeter is irradiated with ionizing radiation. The free radicals from TPO contain benzene groups that emit at around 300-350 nm, stimulating the leuco dye and increasing the fluorescence response to absorbed dose. The dosimeter dose response is, however, exclusively due to the dye and not to the free radicals from the matrix. This was ascertained by EPR measurements, a technique that only measures free radicals. On the contrary, the optical signals are highly influenced by the matrix, since the optical properties of the dye are determined by the matrix.

The requirement for the dye to fluoresce is to be constrained in a rigid environment; otherwise it liberates the excess of energy by non-radiative processes. Therefore,

regarding the polymer matrix, on one hand, it needs to provide rigidity to the dye. On the other hand, the matrix needs to be diffusive. Oxygen and radicals' diffusion is necessary to obtain a homogenous dose response through the whole dosimeter volume. Therefore, the design of the matrix is a compromise between the two characteristics: diffusive and rigid. The main polymer, PEGDA, imparts the main properties to the dosimeter, such as diffusion, water equivalence, flexibility, and transparency. The secondary polymer, HEMA, is used to further the mechanical stability of the host polymer by cross-linking, making it stiffer. The high crosslinking density, high polarity, and high T_g of HEMA, leads to a more rigid PEGDA/HEMA polymer matrix and therefore facilitates the dye fluorescence. This was observed to result in an increase of the fluorescence sensitivity to low doses.

Among the different compositions studied, it was observed that the PEGDA/HEMA/TPO system responds very well for high doses. TPO increases the fluorescence response of the dye to ionizing radiation due to the reactive species in which TPO is decomposed, which stimulate the leuco dye. However, there are two problems related to the remaining TPO after photocuring. One problem is that these remaining species, when irradiated to low doses, may continue photocuring of the matrix or may activate the leuco dye. These are two competitive processes that result in a low fluorescence sensitivity to low doses. The second problem is that these reactive species from TPO are fluorescent and therefore the fluorescence background is high, what hinders the 3D readout of the dosimeter. The fluorescence background was decreased by lowering the amount of dye, lowering the amount of TPO, and changing TPO to other photoinitiators, but the fluorescence sensitivity to low doses did not improve. An improvement was noticed when decreasing TPO at the same time than increasing HEMA.

The manufacturing process of the dosimeter is fast and easy, it only requires mixing of five components (leuco dye, ethanol, PEGDA, HEMA and TPO) for 1h, since the leuco dye is easily dissolved. Regarding the photocuring process, the best sample quality was obtained with *Lamp 3* (15 mW/cm^2), which also allowed to reduce the curing time to just 2 min (also for large 3D samples). Photocuring efficiency of this lamp was ascertained by FTIR spectroscopy, showing near full conversion of PEGDA. It was also observed that a high surface power density and a short curing time reduced the fluorescence background and helped with post-irradiation stability. For fluorescence measurements, excitation with a diode laser at 520 nm showed the best results.

Therefore, in this project, a solid state polymer matrix that allows the dye to fluoresce and that responds to ionizing radiation by increasing fluorescence was developed. It was possible to identify some of the main mechanisms that take place inside the dosimeter. At the moment, fluorescence is not sensitive enough at the medical dose range, but once this is solved, this dosimeter would be a good candidate for use in a clinical basis. The 3D dose distribution from the dosimeter would be measured by optical fluorescence tomography, which would provide a fast readout, high spatial resolution, and high accuracy, allowing ascertaining that the radiotherapy treatment is delivered as intended.

Chapter 6

Future perspectives

The main aspects to take into consideration for future investigations are the following:

The priority at this stage is to increase fluorescence sensitivity for low doses in order to use this dosimeter for radiotherapy. For that purpose, it is suggested to study the effect of increasing the proportion of HEMA and decreasing the proportion of TPO in the polymer matrix. Addition of MEHQ inhibitor would be necessary in case of using high amounts of HEMA, since the amount of this inhibitor in HEMA is too low and it was observed to be necessary to avoid the leuco dye reaction with the polymer. The key is to find the right proportion of the three components (PEGDA, HEMA and TPO). Therefore, it is recommended to carry out another DoE with *Composition 3* (high dye, high HEMA) or *Composition 5* (low dye, high HEMA) as starting point, and study the fluorescence peak difference between 0 and 5 Gy for different proportions of the PEGDA/HEMA/TPO system. Besides, when trying new polymer matrices, the T_g and the Stokes shift should be regarded; in both cases the higher, the better. The photocuring efficiency of new polymer matrices could be studied by FTIR spectroscopy. This technique would also be useful to study post-UV curing effects.

To remove fluorescence quenching by dissolved molecular oxygen in the polymer matrix, amines could be incorporated into the compositions. They are used as anti-fading agents in fluorescence microscopy and tertiary amines are used for film curing to avoid oxygen inhibition. The drawback is, namely, an increased rate of photo-yellowing. A different method to lower oxygen sensitivity could be to try a hybrid photoinitiator system (free radical + cationic).

Studying temperature dependence on the fluorescence of the dosimeter would be the next step, as well as determine the right storage and measurement conditions.

Photocuring of large 3D samples by using *Lamp 3* and the cooling system currently under development would be the final step, taking into consideration that bubble formation should be avoided, since it affects the readout (light scattering).

	Dosimeter	Photocuring			Irradiations		Measurements		
	(Composition)* Shape	(Lamp)* Power (mW/cm²)	Time (min)	Energy (J/cm²)	(Gammacell)* Dose rate (Gy/min)	Dose (Gy)	Type	Laser	Software
Fig. 4.1	(1) Cuvettes	(1) 3.5 & 8.2	5–40	1.05-19.7	(3) 140	1000	-	-	-
Fig. 4.2	(1) Cuvettes	(1) 3.5	5	1.05	(3) 140	1000	Abs.	-	-
Fig. 4.3a	(1) Slides	(1) 4.5	10	2.7	(1) 5	1000	-	-	-
Fig. 4.3b	(3) Several	(3) 15	2	1.8	-	-	-	-	-
Fig. 4.3c	(1) Slides & pellets	(1) 4.5	10	2.7	(1) 5	-	-	-	-
Fig. 4.4a	(1) Sphere 5cmØ	(1) 4.5	90	24.3	-	-	-	-	-
Fig. 4.4b-5	(3) Sphere 3.5cmØ	(3) 15	2	1.8	-	-	-	-	-
Fig. 4.6-7	(1) Slides	(1) 4.5	10	2.7	(3) 140	100, 200, 300, 400, 500, 600, 700, 800, 900, 1000	Abs., Fl.	Nd:YAG	In-house
Fig. 4.8	(1) Slides	(1) 4.5	10	2.7	(3) 140	200, 400, 600, 800, 1000	Abs., Fl.	Nd:YAG	In-house
Fig. 4.9	(1+) Slides	(1) 4.5	10	2.7	(3) 140	1000	Abs., Fl.	Nd:YAG	In-house
Fig. 4.10	(1+) Slides	(1) 4.5	10	2.7	(3) 140	1000	Abs., Fl.	Nd:YAG	In-house
Fig. 4.11	(2+) Slides	(1) 4.5; CQ: (2) 25	10; CQ: 20	2.7; CQ: 30	(3) 140	300	Fl.	Nd:YAG	In-house
Fig. 4.12-13	(2+) Slides	(1) 4.5; CQ: (2) 25	10; CQ:100	2.7; CQ: 150	(1) 5	2, 4, 6, 8, 10, 20, 50, 100, 300, 600, 1000	Abs., Fl.	Nd:YAG	In-house
Fig. 4.14	(5+) Pellets	(1) 4.5	10	2.7	(1) 5	5, 10, 20	Abs., Fl.	Diode	In-house
Fig. 4.15-16	(2, 3) Pellets	(1) 4.5	10	2.7	(1) 5	2, 10, 20, 30, 50, 75, 100	Abs., Fl.	Diode	In-house
Fig. 4.17	(2) Pellets	(1) 4.5	10	2.7	(1) 5	100	Abs., Fl.	Diode	In-house
Fig. 4.18-19	(2) Pellets	(1) 4.5	10	2.7	(1) 5	5, 10, 20, 30, 50, 75, 100	Abs., Fl., EPR	Nd:YAG	In-house
Fig. 4.20-22	(2) Layer	(1) 15	35 s	0.525	-	-	FTIR	-	-
Fig. 4.23	(2) Slides & pellets	(1) 4.5	10	2.7	-	-	Abs., Fl.	Nd:YAG	In-house
Fig. 4.24	(1) Cuvettes	(1) 3.5, 10.7, 17	10	2.1, 6.4, 10.2	(3) 140	100, 200, 300, 400, 500, 600, 700, 800, 900, 1000	Abs.	-	-
Fig. 4.25	(2) Pellets	(3) 5.5, 0.4, 0.065	1, 5, 50	0.33, 0.12, 0.195	(1) 5	50	Abs., Fl.	Diode	SpectraSuite
Fig. 4.26	(2) Slides	(1) 4.5	10	2.7	-	-	Abs.	-	-
Fig. 4.27	(2, 4) Slides	(1) 4.5	10	2.7	-	-	Abs., Fl.	Diode	In-house
Fig. 4.28	(5+) Pellets	(3) 15	2	1.8	(1) 5	50	Abs., Fl.	Diode	SpectraSuite
Fig. 4.29	(3) Pellets	(3) 15	2	1.8	(1) 5	100, 300, 600, 1000	Abs., Fl.	Diode	In-house

*( ) indicate the composition, lamp and gammacell numbers. For the composition, (+) indicate "plus variations".

Annexe I – B. Product specifications

Chemicals		
Product Number	**Product**	**CAS Number**
437441 Sigma-Aldrich	**Poly(ethylene glycol) diacrylate**, average Mn 575	26570-48-9
475629 Sigma-Aldrich	**Poly(ethylene glycol) diacrylate**, average Mn 250	26570-48-9
455008 Sigma-Aldrich	**Poly(ethylene glycol) diacrylate**, average Mn 700	26570-48-9
477028 Sigma-Aldrich	**2-Hydroxyethyl methacrylate**, ≥99%, contains ≤50 ppm monomethyl ether hydroquinone as inhibitor Synonyms: 1,2-Ethanediol mono(2-methylpropenoate), Glycol methacrylate, HEMA	868-77-9
75707 Sigma-Aldrich	**Bis(2,4,6-trichlorophenyl) oxalate**, BioReagent, suitable for chemiluminescence, ≥99.0% (AT) Synonyms: 2,4,6-Trichlorophenyl oxalate, Oxalic acid bis(2,4,6-trichlorophenyl) ester, TCPO	1165-91-9
23100 Sigma-Aldrich	**Chloral hydrate**, crystallized, ≥98.0% (T) Synonym: Trichloroacetaldehyde hydrate	302-17-0
C7129 Sigma-Aldrich	**Citric acid monohydrate**, reagent grade, ≥98% (GC/titration)	5949-29-1
381462 Sigma-Aldrich	**Pentaerythritol tetrakis(3-mercaptopropionate)**, >95%	7575-23-7
415952 Sigma-Aldrich	**Diphenyl(2,4,6-trimethylbenzoyl)phosphine oxide**, 97%	75980-60-8
406317 Sigma-Aldrich	**Isopropyl-9H-thioxanthen-9-one**, mixture of 2- and 4-isomers, 97%	75081-21-9
124893 Sigma-Aldrich	**Camphorquinone**, 97% Synonyms: (±)-Camphorquinone, 2,3-Bornanedione	10373-78-1
06309 Sigma-Aldrich	**1-Chloro-4-propoxy-9H-thioxanthen-9-one**, 97%	142770-42-1
511447 Sigma-Aldrich	**Phenylbis(2,4,6-trimethylbenzoyl)phosphine oxide**, 97%, powder Synonym: BAPOs, Bisacylphosphine oxides	162881-26-7
405655 Sigma-Aldrich	**2-Hydroxy-2-methylpropiophenone**, 97%	7473-98-5
E24905 Aldrich	**Ethyl 4-(dimethylamino)benzoate**, ≥99% Synonym: Parbenate	10287-53-3
234907 Aldrich	**2-(Dimethylamino)ethyl methacrylate**, contains 700-1000 ppm monomethyl ether hydroquinone as inhibitor, 98% Synonym: Methacrylic acid 2-(dimethylamino)ethyl ester	2867-47-2

LEDs			
	Lamp 1	***Lamp 2***	***Lamp 3****
Product Code	LedEngin LZ4-40UA-U5	Luminus Devices PT 121-B-L11-EPG	Luminus Devices CBM-120-UV-C31-L385-21
Specifications	395 nm	460 nm, 16 W	385 nm, 11 W

*The LED from *Lamp 3* is connected to a liquid light guide with the following specifications:
Brand Lumatec Series 250 core diameter, 5mm and length of 2 meters. Product number: 4027.2000

Annexe II – Other experiments

This annexe includes some experiments and considerations that serve as a supplement of the results shown in the thesis. They are the following:

A1. Effect of solvents in the dye dynamics – Studies in solution I
A2. Effect of additives in the dye dynamics – Studies in solution II
A3. Pre-treatments – Trying to improve dose sensitivity I
A4. Other polymers – Trying to improve dose sensitivity II
A5. Polarity of polymers before and after UV exposure
A6. Safety

A1. Effect of solvents in the dye dynamics – Studies in solution I

Objective: The choice of solvent helps with sensitivity and stability of the dye. This was already checked in 1974 (*McLaughlin and Kosanić, 1974*) for solutions of the same dye, where it was observed that a weak acid stabilizes the dye. The purpose of this study is to analyze the effect of different solvents in the dynamics of the dye: stability of the dye before and after irradiation, and sensitivity of the dye to radiation.

Experiment: Absorbance spectra of solutions of 5 mM pararosaniline leuco dye in TBP with different solvents were measured. The solvents that were studied were: ethanol (96 vol% in water), dry ethanol (99 vol% in water), citric acid (20 vol% in water), and water itself. They were studied in the following concentrations: 0.5, 1, 2.5, 5 and 10 vol%, except for citric acid and water where the 10 vol% solutions were not dissolvable. Three cuvettes were measured for each concentration, and they were irradiated to 50 Gy in *Gammacell 3* (dose rate 140 Gy/min). It was analyzed the effect of the solvent on the pre- and post- irradiation stability, and on the dose sensitivity.

Results pre-irradiation stability: Figure A1 shows the effect of the solvent on the pre-irradiation stability of the dye. Cuvettes were measured 20 hours after fabrication. In all cases, stability improves by adding a solvent; and the higher the solvent concentration, the more stable is the dye. For ethanol and dry ethanol, concentrations of 5 vol% and 10 vol% are recommended. Citric acid improves the stability drastically just by adding it in a low concentration (0.5 vol%), and for higher concentrations the stability is maintained. In the case of water, the stability is maintained for concentrations higher than 1 vol%.

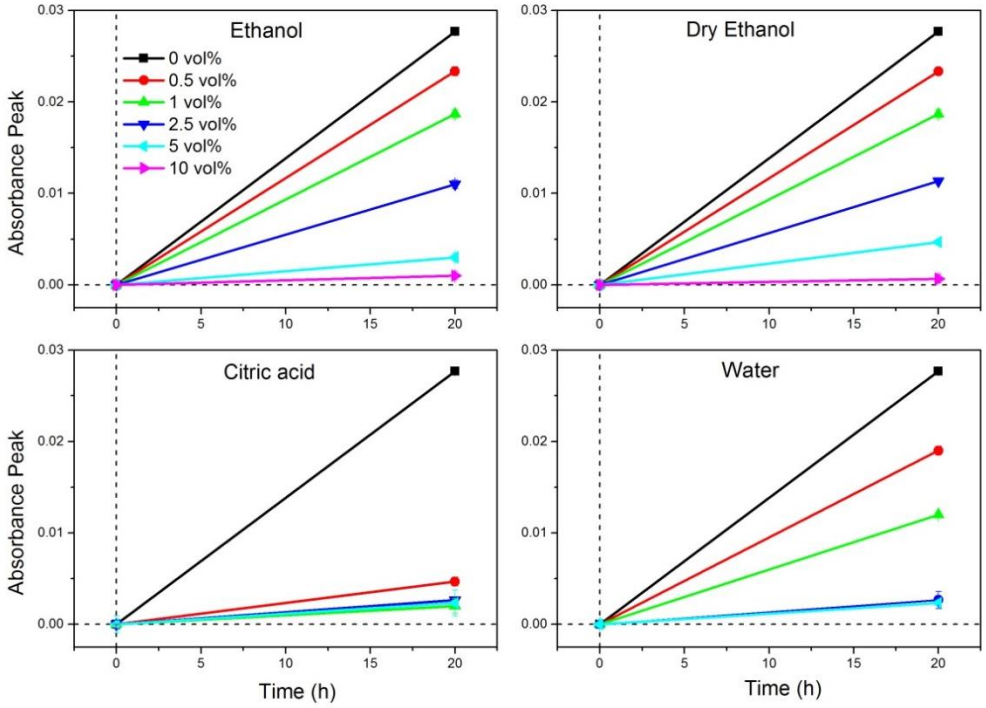

Figure A1: Effect of the solvent on the pre-irradiation stability of the dye. Error bars included, smaller than the markers.

Results dose sensitivity: Figure A2 shows the effect of the solvent on the sensitivity of the dye to radiation. Sensitivity decreases with solvent concentration, but in the case of ethanol and dry ethanol the difference is much smaller than in the case of citric acid and water.

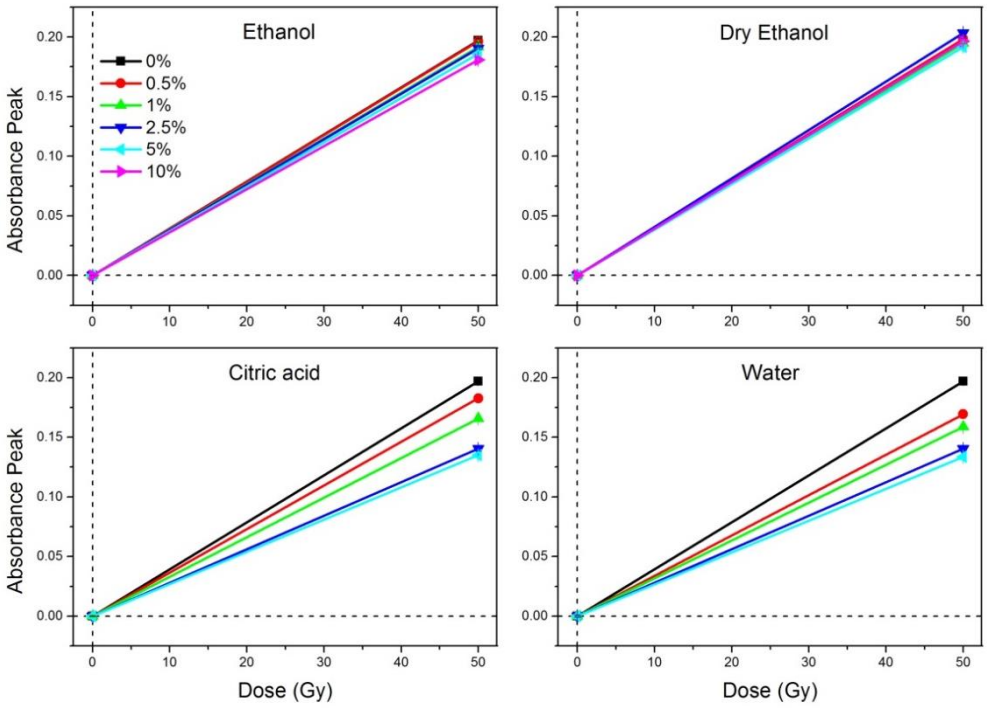

Figure A2: Effect of the solvent on the dose sensitivity of the dye. Error bars included, smaller than the markers.

Results post-irradiation stability: Figure A3 shows effect of the solvent on the post-irradiation stability. Cuvettes were measured 1, 3, 6.5 and 24 hours after irradiation. The stability of the dye after irradiation improves by adding a solvent. The best results are: ethanol and dry ethanol at 5 vol%, citric acid at 0.5 vol% and water at 2.5 vol%.

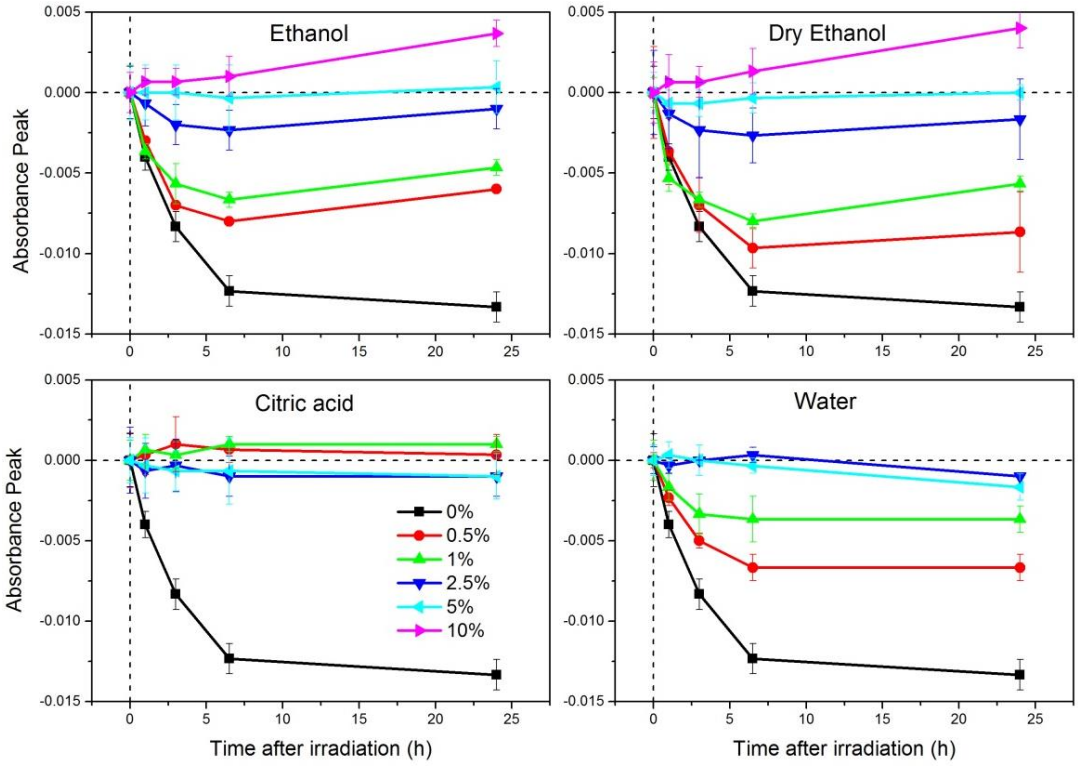

Figure A3: Effect of the solvent on the stability of the dye after irradiation.

Conclusion: Solvents improve pre- and post-irradiation stability, but not dose sensitivity. Ethanol does not decrease sensitivity much, and reaches a very good post-irradiation stability at 5 vol% concentration. For the solid state dosimeter, ethanol at 4.9 vol% (*Composition 1, 2,* and *4*) and 4.5 vol% (*Composition 3,* and *5*) were used. The difference between ethanol and dry ethanol is very low. Citric acid improves stability drastically, but also decreases sensitivity. The effect of citric acid on the stability of the solid state dosimeter was analyzed in chapter 4.5.

A2. Effect of additives in the dye dynamics – Studies in solution II

Objective: Test if additives increase the sensitivity of the dye to radiation.

Experiment & Results: Absorbance spectra of 10 mM solutions of pararosaniline leuco dye in TBP were measured. Citric acid (20 vol% in water), TCPO, and Chloral Hydrate were studied for the following concentrations: 0.1, 1, 2.5 and 5 mM. Cuvettes were irradiated in *Gammacell 3* at 25, 50 and 100 Gy.

Figure A4 shows that TCPO reacts with the dye and that the slope of the absorbance peak vs. dose curve is one order of magnitude lower than without additives. In the case of citric acid and Chloral Hydrate, dose sensitivity decreases when increasing these components (although 0.1 mM citric acid seems to increase sensitivity).

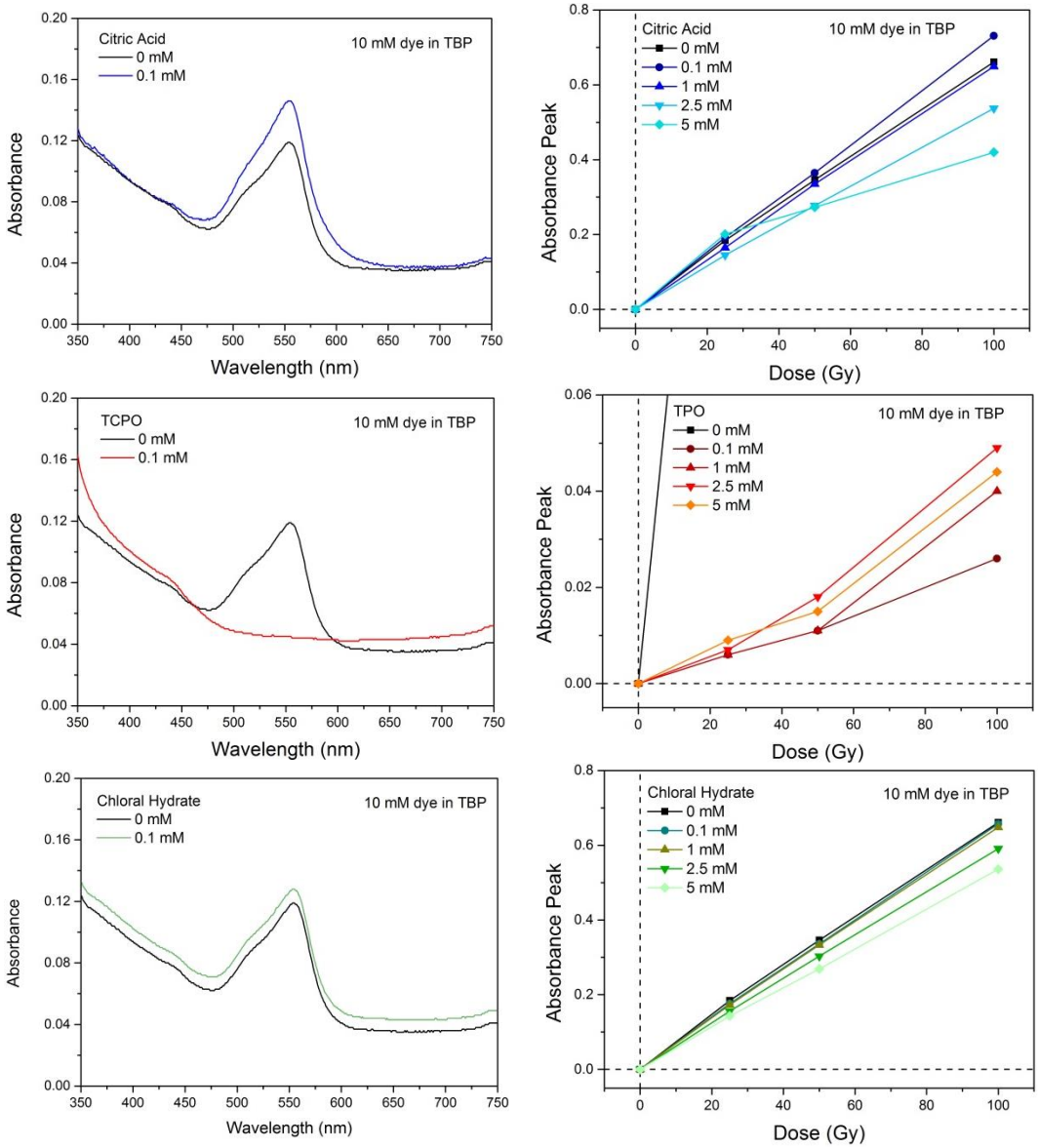

Figure A4: Effect of citric acid, TCPO, and Chloral Hydrate in the dose sensitivity.

Conclusion: Additives decrease dose sensitivity.

A3. Pre-treatments – Trying to improve dose sensitivity I

Objective: Study the effect of heating and irradiating the samples before irradiation to low doses. The hypothesis is that heating and irradiation promote reaction of the species that are left after photocuring, and therefore the sensitivity to low doses would increase since radiation would be used for the leuco dye transformation and not to continue curing of the polymer matrix.

Experiment: The pre-irradiation treatment was done by previously irradiating the slides to 10 Gy, and the pre-heating treatment was done by heating the slides at 60°C (temperature used in the Risø B3 films to stabilize the dye) for 30 min. Slides (3 slides per type of treatment) were made of *Compositions 2* and *4*, and irradiated with *Gammacell 1* (dose rate 5 Gy/min) to 2, 4, 6, 8 and 10 Gy after the pre-treatments. Fluorescence was measured with the diode laser.

Results: Figure A5 shows the dose sensitivity for the pre-irradiation and the pre-heating treatments compared to the case of no pre-treatment.

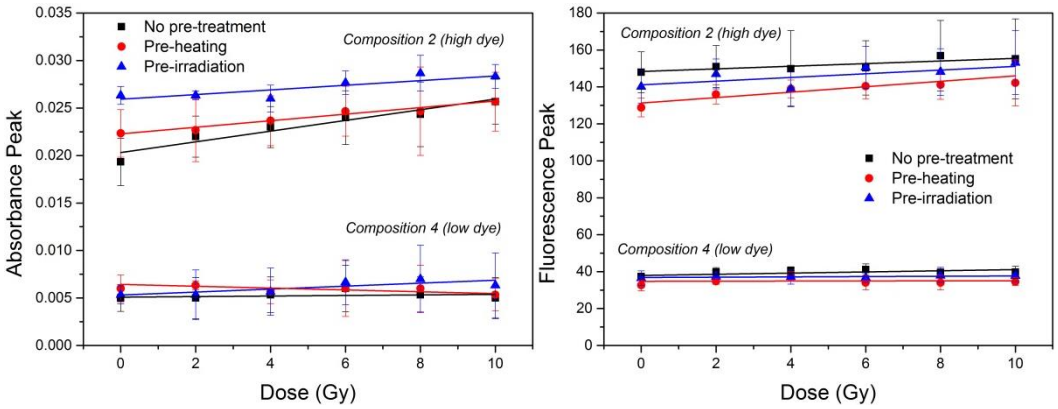

Figure A5: Effect of pre-treatments on the dose sensitivity of slides.

Conclusion: Dose sensitivity does not seem to improve with the pre-treatments.

A4. Other polymers – Trying to improve dose sensitivity II

Objective: Study if sensitivity to low doses for the fluorescence signal improves by using other polymer systems.

Experiment & Results – Proportion of HEMA: The effect of HEMA was analyzed for *Composition 2* (HEMA to PEGDA ratio: 0.6%) by increasing the HEMA to PEGDA ratio to 13%. Pellets were cured with *Lamp 1* for 10 min and irradiated with *Gammacell 1* to 4.4, 8.8, and 17.55 Gy. Fluorescence was excited with the diode laser. Results (figure A6), show an improvement on the sensitivity but not as much as in the result presented in chapter 4.2.6 for *Composition 3*, where the proportion HEMA to PEGDA ratio is 11.6% but the proportion of TPO is lower.

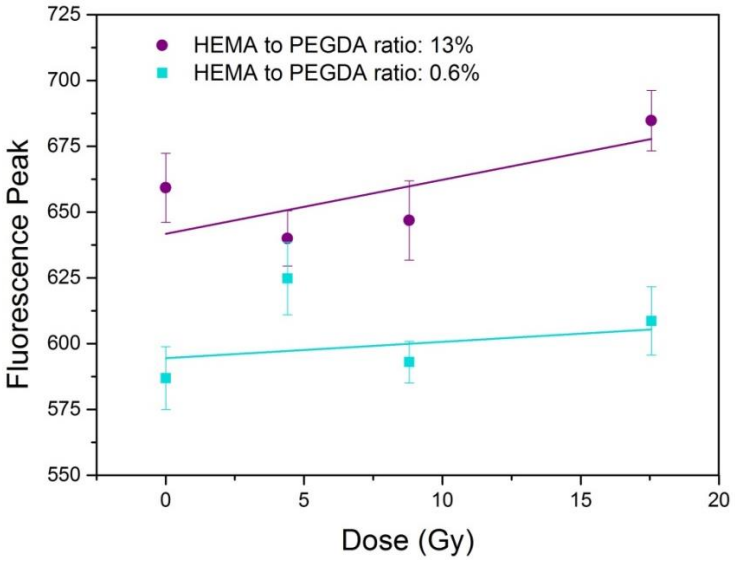

Figure A6: Fluorescence peaks as function of the dose for pellets with different HEMA to PEGDA ratio.

Experiment & Results – Secondary polymers: Pellets of *Composition 5* were made by using different secondary polymers all in the same vol%: HEMA (as usual), 1,6-Hexanediol ethoxylate (Hexanediol), and pentaerythritol tetraacrylate (Tetraacrylate). Pellets were cured with *Lamp 3* for 1 min. Irradiations were done in *Gammacell 1* to 5, 10, 12, 14, 16, and 20 Gy. Fluorescence was excited with the diode laser. Figure A7 shows the results. The slope is similar in all cases, so the dose sensitivity does not improve. However, the fluorescence background is much lower for Tetraacrylate.

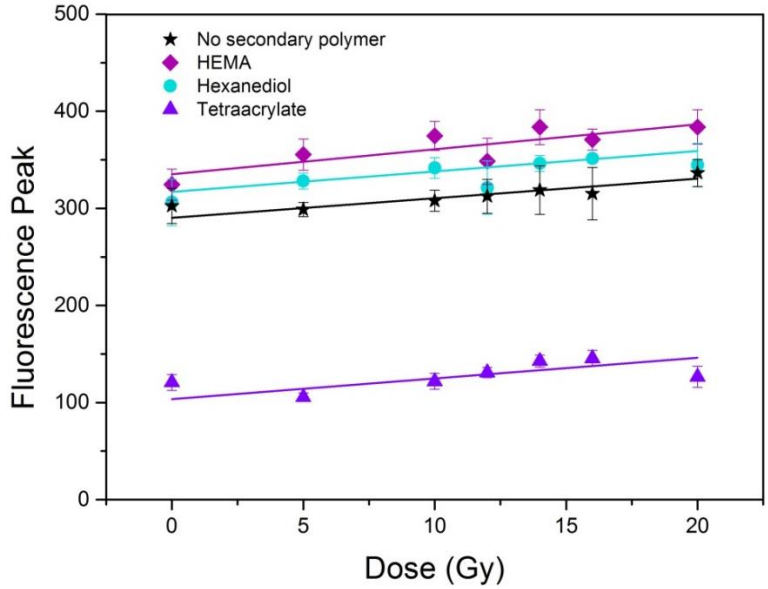

Figure A7: Fluorescence peaks as function of the dose for pellets with different secondary polymers.

Experiment & Results – Other polymers: New systems were tried, such as PEGDA-700 together with propylene carbonate, and Irgacure 819 0.5% in 1-vinyl-2-pyrrolidinone (NVP) as photoinitiator. Pellets (4 pellets per type) were cured in a cooling bath at 3 ^{o}C for 50 sec using *Lamp 2* and post-UV curing with *Lamp 1* for about 20 sec afterwards. Irradiations were done in *Gammacell 1* to 5, 10, and 20 Gy. Fluorescence was excited with the diode laser.

The compositions were the following:

- *New Composition 1:* 10 mg leuco dye, 3 ml propylene carbonate, 3 ml PEGDA-700, and 0.2 ml Irgacure 819 0.5% in NVP.
- *New Composition 2:* 30 mg leuco dye, 120 mg Chloral Hydrate, 5 ml propylene carbonate, 1 ml ethanol, 5 ml PEGDA-700, and 0.5 ml Irgacure 819 0.5% in NVP.
- *New Composition 3:* 30 mg leuco dye, 120 mg Chloral Hydrate, 5 ml propylene carbonate, 1 ml ethanol, 5 ml PEGDA-575, and 0.5 ml Irgacure 819 0.5% in NVP.

Figure A8 shows that the fluorescence now decreases with the dose. Besides, results showed that these samples shrink over time. After irradiations, pellets are attached at the bottom of the holder, and after one week they decreased their size like in half.

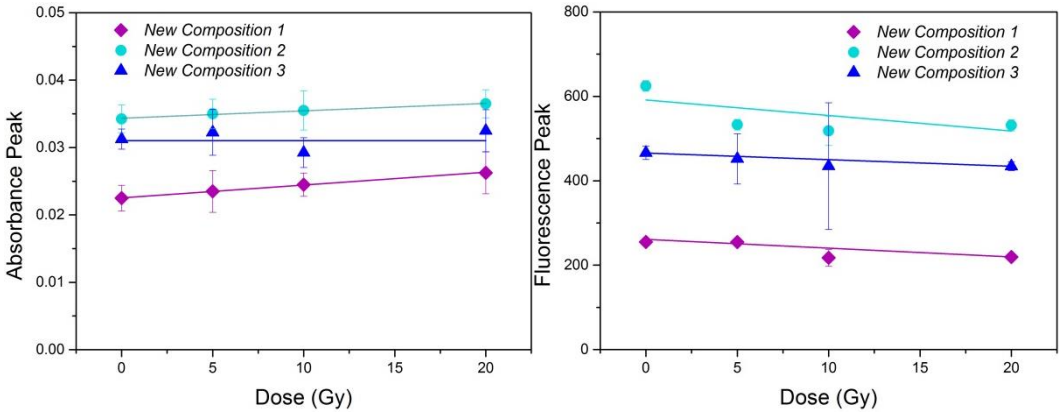

Figure A8: Absorbance and fluorescence peaks as function of the dose for pellets made of new polymer compositions.

Conclusion: These results shown that increasing the amount of HEMA is a good idea to increase dose sensitivity; that tetraacrylate may be used to lower the fluorescence background; and that not all polymer systems are adequate for the matrix, such as is the case of propylene carbonate.

A5. Polarity of polymers before and after UV exposure

Objective: Determine the polarity of different polymers and study if it changes after photocuring.

Experiment & Results: Reichardt's dye (*Reichardt, 1994*), a solvatochromic dye that changes color depending on the solvent polarity, was added to the following solutions (figure A9):

Acetone and ethanol for references
1-vinyl-2-pyrrolidinone (NVP)
Propylene carbonate
PEGDA-575
PEGDA-700
HEMA
1,3,5-triallyl-1,3,5-triazine-2,4,6(1H, 3H, 5H)-trione
Pentaerythritol tetraacrylate
PEGDA-700+Glycerol (ratio 2:3)
Pentaerythritol tetrakis(3-mercaptopropionate)

Figure A9: Solutions used in this experiment. Pictures on the right in the same order.

The mixture of photoinitiators Irgacure 819 + Darocur 1173 was added to the cuvettes (three cuvettes per polymer). When adding the photoinitiator, it was observed that PEGDA-700, and PEGDA-700+Glycerol lose color. Cuvettes were cured with *Lamp 2*. PEGDA-575, PEGDA-700, and tetraacrylate, were the only polymers that were solid after photocuring; NVP was jelly and the others were liquid. While UV exposure, propylene carbonate loses color, while tetraacrylate increases color.

The wavelength that corresponds to the maximum absorbance $\lambda_{max}(nm)$ was measured for the solutions before and after adding the photoinitiator, and after UV exposure. The solvent polarity parameter $E_T(30)$ (molar electronic transition energy), related to solvent polarity, was obtained by the following equation (*Reichardt, 1994*):

$$E_T(30)(kcal\ mol^{-1}) = \frac{28591}{\lambda_{max}(nm)}$$

High $E_T(30)$ values correspond to high solvent polarity (*Reichardt, 1994*). For example, acetone ($E_T(30) = 42.9$) and ethanol ($E_T(30) = 51.9$) have a dielectric constant of $\varepsilon = 20.56$ and $\varepsilon = 24.55$ respectively (*Machado and Machado, 2001*). Figure A10 shows the results. HEMA is the polymer that shows higher polarity, also after UV exposure. In this graph, it can be seen how polarity changes after UV exposure. This is highly notorious in the case of propylene carbonate, decreasing its polarity afterwards. That may be the reason of the bad results (decreasing fluorescence) obtained in the previous experiment (Annexe II – 4).

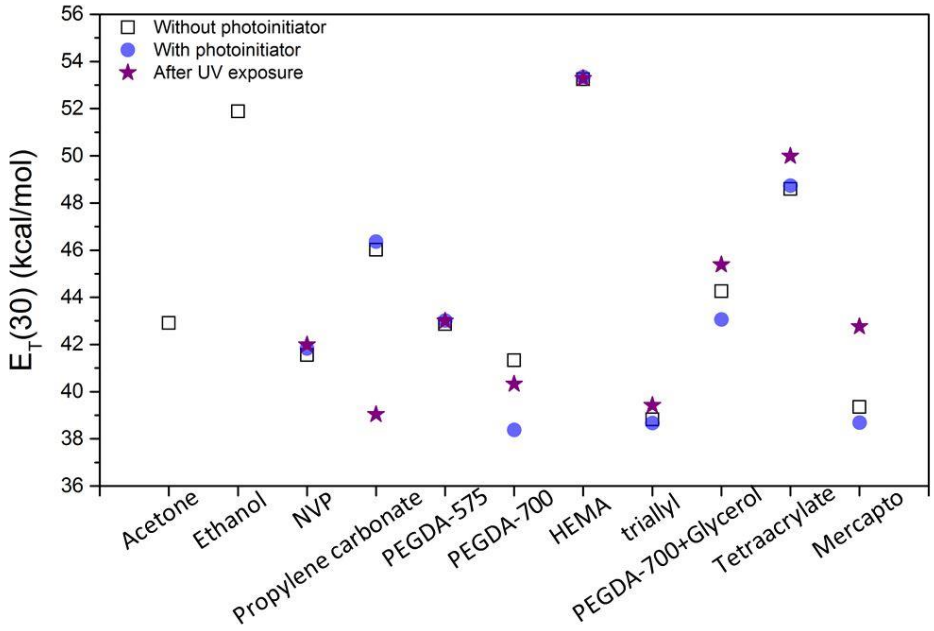

Figure A10: Molar electronic transition energy, $E_T(30)$, of solvents and polymers before adding photoinitiator (squares), after adding it (circles), and after UV exposure (stars). A high $E_T(30)$ indicates high polarity.

Conclusion: This experiment needs further investigation, since interactions of the Reichardt's dye are not discarded. Besides, it was only possible to cure PEGDA-575, PEGDA-700, and tetraacrylate, so it is recommended to try a different photoinitiator and curing with *Lamp 3* (not available at that moment). However, we can conclude that propylene carbonate seems to decrease its polarity after UV exposure, and that the dielectric constant of the host polymer used along this thesis (PEGDA-575) should be higher to get higher dose sensitivity. By incorporating HEMA, the polarity of the matrix increases, increasing therefore the sensitivity (as it was observed in chapter 4.2.6).

A6. Safety

All the work was carried out under the necessary safety conditions: fume chambers and laboratory disposable gloves for chemical preparation, UV protective glasses for photocuring, and a TLD dosimeter worn during irradiations for radiation protection control.

It should be noticed the high safety of the manufacturing of this solid state dosimeter. No toxic chemicals are used in its composition, contrary to gel dosimeters that often contain highly toxic chemical species such as acrylamides, known to be severe neurotoxins and suspected carcinogens. Regarding the curing process, photocuring has the advantage of not evaporating toxic substances, contrary to current solid state dosimeters that use various kinds of organic peroxides, such as chloroform, necessary to cause the oxidation of the leuco dye (*Khezerloo et. al, 2017*). Those components are evaporated since the curing method used is thermal curing by evaporation. UV-curing is a cleaner way of obtaining the solid state dosimeter.

Bibliography

AAPM (1999). AAPM's TG-51 protocol for clinical reference dosimetry of high-energy photon and electron beams. Medical Physics, 26(9): 1847-1870.

Abdel-Fattah, A.A., Beshir, W.B., Hegazy, El-Sayed A., El-Din, H.E. (2001). Photo-luminescence of Risø B3 and PVB films for application in radiation dosimetry. *Radiation Physics and Chemistry 62*, 423-428.

Abramowitz, M., and Davidson, M.W. (2017). Overview of Fluorescence Excitation and Emission Fundamentals. Retrieved on December 2017 from www.olympus-lifescience.com.

Adamovics, J., and Maryanski, M.J. (2006). Characterisation Of Presage™: A New 3-D Radiochromic Solid Polymer Dosimeter For Ionising Radiation. Radiation Protection Dosimetry, 120, 1-4, 107-112, DOI:10.1093/rpd/nci555.

Agostinelli, S., Allison, J., Amako, K., et al. (2003). GEANT4-a simulation toolkit. *Nuclear Instruments and Methods in Physics Research A, 506*, 250-303.

Andreo, P., Burns, D.T., Nahum, A.E., Seuntjens, J., and Attix F.H. (2017). *Fundamentals of Ionizing Radiation Dosimetry*. WILEY-VCH.

Ashland (2017). Gafchromic EBT Films - GAFchromic. Retrieved on December 2017 from www.gafchromic.com.

Attix, F.H. (1986). *Introduction to Radiological Physics and Radiation Dosimetry*. John Wiley & Sons.

Bache, S.T., Juang, T., Belley, M.D., Koontz, B.F., Adamovics, J., Yoshizumi, T.T., Kirsch, D.G., and Oldham, M. (2015). Investigating the accuracy of microstereotactic-body-radiotherapy utilizing anatomically accurate 3D printed rodent-morphic dosimeters. *Medical Physics, 42*(2), DOI: 10.1118/1.4905489.

Baldock C., De Deene Y., Doran S., Ibbott G., Jirasek A., Lepage M., McAuley K. B., Oldham M. and Schreiner L.J. (2010). Polymer gel dosimetry. *Physics in Medicine and Biology, 55*, R1-R63, DOI:10.1088/0031-9155/55/5/R01.

Baskar, R., Lee, K.A., Yeo, R., and Yeoh, K.W. (2012). Cancer and Radiation Therapy: Current Advances and Future Directions. *International Journal of Medical Sciences, 9*(3): 193-199, DOI: 10.7150/ijms.3635.

Beddar, A.S., Mackie, T.R., and Attix, F.H. (1992). Water-equivalent plastic scintillation detectors for high-energy beam dosimetry: I. Physical characteristics and theoretical considerations. *Physics in Medicine and Biology, 37*(10), 1883-1900.

Beierholm, A.R., Lindvold, L.R., Andersen, C.E. (2011). Pulse-resolved radiotherapy dosimetry using fiber-coupled organic scintillators. PhD thesis. Technical University of Denmark, Center for Nuclear Technologies.

Bielajew, A.F. (2013). *Monte Carlo Techniques in Radiation Therapy*. Imaging in Medical Diagnosis and Therapy. Chapter: History of Monte Carlo. CRC Press.

Borca, V.C., Pasquino, M., Russo, G., Grosso, P., Cante, D., Sciacero, P., Girelli, G., La Porta, M. R., and Tofani, S. (2013). Dosimetric characterization and use of GAFCHROMIC EBT3 film for IMRT dose verification. *Journal of Applied Clinical Medical Physics, 14*(2), DOI: 10.1120/jacmp.v14i2.4111.

Brown, F.B. (2003*). MCNP - a general Monte Carlo N-particle transport code,* version 5, Report LA-UR-03-1987, Los Alamos National Laboratory.

CCS (2017). Retrieved on December 2017 from www.ccshc.com.

Chechik, V., Carter, E., and Murphy, D. (2016). *Electron Paramagnetic Resonance*. Oxford University Press.

Day, M.J., and Stein, G. (1950). Chemical effects of ionizing radiation in some gels. *Nature, 166*(4212).

d'Errico, F., Lazzeri, L., Dondi, D., Mariani, M., Marrale, M., Souza, S.O., and Gambarini, G. (2017). Novel GTA-PVA Fricke gels for three-dimensional dose mapping in radiotherapy. *Radiation Measurements, 106*, 612-617, DOI: 10.1016/j.radmeas.2017.07.003.

Drobny, J.G. (2010). *Radiation Technology for Polymers*. CRC Press, 2nd edition.

Duxbury, D.F. (1993). The Photochemistry and Photophysics of Triphenylmethane Dyes in Solid and Liquid Media. *Chemical Reviews, 93*(1): 381-433, DOI: 10.1021/cr00017a018.

Figueiredo, A.G.P.R., Figueiredo, A.R.P., Alonso-Varona, A., Fernandes, S.C.M., Palomares, T., Rubio-Azpeitia, E., Barros-Timmons, A., Silvestre, A.J.D., Neto, C.P., and Freire, C.S.R. (2013). Biocompatible Bacterial Cellulose-Poly(2-hydroxyethyl methacrylate) Nanocomposite Films. *BioMed Research International*, DOI: 10.1155/2013/698141.

Ferlay, J., Soerjomataram, I., Ervik, M., Dikshit, R., Eser, S., Mathers, C., Rebelo, M., Parkin, DM., Forman, D., and Bray, F. (2013). GLOBOCAN 2012 v1.0, Cancer Incidence and Mortality Worldwide: IARC Cancer Base No. 11. *International Agency for Research on Cancer*.

Fox, M. (2007). *Optical Properties of Solids*. Oxford University Press.

Galagan, Y., Hsu, S.H., Su, W.F. (2010). Monitoring time and temperature by methylene blue containing polyacrylate film. *Sensors and Actuators B 144*, 49–55, doi:10.1016/j.snb.2009.10.011.

Gessner, T., and Mayer, U. (2012). *Ullmann's Encyclopedia of Industrial Chemistry*. Chapter: Triarylmethane and Diarylmethane Dyes. Wiley-VCH, DOI: 10.1002/14356007.

Glöckner, P., Jung, T., Struck, S., and Studer, K. (2008). *Radiation Curing. Coatings and Printing Inks*. European Coatings Tech Files, Vincentz.

Gotro, J. (2016). *UV Curing of Thermosets Part 11: Using UV Rheology to Monitor Curing - 2*. Retrieved from https://polymerinnovationblog.com.

Green, W.A. (2010). *Industrial Photoinitiators: A Technical Guide*. CRC Press.

Heidolph (2017). Retrieved on December 2017 from www.heidolph-instruments.com.

Helt-Hansen, J., and Miller, A. (2004). RisøScan - a new dosimetry software. *Radiation Physics and Chemistry, 71*(1-2): 361-364.

Herman, B., Lakowicz, J.R., Murphy, D.B., Fellers, T.J., and Davidson, M.W. (2017). *Confocal Microscopy - Fluorophores for Confocal Microscopy*. Retrieved on December 2017 from www.olympus-lifescience.com.

Holmes, E.O. (1966). The effect of the properties of solvents of various dielectric constants and structures on the photoionization of the leucocarbinols and leucocyanides of malachite green, crystal violet, and sunset orange and related phenomena. *The Journal of Physical Chemistry, 70*(4): 1037-1046.

Høye, E.M., Skyt, P.S., Yates, E.S., Muren, L.P., Petersen, J.B.B., and Balling, P. (2015). A new dosimeter formulation for deformable 3D dose verification. *Journal of Physics: Conference Series, 573*, 012067, DOI:10.1088/1742-6596/573/1/012067.

Hsueh, Y.H., Liaw, W.C., Kuo, J.M., Deng, C.S., and Wu, C.H. (2017). Hydrogel Film-Immobilized Lactobacillus brevis RK03 for ?-Aminobutyric Acid Production. *International Journal of Molecular Science, 18*, 2324, DOI:10.3390/ijms18112324.

IAEA (2000). IAEA Technical Resport Series No. 398. Absorbed dose determination in external beam radiotherapy: An iInternational code of practice for dosimetry based on standards of absorbed dose to water. *International Atomic Energy Agency*.

ICRU (2008). Journal of the ICRU, Vol 8, No 2, Report 80. *International Commission on Radiation Units and Measurements.*

Iverson Lab (2016). Retrieved on December 2017 from iverson.cm.utexas.edu.

Johns, H.E., and Cunningham, J.R. (1983). *The physics of radiology*. Thomas Books, 4th edition.

Kawrakow, I. (2000). Accurate condensed history Monte Carlo simulation of electron transport. I. EGSnrc, the new EGS4 version. *Medical Physics, 27*, 485-98.

Kawrakow, I. (2005). EGSnrc C++ Class Library. Report PIRS-898. *National Research Council Canada*.

Kawrakow, I., Mainegra-Hing, E., Rogers, D.W.O., Tessier, F., and Walters, B.R.B. (2011). The EGSnrc code system: Monte Carlo Simulation of Electron and Photon Transport. NRCC Report PIRS-701, *National Research Council Canada*.

Khezerloo, D., Nedaie, H.A., Takavar, A., Zirak, A., Farhood, B., Movahedinejhad, H., Banaee, N., Ahmadalidokht, I., and Knuap, C. (2017). PRESAGE as a solid 3-D radiation dosimeter: A review article. *Radiation Physics and Chemistry, 141*, 88-97, DOI: 10.1016/j.radphyschem.2017.06.002.

Knoll, G.F. (2010). *Radiation Detection and Measurement*. John Wiley & Sons, 4th edition.

Kopeček, J. (2009). Hydrogels from soft contact lenses and implants to self-assembled nanomaterials. *Journal of Polymer Science Part A: Polymer Chemistry, 47*, 5929-5946, DOI:10.1002/pola.23607.

Kshitij Education India (2015). *Bonding in Benzene*. Retrieved on December 2017, from www.kshitij-iitjee.com/Bonding-in-Benzene.

Lakowicz, J.R. (2006). *Principles of Fluorescence Spectroscopy*. Springer, 3rd edition.

Lin, C.C. (2015). Recent advances in crosslinking chemistry of biomimetic poly(ethylene glycol) hydrogels. *RSC Advances, 5*, 39844-398583, DOI:10.1039/C5RA05734E.

Low, D. (2015). The importance of 3D dosimetry. *Journal of Physics: Conference Series, 573*, DOI:10.1088/1742-6596/573/1/012009.

Machado, C., and Machado, V.G. (2001) An Easy and Versatile Experiment to Demonstrate Solvent Polarity Using Solvatochromic Dyes. *Journal of Chemical Education, 78*(5): 649, DOI: 10.1021/ed078p649.

McLaughlin, W.L., and Kosanić, M. (1974). The Gamma-Ray Response of Pararosaniline Cyanide Dosimeter Solutions. *International Journal of Applied Radiation and Isotopes, 25*, 249-262.

McLaughlin, W.L., Miller, A., Kovács A., and Mehta, K.K. (2011). *Dosimetry Methods*. Handbook of Nuclear Chemistry, Volume 5, Springer.

McMurry, J. (2016). *Organic Chemistry*. Cengage Learning, 9th edition.

Mei, J., Hong, Y., Lam, J.W.Y., Qin, A., Tang, Y., and Tang, B.Z. (2014). Aggregation-Induced Emission: The Whole Is More Brilliant than the Parts. *Advanced Materials, 26*, 5429-5479, DOI: 10.1002/adma.201401356.

Miller, A., and McLaughlin, W. (1980). On a radiochromic dye dosimeter. Risø-M; No. 2254.

MODDE (2014). *User Guide to MODDE*. MKS Umetrics AB, version 10.1.

Modus QA (2017). *3D Dosimetry - Modus QA*. Retrieved on December 2017 from modusqa.com/dosimetry/optical-ct//vista.

Morrison, R.T., and Boyd, R.N. (1973). *Organic Chemistry*. Allyn and Bacon, 3rd edition.

NCK (2016). Retrieved on December 2017 from www.nck.dk.

Nelson, W.R., Hirayama, H., and Rogers, D.W.O. (1985). *The EGS4 code system Report*, SLAC-265, Stanford Linear Accelerator Center.

Neumann, M.G., Schmitt, C.C., Ferreira, G.C., and Corrêa, I.C. (2006). The initiating radical yields and the efficiency of polymerization for various dental photoinitiators excited by different light curing units. *Dental Materials, 22*(6): 576-584. DOI:10.1016/j.dental.2005.06.006.

Noels, L. (2015). *Computational & Multiscale Mechanics of Materials*. University of Liège. Retrieved on December 2017, from http://www.ltas-cm3.ulg.ac.be.

Ocean Optics (2017). Retrieved on December 2017 from oceanoptics.com.

Oldham, M. (2006). 3D dosimetry by optical-CT scanning. *Journal of Physics: Conference Series 56*: 58-71.

Oster, G., Joussot-Dubien J. and Broyde B. (1959). Photoreduction of dyes in rigid media. I. Triphenylmethane dyes. *Journal of American Chemical Society, 81*: 1869-72.

Podgorsak, E.B. (2005). *Radiation Physics for Medical Physicists*. Springer, 2nd edition.

Potsaid, M.S., and Irie, G. (1961). An in-phantom radiation detector. *The New England Journal of Medicine, 265*(23), DOI: 10.1056/NEJM196112072652303.

Rainin (2017). Retrieved on December 2017 from www.shoprainin.com.

Radon, J. (1917). *Über die Bestimmung von Funktionen durch ihre Integralwerte längs gewisser Mannigfaltigkeiten.* Berichte Sächsische Akademie der Wissenschaften, Leipzig, Mathematisch-Physikalische Klasse, 69: 262-277.

Reichardt, C. (1994). Solvatochromic Dyes as Solvent Polarity Indicators. *Chemical Reviews, 94*(8): 2319-2358.

Roffey, C. (1997). *Photogeneration of reactive species for UV curing*. Wiley.

Rogers, D.W.O., Kawrakow, I., Seuntjens, J.P., Walters, B.R.B., and Mainegra-Hing, E. (2010). NRC User Codes for EGSnrc. Report PIRS-702. *National Research Council Canada*.

Sakhalkar, H.S., Adamovics, J., Ibbott, G., and Oldham, M. (2009). A comprehensive evaluation of the PRESAGE/optical-CT 3D dosimetry system. *Medical Physics, 36*(1), DOI: 10.1118/1.3005609.

Salvat, F., Fernández-Varea, J.M., and Sempau, J. (2011). *PENELOPE-2011: A code system for Monte Carlo simulation of electron and photon transport*. NEA/NSC/DOC(2011)5, Nuclear Energy Agency.

Sanders, N.H., (2017). *Towards 3D Dosimetry with Optical Fluorescence Tomography Using a Radiofluorogenic Material: Setup and Data Processing*. PhD thesis. Technical University of Denmark, Center for Nuclear Technologies.

Sartorius (2017). Retrieved on December 2017 from www.sartorius.com.

Schafer, F.P. (1972). *Dye Lasers*. Springer-Verlag.

Schreiner, L.J. (2004). Review of Fricke gel dosimeters. *Journal of Physics: Conference Series, 3*, 9-21, DOI:10.1088/1742-6596/3/1/003.

Shimadzu (2017). Retrieved on December 2017 from www.ssi.shimadzu.com.

Sigma-Aldrich (2017). Retrieved on December 2017 from www.sigmaaldrich.com.

Sobotka, P., Kozicki, M., Maras, P., Boniecki, L., Kacperski, K., and Domański, A.W. (2012). Optical Scanner for 3D Radiotherapy Polymer Gel Dosimetry. *Acta Physica Polonica A, 122*(5).

Supertech (2017). *IMRT Torso Freepoint Phantom, Complete Quality Assurance, CT imaging and Radiation Therapy dose verification*. Retrieved on December 2017 from www.supertechx-ray.com.

Telford, J.K. (2007). *A Brief Introduction to Design of Experiments*. Johns Hopkins APL Technical Digest, 27(3).

Thomas, A., Newton, J., and Oldham, M. (2011). A method to correct for stray light in telecentric optical-CT imaging of radiochromic dosimeters. *Physics in Medicine and Biology, 56*, 4433-4451, DOI:10.1088/0031-9155/56/14/013.

TIR 100-205 (2010). *B3 Radiochromic film dosimetry*. Technical Memorandum, GEX Corporation.

Turro, N.J. (1978). *Modern Molecular Photochemistry*. University Science Books.

Van Blitterswijk, C.A., Moroni, L., Rouwkema, J., Siddappa, R., and Sohier, J. (2008). *Tissue engineering - an introduction*. Academic Press.

Vandecasteele, J., and De Deene, Y. (2013). Evaluation of radiochromic gel dosimetry and polymer gel dosimetry in a clinical dose verification. *Physics in Medicine and Biology, 58*, 6241-6262, DOI:10.1088/0031-9155/58/18/6241.

Waldeland, E., Helt-Hansen, J., and Malinen, E. (2011). Characterization of lithium formate EPR dosimeters for high dose applications - Comparison with alanine. *Radiation Measurements, 46*, 213-218, DOI:10.1016/j.radmeas.2010.11.015.

Walton, D., and Lorimer, P. (2005). *Polymers*. Oxford Chemistry Primers, 2nd edition.

Wang, L., Kielar, K.N., Mok, E., Hsu, A., Dieterich, S., and Xing, L. (2012). An end-to-end examination of geometric accuracy of IGRT using a new digital accelerator equipped with onboard imaging system. *Physics in Medicine and Biology, 57*(3): 757-69, DOI:10.1088/0031-9155/57/3/757.

Warman, J.M., de Haas, M.P., Luthjens, L.H., Denkova, A.G., Kavatsyuk, O., van Goethem, M.J., Kiewiet, H.H., and Brandenburg, S. (2013). Fixed fluorescent images of an 80 MeV proton pencil beam. *Radiation Physics and Chemistry, 85*, 179-181, DOI: 10.1016/j.radphyschem.2012.11.011.

Watanabe, Y., Warmington, L., and Gopishankar, N. (2017). Three-dimensional radiation dosimetry using polymer gel and solid radiochromic polymer: From basics to clinical applications. *World Journal of Radiology, 9*(3): 112-125, DOI: 10.4329/wjr.v9.i3.112.

Wayne, C.E., and Wayne, R.P. (2005). *Photochemistry*. Oxford Chemistry Primers, 2nd edition.

Wegner, G. (2006). Polymers as functional components in batteries and fuel cells. *Polymers for Advanced Technologies, 17*(9-10), 705-708.

Wu, K.C., Halloran, J.W. (2005). Photopolymerization monitoring of ceramic stereolithography resins by FTIR methods. *Journal of Materials Science 40*, 71-76.

Yang, W., Yu, H., Liang, W., Wang, Y., and Liu, L. (2015). Rapid Fabrication of Hydrogel Microstructures Using UV-Induced Projection Printing. *Micromachines, 6*, 1903-1913, DOI:10.3390/mi6121464.

Zaragoza, J.R. (1992). *Física e Instrumentación Médicas*. Masson-Salvat Medicina.

PAPER I

Bernal-Zamorano, M.R., Sanders, N.H., Lindvold, L., Andersen, C.E. (2017). Radiochromic and radiofluorogenic 3D solid polymer dosimeter; initial results for high doses.
Journal of Physics: Conference Series, 847, 012016. Published.
DOI: 10.1088/1742-6596/847/1/012016.

Radiochromic and radiofluorogenic 3D solid polymer dosimeter; initial results for high doses

María del Rocío Bernal-Zamorano, Nicolai Højer Sanders, Lars René Lindvold, Claus E. Andersen

Center for Nuclear Technologies, Technical University of Denmark, 4000 Roskilde, Denmark

E-mail: mroc@dtu.dk

Abstract. The complexity of dose distributions has increased with the advent of intensity modulated radiation therapy (IMRT). For that reason, experimental measurements using 3D dosimeters with high spatial resolution are required to check the delivered dose. In this study a new 3D solid polymer dosimeter with absorbance and fluorescence responses to radiation is presented. Measuring fluorescence instead of absorbance improves the spatial resolution and eases the read out of the dosimeter. The proposed dosimeter is tissue-equivalent and can be moulded in any shape by a controllable and fast photopolymerization process.

1. Introduction

Modern radiotherapy requires complex dose distributions; therefore, there is an increasing demand for a high spatial resolution system suitable for dose verification to ensure treatment quality. Over the last years, 3D dosimetry systems have been developed for this purpose. They may be classified into polymerizing dosimeters or radiochromic dosimeters, which use magnetic resonance imaging (MRI) [1] or optical computed tomography (CT) [2] as readout systems. These dosimeters change chemical properties upon irradiation. While polymerizing dosimeters consist of a gel matrix that polymerizes with radiation [3], radiochromic dosimeters consist of a gel, plastic or silicone matrix with a radiation sensitive dye that changes color with radiation exposure [4].

It is important to remember that a dosimetry system is not only the dosimeter itself but also the readout technique used for extracting the dose information after irradiation. Oldham *et al* [5] applied both techniques (MRI and CT) to the same gel dosimeter and they obtained a higher resolution for CT. Besides that, MRI scanners have significant disadvantages like its cost and availability, and they may be susceptible to several uncertainty sources like field homogeneity and temperature [6]. These uncertainties are well understood and can be compensated. However, there are still issues concerning the material properties of the gels. It is known that the radiation induced cross-linking of the gel is highly dependent on its oxygen level, pH, and temperature, just to mention a few parameters. For those reasons CT is more commonly used [7].

Some problems of the CT scan are the light scattering and the acquisition time. Gel dosimeters require the use of a container, which adds scatter artifacts in the read out due to reflections [8]. Therefore, the scattering may be reduced by using a solid dosimeter that does not need a holder. Solid dosimeters also avoid the diffusion problem present in gel dosimeters, which causes blurring of the dose distribution image over time. For some systems, the acquisition of the image may be time consuming since current CT readout systems require scanning of several slices while the sample

rotates to acquire data at different angles. For example, the 3D scan of the commercially available PRESAGE™/OCTOPUS™ dosimetry system needs 15 slices and takes 8-9 minutes per slice [9]. This gives a total scanning time of 2 hours, followed by a computer intensive image reconstruction. A simple, *in-situ* and fast reading of the dosimeter would facilitate the use of the 3D dosimeter in a clinical basis.

A way to increase the scanning speed is by using scanners based on charge-coupled device (CCD) cameras, since it is possible to obtain a complete 2D image in one go [7]. This technique can be used to measure the fluorescence [10] instead of the attenuation as the CT does. We have developed a 3D readout based on a black and white CCD camera. Detecting small signals is difficult when measuring the absorbance (or attenuation) in the dosimeter; however, measuring fluorescence allows us to use color filters to ensure that the vast majority of the signal comes from the dye in the sample.

In this paper we present a sensitive, soft-tissue equivalent and moldable 3D solid polymer dosimeter that is not only radiochromic but also radiofluorogenic. The underlying mechanism involves the conversion of a non-fluorescent dye molecule into a fluorescent form when incorporated into a rigid polymeric matrix and irradiated. The imaging of the dose distribution is obtained by measuring the fluorescence intensity, which can be recorded using a conventional digital camera. This gives a higher accuracy, a higher spatial resolution and a faster read out, compared to the current commercially available 3D dosimetry systems.

2. Materials and methods

2.1. The dosimeter

We use a poly(ethylene glycol) diacrylate matrix (PEGDA-575 g/mol) containing pararosaniline leuco dye [11]. The radiation chemistry involved in the transformation from leuco dye to dye is presented in figure 1 [12]. This polymer enables the solidification of the material through a photopolymerization process. We use diphenyl(2,4,6-trimethylbenzoyl)phosphine oxide (TPO) as photoinitiator.

The dosimeter can be molded in any shape by light of approximately 400 nm, which does not affect the dye. This is a controllable and fast process that only takes up to 10 minutes. After curing, the dosimeter can be removed from the mold. This property could open up for a significant number of clinical applications relative to making patient-like geometries, or using it as a thin 2D dosimeter (film) for the radiation field verification as a quality control test.

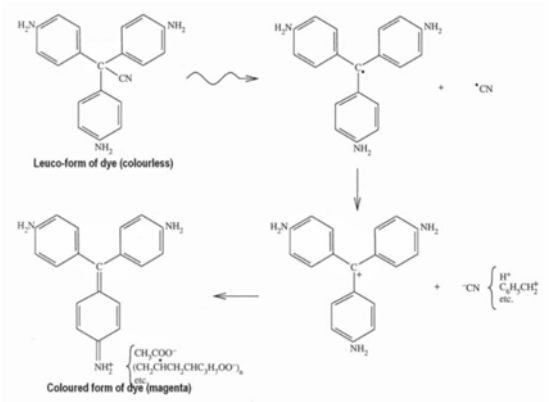

Figure 1. Chemical reaction of the leuco dye due to radiation.

2.2. The readout system

Optical fluorescence tomography is used for read out of the dose distribution in the dosimeter (figure 2) [13]. The dosimeter is submerged in an index matching fluid tank and excited with a green laser. Pictures of the fluorescent emission are taken with a CCD black and white camera to get the 2D dose

distribution. 3D information is obtained by moving the sample through the light sheet while taking pictures.

The scanning speed is up to 2 millimeters per second, so the total scanning of the dosimeter is finished within minutes, which avoids problems of chemical changes during scanning. This technique allows having an *in-situ* reading and the device is easy to use. These characteristics would facilitate its use in the clinic.

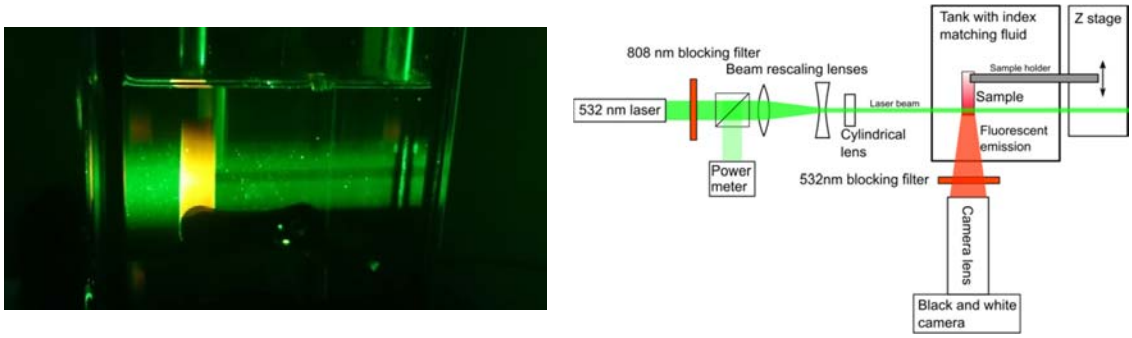

Figure 2. Picture of the dosimeter inside the index matching fluid tank and scheme of the readout system.

2.3. Irradiations and measurements

Irradiations were carried out in a ^{60}Co gamma source with a dose rate of 139.3 Gy/min. The uncertainty on the delivered dose is 1.3%. Absorbance was measured with a Shimazdu UV-2700 spectrophotometer. Fluorescence is excited with a 532 nm Nd:YAG laser, and measured with an Ocean Optics QE6500 spectrometer.

3. Results and discussion

A slide of 1 mm thickness is cured between two glass plates to ensure the best optical quality and irradiated up to 1 kGy in steps of 100 Gy. Normalized absorbance and fluorescence spectra as function of the dose are shown in figure 3. The results show that the fluorescence response is strong enough to be used. In figure 4 we present the fits of the responses with the absorbed dose for different parts of the spectrum. While the absorbance response is linear with the dose, the fluorescence response is exponential in overall and linear for the clinical dose range.

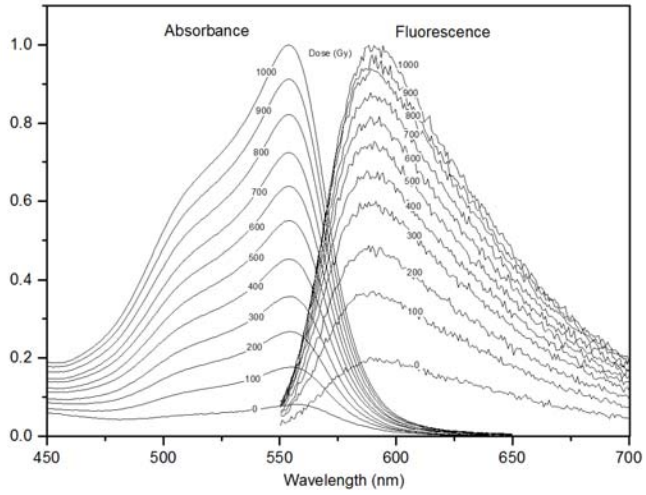

Figure 3. Normalized absorbance and fluorescence spectra.

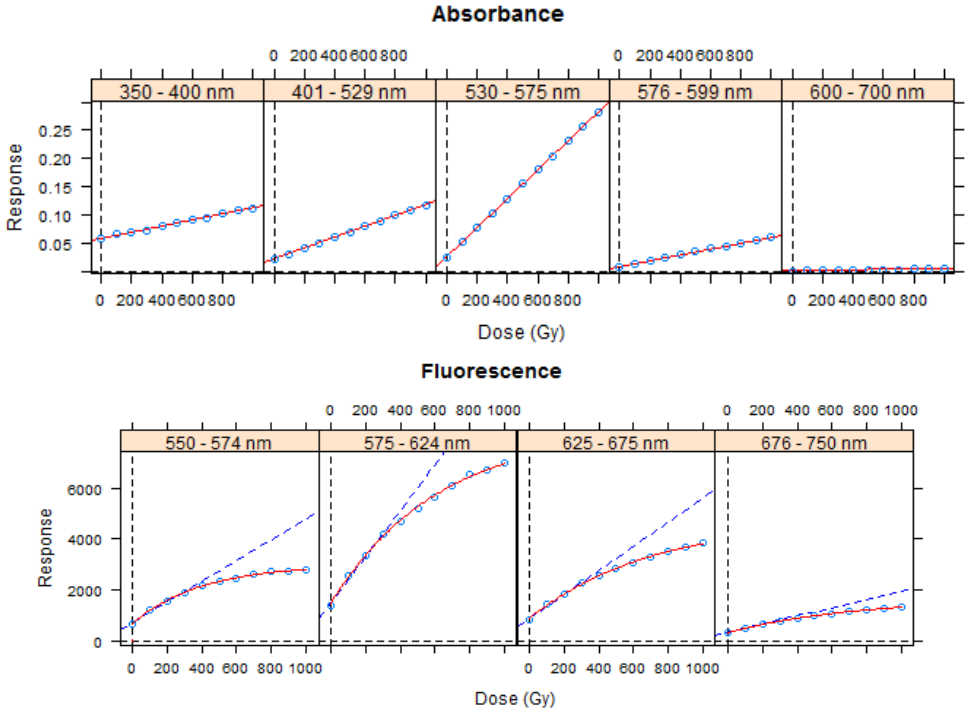

Figure 4. Absorbance and fluorescence fits as function of the absorbed dose.

4. Conlusions

We have developed a passive solid dosimeter that is tissue equivalent, can be molded in the desired form and does not need a container. The dosimeter responds to irradiation in the same way as radiochromic films (oxidation of a leuco dye) but we have established a polymer matrix for this dye that allows us to measure not only the absorbance of the material but also its fluorescence. The main difference with current 3D solid polymer dosimeters is the readout technique. While current 3D dosimetry systems mainly use CT to extract dose information, we can measure the fluorescence, which potentially is a faster and more sensitive method. The response range of this dosimeter is very high (up to 1 kGy), but future studies will focus on optimizing the dosimeter at low doses for its clinical application.

5. References

[1] Gore *et al*, 1984 *Phys. Med. Biol.* **29** (10) 1189–1 197
[2] Gore *et al*, 1996 *Phys. Med. Biol.* **41** 2695–2704
[3] Baldock *et al*, 2010 *Phys. Med. Biol.* **55** R1–R63
[4] Høye *et al*, 2015 *J. Phys. Conf. Ser.* **573** 012067
[5] Oldham *et al*, 2001 *Med. Phys.* **28** (7) 1436–1445
[6] Vandecasteele *et al*, 2013 *Phys. Med. Biol.* **58** 63–85
[7] Doran *et al*, 2006 *J. Phys. Conf. Ser.* **56** 45–57
[8] Oldham, 2006 *J. Phys. Conf. Ser.* **56** 58–71
[9] Sakhalkar *et al*, 2009 *Med. Phys.* **36** 71–82
[10] Warman *et al*, 2013 *Rad. Phys.Chem.* **85** 179–181
[11] Bernal-Zamorano *et al*, 2016. 3D dosimetry material with absorbance and fluorescence responses to ionizing radiation. Presented at the 18th Solid State Dosimetry conference.
[12] Journal of the ICRU Vol 8 No 2 (2008) Report 80
[13] Sanders *et al*, 2016. Measuring radiation dose in 3D in a radiofluorogenic sample; a proof of concept setup. Presented at the 18th Solid State Dosimetry conference.

PAPER II

Bernal-Zamorano, M.R., Sanders, N.H., Lindvold, L., Andersen, C.E. (2017). Radiochromic and radiofluorogenic 3D solid polymer dosimeter; effect of the photoinitiator.
Radiation Measurements, 106, 192-195. Published.
DOI: 10.1016/j.radmeas.2017.03.012.

Radiation Measurements 106 (2017) 192–195

Contents lists available at ScienceDirect

Radiation Measurements

journal homepage: www.elsevier.com/locate/radmeas

Radiochromic and radiofluorogenic 3D solid polymer dosimeter; effect of the photoinitiator

M.R. Bernal-Zamorano*, N.H. Sanders, L. Lindvold, C.E. Andersen

Center for Nuclear Technologies, Technical University of Denmark, Risø Campus, Frederiksborgvej 399, 4000 Roskilde, Denmark

HIGHLIGHTS

- Fluorescence response is strong enough to be used.
- Absorbance and fluorescence responses increase with the absorbed dose.
- The water equivalent material is cured in the desired form by a photopolymerization process.
- The type of photoinitiator affects the response to ionizing radiation.

ARTICLE INFO

Article history:
Received 30 September 2016
Received in revised form
21 December 2016
Accepted 14 March 2017
Available online 16 March 2017

Keywords:
3D dosimetry
Solid polymer dosimeter
Absorbance
Fluorescence
Pararosaniline leuco dye
Photoinitiator

ABSTRACT

Due to the recent increase in the complexity of external radiotherapy treatments, there is a need for a dosimeter capable of rendering a 3D dose profile to verify the absorbed dose with high spatial resolution. We are developing a solid and moldable 3D dosimeter material with the objective of determining the absorbed dose by measuring its fluorescence instead of the absorbance, which is a more established method. Measuring fluorescence could potentially provide higher sensitivity and spatial resolution, which is critical for 3D dosimetry. In this study, absorbance and fluorescence responses to gamma radiation are presented for doses up to 1 kGy. Since the material is cured by a photopolymerization process, the effect of the photoinitiator is also analyzed.

1. Introduction

The goal of external radiotherapy is to deliver the appropriate dose to the tumor without damaging the healthy tissue. To achieve this, the complexity of radiotherapy has increased over time, especially by advances in Intensity Modulated Radiation Therapy (IMRT) and computerized treatment planning systems. These advanced techniques are more sensitive to errors, which demands dose verification with high spatial resolution (Low, 2015).

Radiochromic films have been used for long time as 2D dosimeters (Mclaughlin et al., 1977; Niroomand-Rad et al., 1998). They are usually colorless polymeric films based on a colorless leuco dye precursor that acquires color after irradiation due to the chemical change of the radiochromic dye. The dose is determined by measuring the optical density or absorbance; that is the dose-induced color change (ICRU, 2008). Some of the commercially available films are the GafChromic™ film (Chu et al., 1990) that is based on polydiacetylene; and the B3 Radiochromic™ film (Miller and Mclaughlin, 1980), whose colorless precursor leuco dye (pararosaniline) belongs to the triarylmethane dyes family. These films are widely used as routine dosimetry systems. However, the new treatment modalities require a dosimetry system capable of measuring 3D dose distributions to assure treatment quality (Wuu, 2015).

3D dosimeters may be classified according to their response to radiation: polymerizing or radiochromic dosimeters. A polymerizing dosimeter is a gel that polymerizes with radiation, while a radiochromic dosimeter may be a gel or solid that changes its color due to radiation. 3D dosimeters may also be classified according to their polymeric matrix: gel or solid dosimeters. Gel polymer dosimeters have important limitations such as the high diffusion

* Corresponding author.
E-mail address: mroc@dtu.dk (M.R. Bernal-Zamorano).

http://dx.doi.org/10.1016/j.radmeas.2017.03.012
1350-4487/

inside the gel and the need of a supporting container that adds artifacts in the readout (De Deene, 2004; Baldock et al., 2010). Solid polymer dosimeters, such as PRESAGE™ (Guo et al., 2006), which also uses a triarylmethane dye (malachite green), avoid these problems. However, the readout technique (optical computed tomography) is a long process that takes several hours due to the scanning procedure and image reconstruction (Sakhalkar et al., 2009).

The dose is usually determined by measuring the optical density (or absorbance) (Høye et al., 2015). Measuring fluorescence instead, could potentially provide higher sensitivity and spatial resolution (Cullum et al., 2000; Warman et al., 2013) and the 3D readout device would be quicker and easier to use than current scans (Sanders et al., 2016). Since some of the triarylmethane dyes are fluorescent when embedded in a rigid matrix (Oster et al., 1958), the objective of our study was to test if it is possible to use pararosaniline leuco dye (used in B3 Radiochromic™ films) to determine the absorbed dose by measuring fluorescence. The polymer that we use, poly(-ethylene glycol) diacrylate (PEGDA), allows us to cure the material in the desired form by light. This requires the use of a photoinitiator that creates reactive species to induce polymerization (Neumann et al., 2005). Depending on the type of reaction needed to generate free radicals, photoinitiators can be classified into type I (unimolecular reaction) and type II (bimolecular reaction). In this study we tested the absorbance and fluorescence response to radiation for the two types of photoinitiators.

2. Materials and methods

2.1. Fabrication

Pararosaniline leuco dye is dissolved in a poly(ethylene glycol) diacrylate (PEGDA - 575 g/mol) matrix. This polymer enables the material to cure through a photopolymerization process, which allows a time- and space-controlled polymerization. We use two photoinitiators: diphenyl(2,4,6-trimethylbenzoyl) phosphine oxide (TPO) and isopropylthioxanthone (ITX). TPO is a type I photoinitiator, while ITX belongs to type II so it needs to interact with a second molecule (co-initiator) to generate free radicals. We use ethyl 4-dimethylaminobenzoate (EDB) as co-initiator in a 1:2 photoinitiator to co-initiator ratio by weight.

We dissolved the dye (61 mM) in ethanol (0.83 M), PEGDA-575 (1.62 M) and 2-hydroxyethyl methacrylate (HEMA) (41 mM). We used a vortex rotor for homogenization. Photoinitiators are dissolved in PEGDA-575 and added to the dye solution in a 9.85% vol. The concentration of each photoinitiator in the total solution was: 1.41 mM and 0.60 mM for TPO; and 1.41 mM for ITX. Solutions were kept in brown glass bottles to avoid curing.

The material was cured in the desired form (slides of 1 mm thickness) with a 395 nm LED. These wavelengths do not stimulate the dye, but shorter wavelengths can produce unwanted exposure in the material. We made 5 slides per dosimeter and we cured them all at the same time between two glass plates to ensure the best optical quality. Curing time was 10 min. Afterwards the material was removed from the mold.

2.2. Irradiations and measurements

Irradiations were carried out in a ^{60}Co gamma source (dose rate: 4.64 Gy/min). The uncertainty on the delivered dose is 1.3%. Afterwards, the absorbance of the dosimeter film was measured with a Shimazdu UV-2700 spectrophotometer. Fluorescence was excited with a 532 nm Nd:YAG laser, and measured with an Ocean Optics QE6500 spectrometer. One absorbance measurement and three fluorescence measurements were taken for each slide. In order to measure the accumulated absorbed dose, the same slides were irradiated and measured at 12 dose levels (0, 2, 4, 6, 8, 10, 20, 50, 100, 300, 600, 1000 Gy).

3. Results and discussion

3.1. Material quality

PEGDA provides excellent physical properties for a dosimeter: optical clarity, adhesion to surfaces, toughness and flexibility. The material is moldable in the desired form by a controllable and fast photopolymerization process. Fig. 1 shows the good mechanical and optical properties of the dosimeter.

3.2. Water equivalence

The protocols used in radiotherapy departments are based on reporting the absorbed dose to water (Almond et al., 1999; IAEA TRS-398, 2000). Therefore, it is very important to use a detector with characteristics as similar as possible to water. Some physical parameters can be used to quantify water equivalence, such as the effective atomic number (Z_{eff}), the mass density (ρ) and the electron density (ρ_{el}). The properties of our dosimeter are dominated by the properties of PEGDA, since it comprises 83% vol. of the total solution.

The effective atomic number is defined in Eq. (1), where a is the element-specific ratio of the number of electrons to the total electronic number, Z is the atomic number of each element, and m is an energy-dependent number ($m = 3.5$ is commonly used) (Johns and Cunningham, 1983).

$$Z_{eff} = \sqrt[m]{a_1 Z_1^m + a_2 Z_2^m + \ldots} \tag{1}$$

The chemical formula of PEGDA is $(C_3H_3O)(C_2H_4O)_n(C_3H_3O_2)$, where $n \sim 10$ for a molecular weight of 575 g/mol. Thus, carbon ($Z = 6$) contributes with 26×6 electrons, hydrogen ($Z = 1$) with 46×1 electrons and oxygen ($Z = 8$) with 13×8 electrons. Therefore, $Z_{eff}(PEGDA) \sim 5.9$.

The mass density of PEGDA is 1.12 g/ml in liquid state, but the density of the dosimeter is a bit lower since the material shrinks when it solidifies.

The electron density is calculated by using Eq. (2), where N_A is Avogadro's number, ρ_m is the mass density, and N_i, Z_i, A_i are: number of atoms of specie i, atomic number and mass number of such atoms.

$$\rho = N_A \rho_m \frac{\sum N_i Z_i}{\sum N_i A_i} \tag{2}$$

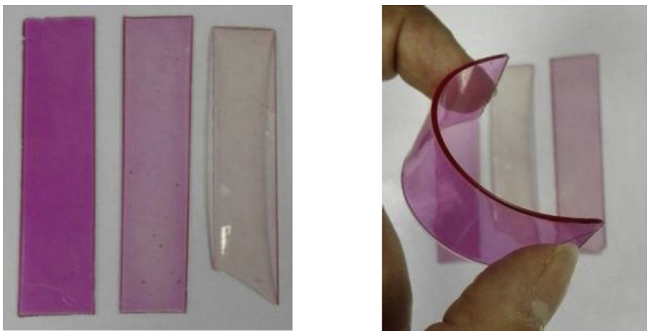

Fig. 1. Slides after irradiation to 1 kGy. From left to right: TPO-1.41 mM, TPO-0.60 mM, ITX + EDB-1.41 mM.

Table 1
Physical parameters to quantify water equivalence.

Material	Z_{eff} (m = 3.5)	$\rho(g/cm^3)$	$\rho_{el}(e^-/g)$ relative to water
Water	7.51	1.00	1.000
Alanine	5.96	1.23	0.976
BCF-60 scintillator	5.70	1.06	0.975
PEGDA	6.66	1.12	1.087

Results for PEGDA and values for water and commonly used dosimeters such as alanine and plastic scintillator (Azangwe et al., 2014) are shown in Table 1. From this perspective, our material is water equivalent, and therefore, soft-tissue equivalent, which is one of the requirements for a good medical dosimeter.

3.3. *Fluorescence and absorbance responses to gamma radiation*

Although this dye in solution is not fluorescent (Oster et al., 1958), a strong fluorescence response is detected when the dye is embedded in the rigid polymer matrix. The polymer dosimeter responds to irradiation by changing color, due to a chemical change in the pararosaniline leuco dye (Fig. 2a) (ICRU, 2008). We have observed that this change is accompanied by a change in the fluorescence response (Fig. 2b and c).

In Fig. 3 we present the absorbance and fluorescence peaks as function of absorbed dose – up to 1 kGy. We observe an increase in the fluorescence intensity when increasing the dose, contrary to the results shown in an earlier study with polymer films of the same dye (Abdel-Fattah et al., 2001). However, the material response is currently not sensitive enough for its clinical application. The low slope for low doses can be noted in the insets of Fig. 3, where data are presented in the logarithmic scale.

The radiation response is different for the different dosimeters due to the secondary species released by the photoinitiators. After irradiation, TPO breaks into reactive species (benzene groups) that have their emission wavelength around 300–350 nm, which stimulates the dye (Noakes and Culp, 1982). Therefore, it is not only radiation that affects the dye, but also these secondary species. For that reason, the dosimeter with TPO in high concentration has the highest response. On the other hand, ITX + EDB has the lowest response due to the sulfur in the chemical structure of ITX. Heavy-atom substituents like sulfur increase the spin-orbit coupling and yield a dye that is nonfluorescent (Schäfer, 1972; Turro, 1978). However, we notice a fluorescent response in this case due to the co-initiator, EDB, which releases also a benzene group.

4. Conclusions

There is an increasing demand for a highly sensitive and accurate 3D dosimeter. Our material is a good candidate for this purpose, since it is water equivalent and can be molded in any shape. It is solid, so it avoids the inconveniences of gel dosimeters such as the high diffusion inside the gel and the need of a supporting container. It has good optical and mechanical properties, and it is possible to measure not only its absorbance but also its fluorescence. In this study we have presented the absorbance and fluorescence responses as function of the absorbed dose. We have also observed that the photoinitiator used for curing plays an important role on the response of the dosimeter. It is not only radiation that changes the form of the leuco dye, but also the secondary species released by the photoinitiator. Currently, this dosimeter has a good response for doses up to 1 kGy, but cannot be used in the medical range. A typical dose in radiotherapy is 2 Gy per fraction and 50 Gy for a full treatment, and the dosimeter therefore needs to be optimized and characterized for lower doses than was studied in this work.

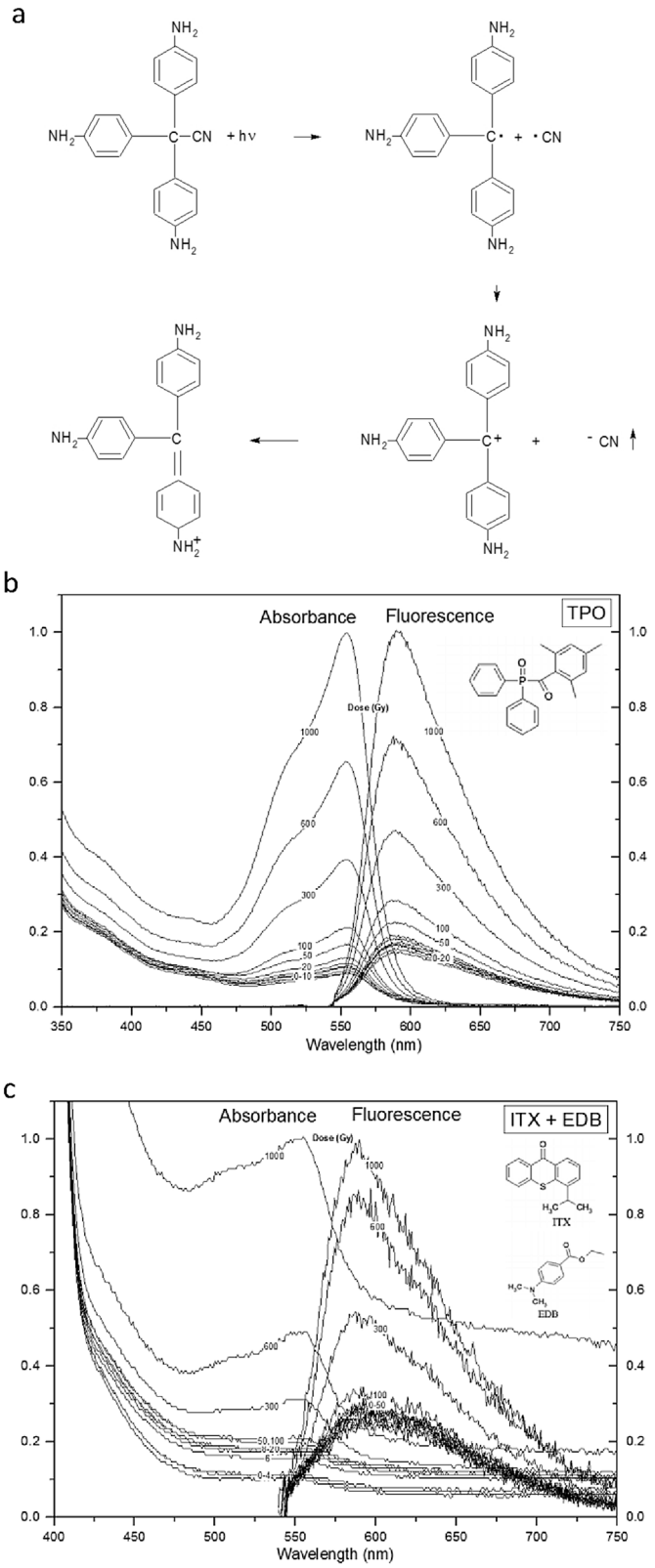

Fig. 2. a. Radiation chemistry involved in the transformation from leuco dye to dye. **b, c.** Normalized spectra for a single slide for the two different photoinitiators (1.41 mM). Insets: chemical structure of each photoinitiator (and co-initiator, EDB).

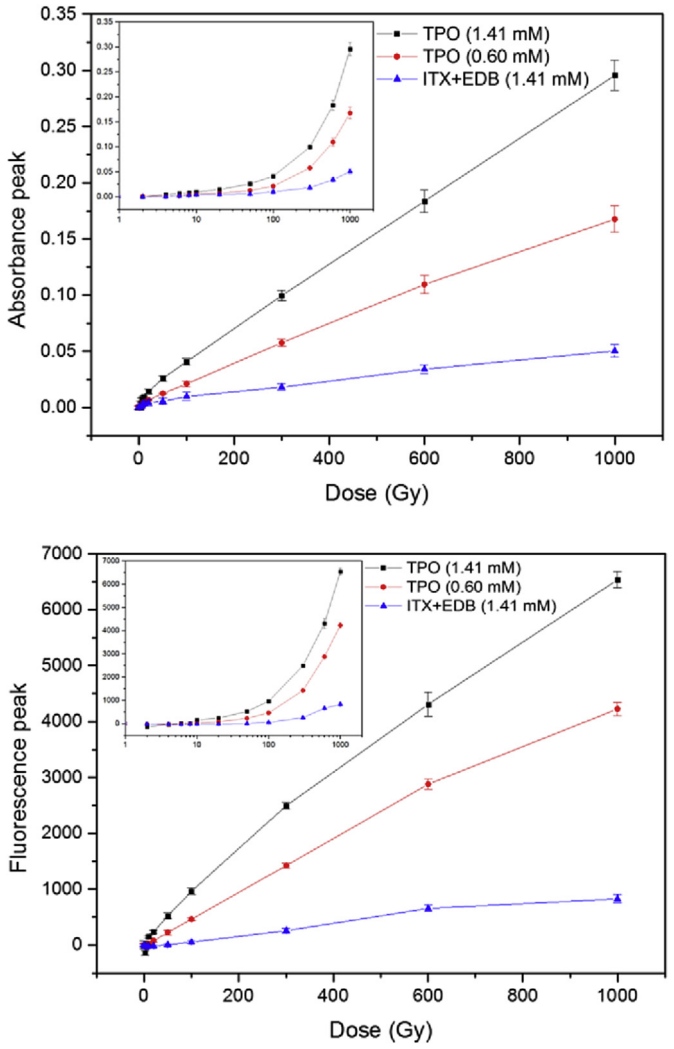

Fig. 3. Absorbance and fluorescence peaks as a function of the dose. Insets: same data in the logarithmic scale to show the low slope in the low dose range (medical range). Black square: TPO-1.41 mM, red circle: TPO-0.60 mM, blue triangle: ITX + EDB-1.41 mM.

Acknowledgements

M. Bailey and A. Miller for help with irradiations at the Center for Nuclear Technologies, Technical University of Denmark.

References

Abdel-Fattah, A.A., Beshir, W.B., Hegazy, E.S.A., El-Din, H.E., 2001. Photo-luminescence of Risø B3 and PVB films for application in radiation dosimetry. Radiat. Phys. Chem. 62 (5–6), 423–428.
Almond, P.R., Biggs, P.J., Coursey, B.M., Hanson, W.F., Huq, M.S., Nath, R., Rogers, D.W.O., 1999. AAPM TG-51 protocol for clinical reference dosimetry of high-energy photon and electron beams. Med. Phys. 26, 9.
Azangwe, G., Grochowska, P., Georg, D., Izewska, J., Hopfgartner, J., Lechner, W., Andersen, C.E., Beierholm, A.R., Helt-Halsen, J., Mizuno, H., Fukumura, A., Yajima, K., Gouldstone, C., Sharpe, P., Meghzifene, A., Palmans, H., 2014. Detector to detector corrections: a comprehensive experimental study of detector specific correction factors for beam output measurements for small radiotherapy beams. Med. Phys. 41, 072103.
Baldock, C., De Deene, Y., Doran, S., Ibbott, G., Jirasek, A., Lepage, M., McAuley, K.B., Oldham, M., Schreiner, L.J., 2010. Polymer gel dosimetry. Phys. Med. Biol. 55, R1–R63.
Chu, R.D.H., Vandyk, G., Lewis, D.F., Ohara, K.P.J., Buckland, B.W., Dinelle, F., 1990. Gafchromic™ dosimetry media: a new high dose, thin film routine dosimeter and dose mapping tool. Radiat. Phys. Chem. 35 (4–6), 767–773.
Cullum, B.M., Mobley, J., Bogard, J.S., Moscovitch, M., Phillips, G.W., Vo-Dinh, T., 2000. Three-Dimensional optical random access memory materials for use as radiation dosimeters. Anal. Chem. 72, 5612–5617.
De Deene, Y., 2004. Essential characteristics of polymer gel dosimeters. J. Phys. Conf. Ser. 3, 34–57.
Guo, P.Y., Adamovics, J.A., Oldham, M., 2006. Characterization of a new radiochromic three-dimensional dosimeter. Med. Phys. 33 (5), 1338–1345.
Høye, E.M., Skyt, P.S., Yates, E.S., Muren, L.P., Petersen, J.B.B., Balling, P., 2015. J. Phys. Conf. Ser. 573, 012067.
IAEA TRS-398, 2000. Absorbed Dose Determination in External Beam Radiotherapy: An International Code of Practice for Dosimetry Based on Standards of Absorbed Dose to Water.
Johns, H.E., Cunningham, J.R., 1983. The Physics of Radiology, fourth ed.
J. ICRU 8 (No 2), 2008. Report 80.
Low, D., 2015. The importance of 3D dosimetry. J. Phys. Conf. Ser. 573, 012009.
Mclaughlin, W.L., Miller, A., Fidan, S., Pejtersen, K., 1977. Radiochromic plastic films for accurate measurement of radiation absorbed dose and dose distributions. Radiat. Phys. Chem. 10 (2), 119–127.
Miller, A., Mclaughlin, W.L., 1980. On a radiochromic dye dosemeter. Risø-M, 2254.
Neumann, M.G., Schmitt, C.C., Giovana, C.F., Correa, I.C., 2005. The initiating radical yields and the efficiency of polymerization for various dental photoinitiators excited by different light curing units. Dent. Mat. 22, 576–584.
Niroomand-Rad, A., Chiu-Tsao, S., Trichter, S., Das, I., 1998. Radiochromic Film Dosimetry. AAPM. Report No. 63.
Noakes J.E., Culp, R.A., 1982. US 4507226. United States Patent.
Oster, G., Joussot-Dubien, J., Broyde, B., 1958. Photoreduction of dyes in rigid media. I. Triphenylmethane dyes. J. Am. Chem. Soc. 81 (8), 1869–1872.
Sakhalkar, H.S., Adamovics, J., Ibbott, G., Oldham, M., 2009. A comprehensive evaluation of the PRESAGE/optical-CT 3D dosimetry system. Med. Phys. 36 (1), 71–82.
Sanders, N.H., Bernal-Zamorano, M.R., Lindvold, L.R., Andersen, C.E., 2016. Designing an optical setup for readout of the 3D dose distribution from a radiofluorogenic polymer. Submitted to Radiation Measurements.
Schäfer, F.P., 1972. Dye Lasers. Editorial: Topics in Applied Physics, vol. 1.
Turro, N.J., 1978. Modern Molecular Photochemistry. Benjamin/Cummings, Editorial.
Warman, J.M., de Haas, M.P., Luthjens, L.H., Denkova, A.G., Kavatsyuk, O., van Goethem, M.-J., Kiewiet, H.H., Brandenburg, S., 2013. Fixed fluorescent images of an 80MeV proton pencil beam. Radiat. Phys. Chem. 85, 179–181.
Wuu, C., 2015. Clinical applications of 3-D dosimeters. J. Phys. Conf. Ser. 573, 012011.

PAPER III

Bernal-Zamorano, M.R., Sanders, N.H., Lindvold, L., Andersen, C.E.
Radiochromic and radiofluorogenic 3D solid polymer dosimeter; a third signal: Electron Paramagnetic Resonance (EPR).
Submitted to Radiation Measurements on December 2017.

Title: "Radiochromic and radiofluorogenic 3D solid polymer dosimeter; a third signal: Electron Paramagnetic Resonance (EPR)"

Authors: M.R. Bernal-Zamorano[a*], N.H. Sanders[a], L. Lindvold[a], C.E. Andersen[a].

[a]Center for Nuclear Technologies, Technical University of Denmark, Risø Campus, Frederiksborgvej 399, 4000 Roskilde, Denmark.

* Corresponding author.
E-mail: mroc@dtu.dk

HIGHLIGHTS

- EPR signal from the dosimeter is detected and it increases with the dose, linearly for the medical dose range.
- Three signals for the solid polymer dosimeter's characterization: absorbance, fluorescence and EPR.
- EPR as supporting feature to the optical signals from the dosimeter.
- The measured EPR signal originates from radiation induced changes of the radiochromic dye and not the matrix polymer.

KEYWORDS

3D dosimetry; solid-state polymer dosimeter; EPR; fluorescence; pararosaniline leuco dye, free radical.

ABSTRACT

We have developed a water-equivalent solid polymer dosimeter material aimed for 3D dosimetry in radiotherapy beams. The material responds to ionizing radiation by changes in its optical absorbance and by generation of fluorescence species. The latter signal is of particular interest as the fluorescence facilitates detailed mapping of the 3D dose distribution by using laser stimulation.
In addition to the optical signals we also expect an electron paramagnetic resonance (EPR) dose response from the material, related to the formation of stable free radicals.
To test this hypothesis, point detector experiments were performed. The material was casted into 4.75 mm diameter pellets, identical in size to the alanine dosimeters that are routinely used for reference EPR dosimetry in our laboratory. The pellets of the new dosimeter and alanine were irradiated in ^{60}Co beams and first derivative EPR spectra were recorded subsequently. Results show an EPR signal for the solid polymer dosimeter, whose peak-to-peak amplitude is linear with the dose in the medical dose range and saturates for high doses. It was also seen that the matrix does not yield free radicals under irradiation.

1. Introduction

Electron paramagnetic resonance (EPR) has been used to study free radicals formed in solid materials, since they typically produce an unpaired spin on the molecule from which an electron is removed. This technique is commonly used to determine the absorbed dose in alanine, which is used as a reference dosimeter due to its water equivalence, high stability, low fading and high dose range response (Helt-Hansen *et al.*, 2009)(ICRU 80,2008). However, alanine dosimetry can only be used as a point detector and, currently, 3D dosimetry is in high demand (Watanabe *et al.*,2017*)*. Improvements of treatment planning in radiotherapy require experimental verification in three dimensions with high spatial resolution, sensitivity and accuracy.

We presented in a previous work (Bernal-Zamorano *et al.*, 2017a) a good candidate for 3D dosimetry, since the dosimeter is solid, water equivalent, and can be molded in any shape. It is based in pararosaniline leuco dye, which is chemically transformed into its dye-form by the effect of radiation (Fig. 1) (ICRU 80, 2008). This solid-state polymer dosimeter responds to radiation by changes in its absorbance (as current 3D dosimeters do) but also by changes in its fluorescence, which would be a more sensitive and faster method to obtain the absorbed dose point by point. The objective of this study is to make point detectors with this dosimeter to test if it is possible to measure the EPR signal as it is done with alanine. This would allow us to compare our dosimeter with a reference dosimeter, as it is usually done in dosimetry (Waldeland *et al.*, 2011), and to have a third signal that gives us more information of the mechanisms of this new dosimeter.

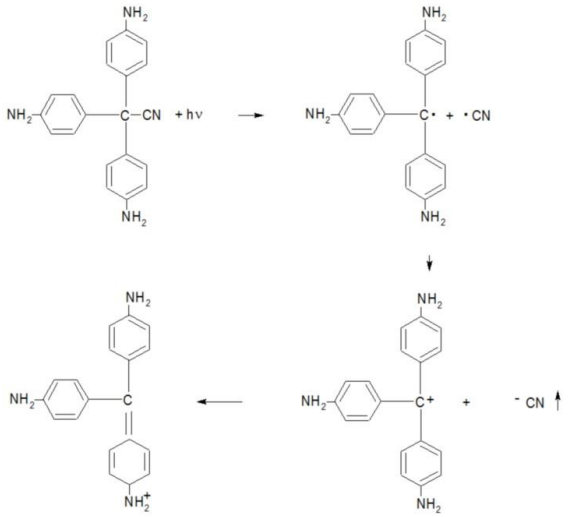

Fig.1. Chemistry involved in the response of the dye to radiation.

2. Materials and methods

2.1. Fabrication

Pararosaniline leuco dye is contained in a poly(ethylene glycol) diacrylate (PEGDA average M_n 575) (Sigma Aldrich 437441) matrix that includes ethanol, 2-hydroxyethyl methacrylate (HEMA) (Sigma Aldrich 128635), and diphenyl(2,4,6-trimethylbenzoyl) phosphine oxide (TPO)(Sigma Aldrich 415952) for photocuring. We used the same composition and procedure that we used in a previous work with slides (Bernal-Zamorano *et al.*, 2017b) (Fig. 2a): dye-61 mM, ethanol-0.83 M, PEGDA-1.62 M, HEMA-41 mM and TPO-1.41 mM. Solutions were mixed in a vortex rotor for half an hour before adding the photoinitiator and for half an hour more afterwards. They were kept in the darkness until the next day when they were cured and irradiated. The matrix of the dosimeter (without dye) was also tested.

We made cylindrical pellets of 4.75 mm diameter and 2.78 mm thickness of the same size than alanine pellets used in this work. We cured the solution by using an aluminum mold between two glass plates to ensure the best optical quality, irradiating with a 407 nm LED from a distance of 9 cm (surface power density 4.5 mW/cm^2) for 10 minutes (Fig. 2b, c, d).

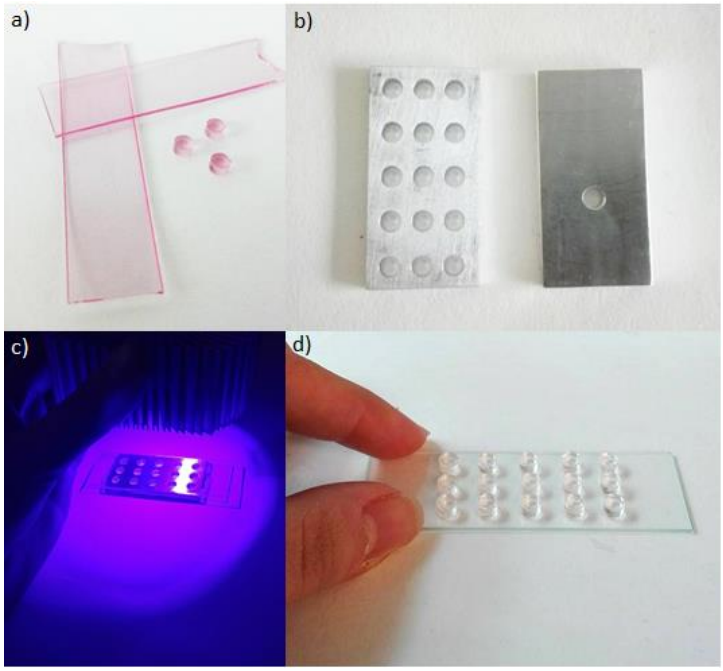

Fig.2. a. Slides and pellets of the dosimeter material. b. Aluminum mold for fabrication and holder for optical measurements. c. Curing process. d. Result after curing.

2.2. Irradiations and measurements

Four pellets of each type (alanine, dosimeter and dosimeter's matrix) were irradiated in a ^{60}Co gamma source with a dose rate of about 5 Gy min^{-1}. They were given doses of: 5, 10, 20, 30, 50, 75 and 100 Gy. After each irradiation, the absorbance, fluorescence and EPR signals of each pellet of the dosimeter and its matrix were measured. The EPR signal of alanine pellets was also measured. Fig. 3 shows the pellets and the holders that were used.

Absorbance spectra of the pellets were measured with a Shimazdu UV-2700 spectrophotometer, and fluorescence spectra with an Ocean Optics QE6500 spectrometer. Fluorescence was excited with a 520 nm diode laser. The EPR signal was obtained by a Bruker EMX-micro spectrometer by inserting each pellet into the resonator in a quartz tube. Before taking each measurement, fine tuning of the cavity was performed. Peak-to-peak amplitude of the first derivative EPR spectrum for alanine is obtained directly through the Risø EPR user interface. In the case of the new dosimeter, peaks are obtained by fitting both the maximum and the minimum of each first derivative EPR spectrum to a fourth degree polynomial, separately. The magnetic sweep width was 50 G with a resolution of 1024 points, the modulation amplitude was 1 G, the frequency 100 kHz, the sweep time 5.24 s and the time constant 1.25 ms. The microwave frequency was 9.75 GHz.

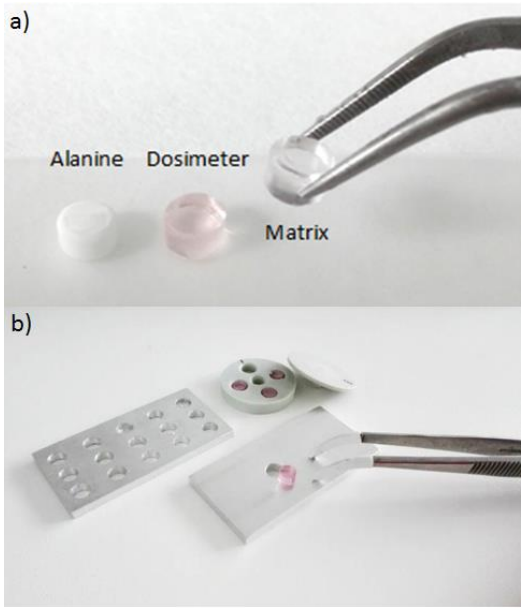

Fig.3. a. Pellets of alanine, solid polymer dosimeter and matrix of the dosimeter (no dye). b. Mold for fabrication, holder for optical measurements and poly(methyl methacrylate) (PMMA) holder for irradiation of 4 pellets.

3. Results and discussion

Fig. 4 shows the results of the EPR of alanine pellets and Fig. 5 shows the results of the EPR, absorbance and fluorescence signals of the new dosimeter and its matrix. Table 1 collects the results with the corresponding uncertainties.

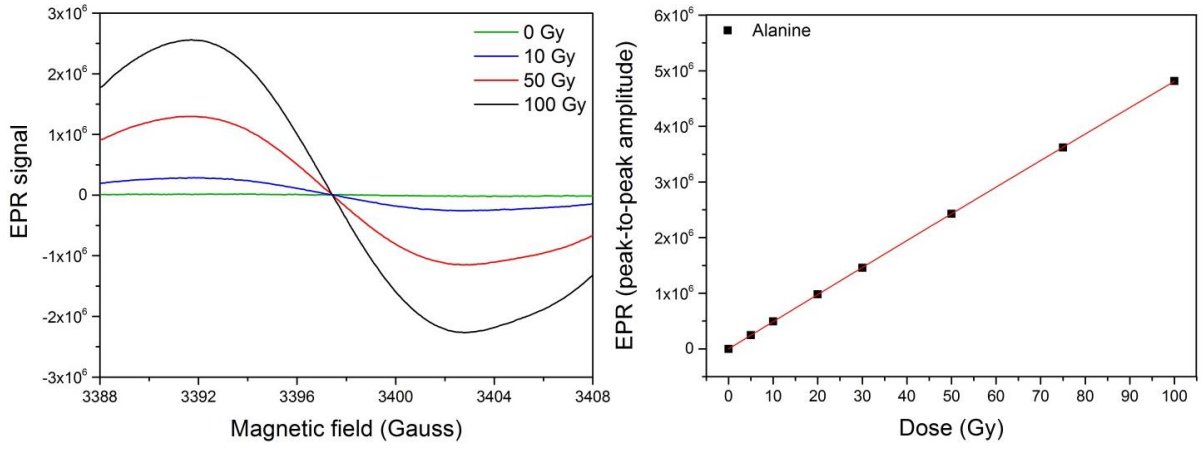

Fig. 4: EPR signal (first derivative of the EPR absorption spectra) of an alanine pellet irradiated to several doses, and peak-to-peak amplitude of the EPR signal as function of the dose for 4 alanine pellets. Error bars representing the statistically spread out of the measurements of the 4 pellets (standard deviation) are smaller than the markers.

3.1. EPR signal

A clear EPR signal was obtained for our material (Fig. 5a), increasing with the dose. As presented in (Bernal-Zamorano *et al.*, 2017b), alanine and PEGDA have similar characteristics in terms of its water equivalence (similar effective atomic number, mass density and electronic density). However, in this study we have observed that their response to radiation is very different (Fig. 4b, Fig. 5b): for the solid polymer dosimeter, the EPR signal saturates at high doses while it continues linear in the case of alanine. This difference is due to the interaction of the un-paired electron from the radical with its environment, which affects the details of the EPR spectrum. While alanine pellets are alanine microcrystals contained in compact wax, our dosimeter is similar to tissue: compact on the surface but diffusive inside. Looking at the chemical composition of our dosimeter, it may contain free water molecules moving within the dosimeter's matrix by diffusion processes and/or bound water, which is chemically attached to other molecules. Therefore, since water has a strong absorption band in the microwave region (Mehdizadeh, 2009), at the microwave frequency used here (9.75 GHz) most energy is absorbed by the dosimeter, resulting in a saturation of the EPR signal from the dye. However, despite this earlier saturation compared to alanine, the EPR signal of our dosimeter is linear for medical doses, which is the main application thought for this dosimeter.

The saturation dose can be obtained by fitting the peak-to-peak amplitude of the EPR spectra to Eq. (1) (Waldeland *et al.*, 2011) (Rotblat and Simmons, 1963), where $N(D)$ is the number of free radicals as function of the dose, N_∞ is the number of radicals at saturation, and D_0 is the characteristic saturation dose of the dosimeter. By fitting the dosimeter curve in Fig.5b (but with background correction; data starting in the origin) the saturation dose was obtained: $D_0 = (48.1 \pm 3.0)$ Gy.

$$N(D) = N_\infty(1 - e^{-\frac{D}{D_0}})$$

Consequently to Eq. (1), the peak-to-peak amplitude of the EPR signal provides a measurement of the free radicals present in the dosimeter. We have observed how these free radicals are only present in the dosimeter with dye and not in the matrix without it (Fig. 5b). The curve for the matrix is flat following the first irradiation, since from 0 to 5 Gy the EPR peak-to-peak amplitude decreases in a 53%. This decrease is due to the remaining radical species from the photoinitiator, which have not completely disappeared after curing and they disappear with the first irradiation. Therefore, the dose response of the dosimeter is only due to the dye. It is important to ascertain that the matrix is not liberating free radicals that respond to radiation and that may interact with those from the dye.

3.2. Absorbance and fluorescence signals

Regarding the absorbance results, in Fig.5c we see how the absorbance spectra are very spread out for the different doses, and the peaks are linear with the dose for the whole dose range (Fig.5d). For the fluorescence, the spectra are less spread out, which decreases sensitivity. Besides, the background fluorescence is very high, which makes indistinguishable the responses for low doses (Fig.5c, e). In Fig. 5e we also observe that the fluorescence of the dosimeter decreases with the first irradiation. Since the photoinitiator is fluorescent, this decrease may be related with the disappearance of the photoinitiator species with the first irradiation, observed in the EPR signal from the matrix. Therefore, the role of the matrix in the fluorescence response of the dosimeter is very important and the EPR signal helps us in studying it in more detail.

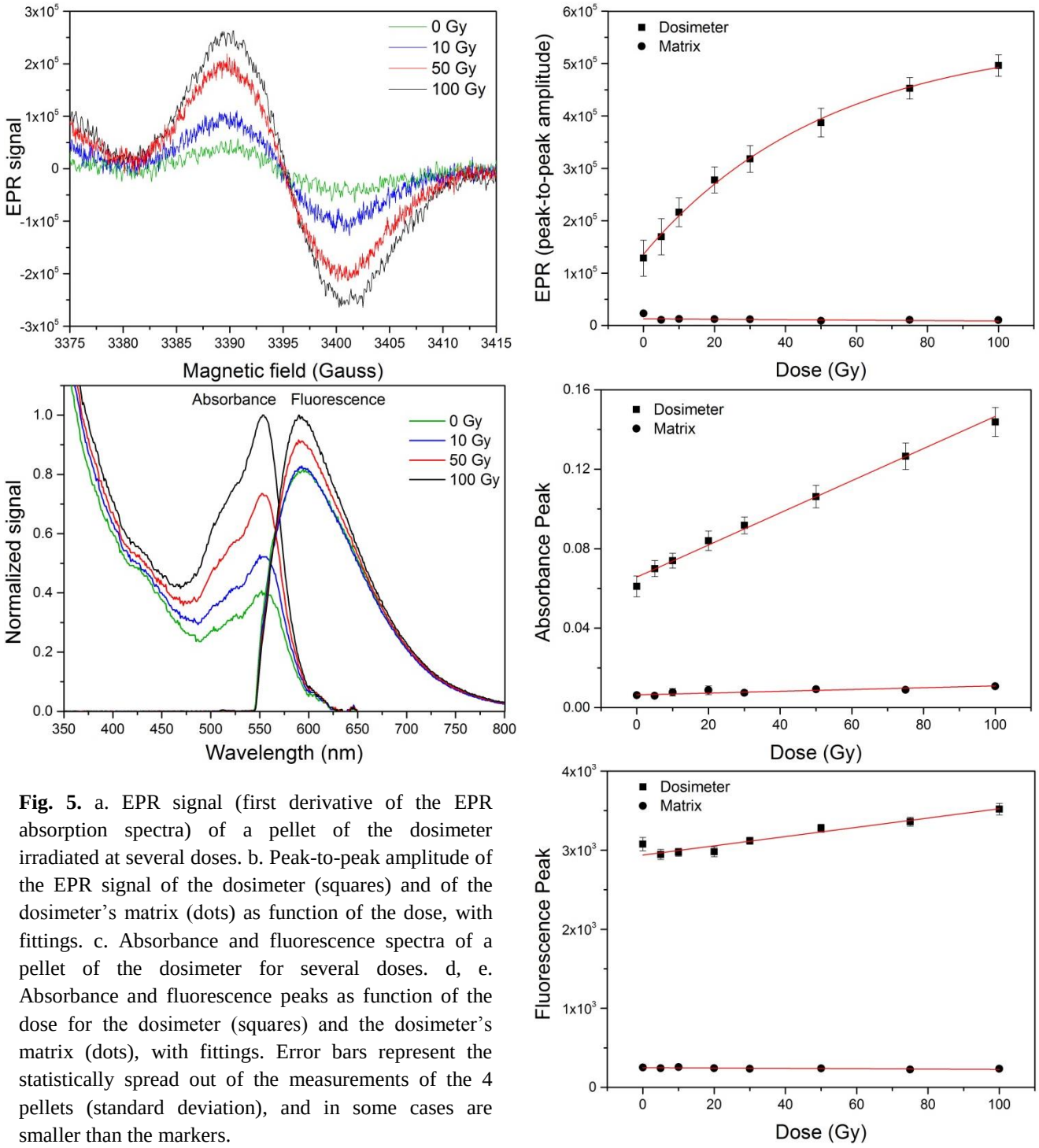

Fig. 5. a. EPR signal (first derivative of the EPR absorption spectra) of a pellet of the dosimeter irradiated at several doses. b. Peak-to-peak amplitude of the EPR signal of the dosimeter (squares) and of the dosimeter's matrix (dots) as function of the dose, with fittings. c. Absorbance and fluorescence spectra of a pellet of the dosimeter for several doses. d, e. Absorbance and fluorescence peaks as function of the dose for the dosimeter (squares) and the dosimeter's matrix (dots), with fittings. Error bars represent the statistically spread out of the measurements of the 4 pellets (standard deviation), and in some cases are smaller than the markers.

Table 1

Values of Fig.5b, d and e with their correspondent standard deviation.

Dose (Gy)	EPR (x 10^5)		Absorbance peak (x 10^{-3})		Fluorescence peak (x 10^3)	
	Dosimeter	Matrix	Dosimeter	Matrix	Dosimeter	Matrix
0	1.29 ± 0.34	0.232 ± 0.022	61.0 ± 5.2	6.25 ± 0.83	3.077 ± 0.085	0.252 ± 0.013
5	1.69 ± 0.34	0.109 ± 0.012	70.0 ± 4.1	6.00 ± 0.71	2.946 ± 0.064	0.244 ± 0.010
10	2.16 ± 0.27	0.126 ± 0.021	74.0 ± 3.7	7.8 ± 1.8	2.974 ± 0.049	0.2560 ± 0.0076
20	2.78 ± 0.25	0.121 ± 0.012	84.0 ± 4.9	8.8 ± 2.2	2.980 ± 0.063	0.2426 ± 0.0069
30	3.18 ± 0.26	0.119 ± 0.019	91.8 ± 4.3	7.5 ± 1.1	3.118 ± 0.045	0.2359 ± 0.0089
50	3.87 ± 0.27	0.0895 ± 0.0082	106.3 ± 5.6	9.25 ± 0.43	3.278 ± 0.050	0.2403 ± 0.0093
75	4.53 ± 0.20	0.1064 ± 0.0093	126.5 ± 6.7	9.00 ± 0.71	3.360 ± 0.057	0.2258 ± 0.0098
100	4.96 ± 0.21	0.105 ± 0.018	143.8 ± 7.3	10.75 ± 0.83	3.518 ± 0.073	0.236 ± 0.010

4. Conclusions

An EPR signal from the solid-state polymer dosimeter has been observed. It increases monotonically with the dose in the medical dose range and saturates for higher doses. Therefore, three signals can be obtained for the dosimeter's characterization: absorbance, fluorescence and EPR.

Due to the EPR it has been observed that free radicals present in the dosimeter are the species that originate from the radiochromic dye and not from the matrix. Therefore, the matrix provides the required properties for the dosimeter, such as solid support, water equivalence, moldable, flexibility, optical clarity, good mechanical and optical properties, without interfering in the radiation response from the dye.

EPR signal could be a source of improved understanding of the underlying dosimetric characteristics of this material and it may be a supporting feature to the optical signals from the dosimeter.

Besides, interesting applications in particle therapy beams are anticipated as the signal production in solid-state dosimeters are generally dependent on the ionization density.

5. Acknowledgements

Mark Bailey, Torben E. Mølholt and Arne Miller for their help with the EPR technique. Søren V. Dalsgaard and Jan S. Andersen for their help with the fabrication of aluminium molds.

References

Bernal-Zamorano M.R., Sanders N.H., Lindvold L., Andersen C.E. (2017a). Radiochromic and radiofluorogenic 3D solid polymer dosimeter: initial results for high doses. Journal of Physics: Conference Series, Vol. 847, 012016, DOI: 10.1088/1742-6596/847/1/012016.

Bernal-Zamorano M.R., Sanders N.H., Lindvold L., Andersen C.E. (2017b). Radiochromic and radiofluorogenic 3D solid polymer dosimeter; effect of the photoinitiator. Radiation Measurements, DOI: 10.1016/j.radmeas.2017.03.012.

Helt-Hansen J., Rosendal F., Kofoed I.M., Andersen C.E. (2009). Medical reference dosimetry using EPR measurements of alanine: Development of an improved method for clinical dose levels. Acta Oncologica, 48:2, 216-222, DOI: 10.1080/02841860802279725.

ICRU (2008). Journal of the ICRU Vol 8 No 2 Report 80.

Mehdizadeh M. (2009). Microwave/RF Applicators and Probes for Material Heating, Sensing, and Plasma Generation. Chapter 1. Elsevier.

Rotblat, J., Simmons, J.A. (1963). Dose-response relationship in yield of radiationinduced free radicals in amino acids. Physics in Medicine and Biology 7, 489e497.

Waldeland E., Helt-Hansen J., Malinen E. (2011). Characterization of lithium formate EPR dosimeters for high dose applications – Comparison with alanine. Radiation Measurements, DOI: 10.1016/j.radmeas.2010.11.015.

Watanabe Y., Warmington L., Gopishankar N. (2017). Three-dimensional radiation dosimetry using polymer gel and solid radiochromic polymer: From basics to clinical applications. World Journal of Radiology, DOI: 10.4329/wjr.v9.i3.112.